Report No. K-TRAN: KSU-02-6
FINAL REPORT

RESILIENT MODULUS AND THE FATIGUE PROPERTIES OF KANSAS HOT MIX ASPHALT MIXES

Stefan A. Romanoschi, Ph.D., P.E.
Nicoleta I. Dumitru
Octavian Dumitru

Kansas State University
Manhattan, Kansas

AUGUST 2006

K-TRAN

1 Report No. K-TRAN: KSU-02-6	2 Government Accession No.	3 Recipient Catalog No.
4 **Title and Subtitle** RESILIENT MODULUS AND THE FATIGUE PROPERTIES OF KANSAS HOT MIX ASPHALT MIXES		5 **Report Date** August 2006
		6 **Performing Organization Code**
7 **Author(s)** Stefan A. Romanoschi, Ph.D., P.E., Nicoleta I. Dumitru and Octavian Dumitru		8 **Performing Organization Report No.**
9 **Performing Organization Name and Address** Kansas State University Department of Civil Engineering 2118 Fiedler Hall Manhattan, Kansas 66506-2905		10 **Work Unit No. (TRAIS)**
		11 **Contract or Grant No.** C1319
12 **Sponsoring Agency Name and Address** Kansas Department of Transportation Bureau of Materials and Research 700 SW Harrison Street Topeka, Kansas 66603-3754		13 **Type of Report and Period Covered** Final Report November 2001 – April 2006
		14 **Sponsoring Agency Code** RE-0281-01

15 **Supplementary Notes**
For more information write to address in block 9.

16 **Abstract**

This research study aimed to determine the dynamic modulus, bending stiffness and fatigue properties of four representative Superpave HMA mixtures used in the construction of base layers of Kansas flexible pavements and to compare the measured values with those predicted by the NCHRP Design Guide. To achieve these objectives, asphalt concrete beams were tested in third point-bending at constant strain, at four temperatures and four levels of strain. Dynamic resilient modulus tests were performed on asphalt cylindrical specimens at five temperatures and five loading frequencies. Multi-linear regression analysis was performed to develop a linear relationship between the bending stiffness and the fatigue life for the asphalt mixes tested. It was found that the dynamic modulus is not a good indicator of the fatigue performance of HMA mixes. At all temperatures and strain levels, the mix containing SBS polymer modified binder had a much longer fatigue life while having similar dynamic moduli with those of mixes with unmodified binders. The measured dynamic moduli on all four mixes were, in most cases, more than two times the dynamic moduli predicted by the NCHRP Design Guide. At the same temperatures and at the same loading frequency of 10 Hz, the measured dynamic moduli were more than two times larger than the corresponding bending stiffnesses. The fatigue model incorporated in the NCHRP Design Guide over-predicted the fatigue lives of the mixes with virgin binder and severely under-predicted the fatigue life of the mix with SBS polymer modified binder.

17 **Key Words** Asphalt Concrete, Fatigue, HMA, Hot Mix Asphalt, Mix Design, Pavement, Superpave and Testing.		18 **Distribution Statement** No restrictions. This document is available to the public through the National Technical Information Service, Springfield, Virginia 22161	
19 **Security Classification (of this report)** Unclassified	20 **Security Classification (of this page)** Unclassified	21 **No. of pages** 143	22 **Price**

Form DOT F 1700.7 (8-72)

RESILIENT MODULUS AND THE

FATIGUE PROPERTIES OF KANSAS HOT MIX

ASPHALT MIXES

Final Report

Prepared by

Stefan A. Romanoschi, Ph.D., P.E.
Nicoleta I. Dumitru
Octavian Dumitru

A Report on Research Sponsored By

THE KANSAS DEPARTMENT OF TRANSPORTATION
TOPEKA, KANSAS

and

KANSAS STATE UNIVERSITY
MANHATTAN, KANSAS

August 2006

PREFACE

The Kansas Department of Transportation's (KDOT) Kansas Transportation Research and New-Developments (K-TRAN) Research Program funded this research project. It is an ongoing, cooperative and comprehensive research program addressing transportation needs of the state of Kansas utilizing academic and research resources from KDOT, Kansas State University and the University of Kansas. Transportation professionals in KDOT and the universities jointly develop the projects included in the research program.

NOTICE

The authors and the state of Kansas do not endorse products or manufacturers. Trade and manufacturers names appear herein solely because they are considered essential to the object of this report.

This information is available in alternative accessible formats. To obtain an alternative format, contact the Office of Transportation Information, Kansas Department of Transportation, 700 SW Harrison, Topeka, Kansas 66603-3754 or phone (785) 296-3585 (Voice) (TDD).

DISCLAIMER

The contents of this report reflect the views of the authors who are responsible for the facts and accuracy of the data presented herein. The contents do not necessarily reflect the views or the policies of the state of Kansas. This report does not constitute a standard, specification or regulation.

ABSTRACT

This research study aimed to determine the dynamic modulus, bending stiffness and fatigue properties of four representative Superpave HMA mixtures used in the construction of base layers of Kansas flexible pavements and to compare the measured values with those predicted by the NCHRP Design Guide. To achieve these objectives, asphalt concrete beams were tested in third point-bending at constant strain, at four temperatures and four levels of strain. Dynamic resilient modulus tests were performed on asphalt cylindrical specimens at five temperatures and five loading frequencies. Multi-linear regression analysis was performed to develop a linear relationship between the bending stiffness and the fatigue life for the asphalt mixes tested. It was found that the dynamic modulus is not a good indicator of the fatigue performance of HMA mixes. At all temperatures and strain levels, the mix containing SBS polymer modified binder had a much longer fatigue life while having similar dynamic moduli with those of mixes with unmodified binders. The measured dynamic moduli on all four mixes were, in most cases, more than two times the dynamic moduli predicted by the NCHRP Design Guide. At the same temperatures and at the same loading frequency of 10 Hz, the measured dynamic moduli were more than two times larger than the corresponding bending stiffnesses. The fatigue model incorporated in the NCHRP Design Guide over-predicted the fatigue lives of the mixes with virgin binder and severely under-predicted the fatigue life of the mix with SBS polymer modified binder.

TABLE OF CONTENTS

LIST OF TABLES

LIST OF FIGURES

CHAPTER 1

INTRODUCTION

1.1   Introduction

A new design guide for pavement structures, based on a mechanistic design method, could be adopted by AASHTO in the near future and will replace the current version used by KDOT in the structural design of flexible and rigid pavements. The mechanistic design procedure relates pavement deterioration and thus, pavement life, to the magnitude of stresses and strains developed in the road structure under traffic. Any mechanistic design procedure for asphalt pavements includes models for the rut depth evolution, as well as for the initiation and development of fatigue cracking. Fatigue cracking models use as input parameters the fatigue properties and stiffness of the asphalt concrete. These models are effective only when the appropriate fatigue parameters are selected in the design. It is therefore imperative to know the fatigue parameters for the typical HMA mixes used on Kansas roads in order to use the new AASHTO method in the design of new and reinforced Kansas roads.

Currently, the asphalt pavements in Kansas commonly exhibit severe rutting before the fatigue cracks reach a severe level. However, even fatigue cracking is not a major distress type for asphalt pavements in the State, appropriate input parameters in the fatigue model will be required to ensure an efficient structural design. Therefore, research is needed to determine the fatigue characteristics of the typical asphalt concrete mixes used in Kansas.

Research is also needed to establish the correlation between stiffness and fatigue characteristics of the typical asphalt concrete mixes used in Kansas. The experience has proven that the fatigue life of asphalt concrete is related to its stiffness; under the same loading and

temperature, a stiffer mix is more brittle and has reduced fatigue resistance. It is therefore desirable to know the relationship between the fatigue characteristics and the mix stiffness or resilient modulus for each type of HMA mix used in Kansas.

The stiffness of asphalt concrete is commonly measured in laboratory using the bending tests on asphalt concrete beams. Because it is assumed that dynamic modulus and stiffness have similar values, especially for mixes at low temperature and loaded at high frequencies, measurements of dynamic modulus are more popular. Modulus determination is preferred also because it can be determined in field tests. The backcalculation from the field measured FWD deflections represents a popular technique for estimating the dynamic modulus of the asphalt layer. It is therefore desirable to know the relationship between the mix stiffness and dynamic modulus for each representative Kansas HMA mix.

1.2   Objectives

The objectives of this research are:

- to characterize the fatigue properties of the Superpave HMA mixes;
- to determine the typical resilient modulus for the typical Kansas HMA mixes;
- to develop a relationship between the fatigue properties and the stiffness for each typical Kansas HMA mix
- to develop a relationship between stiffness and dynamic modulus for each typical Kansas HMA mix

CHAPTER 2

BACKGROUND

Fatigue cracking represents a major distress that affects the service life of flexible pavements. Due to the rheological properties of the HMA mixes, after the passing of a vehicle, the asphalt concrete layer tends to return to its original condition. But, due to the cycling nature of the loading, the asphalt concrete exhibits the fatigue cracking. Cracking usually starts from the bottom of the asphalt layer, where the material is in tension when wheel loads are applied at the pavement surface, and propagates up to the surface. Once they reach the surface, the cracks represent avenues for water to enter the pavement and cause the deterioration of the foundation layers. The cracks may also lead to the formation of potholes, which greatly reduces the rideability of the pavement, the comfort and safety of road users. Therefore, understanding the phenomenon of fatigue cracking and measuring the fatigue properties of asphalt concrete is essential for the design of flexible pavements (Monismith et al., 1985).

Load associated cracking may also develop at the surface of the pavement and then progress down into the surface layer. These cracks develop typical in the wheel-path, in longitudinal direction. The mechanism of initiation and progression of top-down cracks is not well understood. However, it is commonly assumed that high concentration of stresses at the tire-pavement contact surface, right underneath the tire walls, is the major cause for these cracks.

In addition to load associated cracking, asphalt pavements also exhibit temperature related cracking. At very low temperatures, the asphalt concrete surface layer contracts. The friction between the surface layers and the layers underneath prevent the surface layers from contracting. This causes the formation of low-temperature cracks, which are transverse cracks

that develop typically over the entire width of the pavement, with spacing between 15 and 25 feet.

The determination of fatigue properties of asphalt concrete is done through fatigue tests. A variety of fatigue tests are reported in the literature, each having specific configuration. The results of the fatigue tests are influences by:

- loading conditions: bending beam, rotating cantilever, trapezoidal cantilever, plate bending
- load rate or frequency and magnitude;
- environmental conditions: temperature, moisture;
- mixture variables (stiffness, air void content, asphalt content and grade).

2.1   Fatigue Tests for Asphalt Mixes

The fatigue characteristics of asphalt mixes are usually expressed as relationships between the initial stress or strain and the number of load repetitions to failure determined in fatigue tests (repeated flexure, direct tension, or diametral tests) performed at several levels of stress or strain (SHRP, 1994). A typical fatigue model has the following form:

$$N_f = a \, (1/e_h)^b \, x \, (1/S)^c \qquad\qquad (2.1)$$

where:

N_f = fatigue life or number of load repetitions to failure,

e_h = horizontal tensile strain,

S = initial mix stiffness

a, b, c = experimentally determined coefficients; c = 1 in some simple models.

The fatigue life and behavior of bituminous mixture depends on variables related to the loading: (load history, rate of load application, wave form, type of specimen), mixture characteristics: (air void content, stiffness, asphalt content, aggregate type and gradation, asphalt

type and hardness), and environmental conditions: (temperature, moisture). Due to the variety of testing configuration used and materials tested, many fatigue relationships are reported in the literature, as shown in Figure 2.1.

Generally is accepted that the number of cycles causing significant fatigue cracking in asphalt concrete layers subjected to real traffic is greater than the number of cycles to failure of the same asphalt concrete, when subjected to laboratory fatigue tests. The fatigue life may be defined as the number of cycles required to reduce flexural stiffness of an asphalt mix to half of its initial value (Zaitsev, 1994). Some of the most used fatigue tests are: simple flexure, direct axial, diametral, fracture tests, laboratory wheel-track testing.

2.1.1   Simple Flexure

The majority of fatigue tests have been done using a simple flexure test. A number of different types of flexural equipment have been developed to study the fatigue characteristics of asphalt concrete mixtures. They include:

- Flexure tests in which the cyclic loads are applied under center-point or third-point loading;
- Rotating cantilever beams subjected to sinusoidal loads;
- Trapezoidal cantilever beams subjected to sinusoidal loads or deformations.
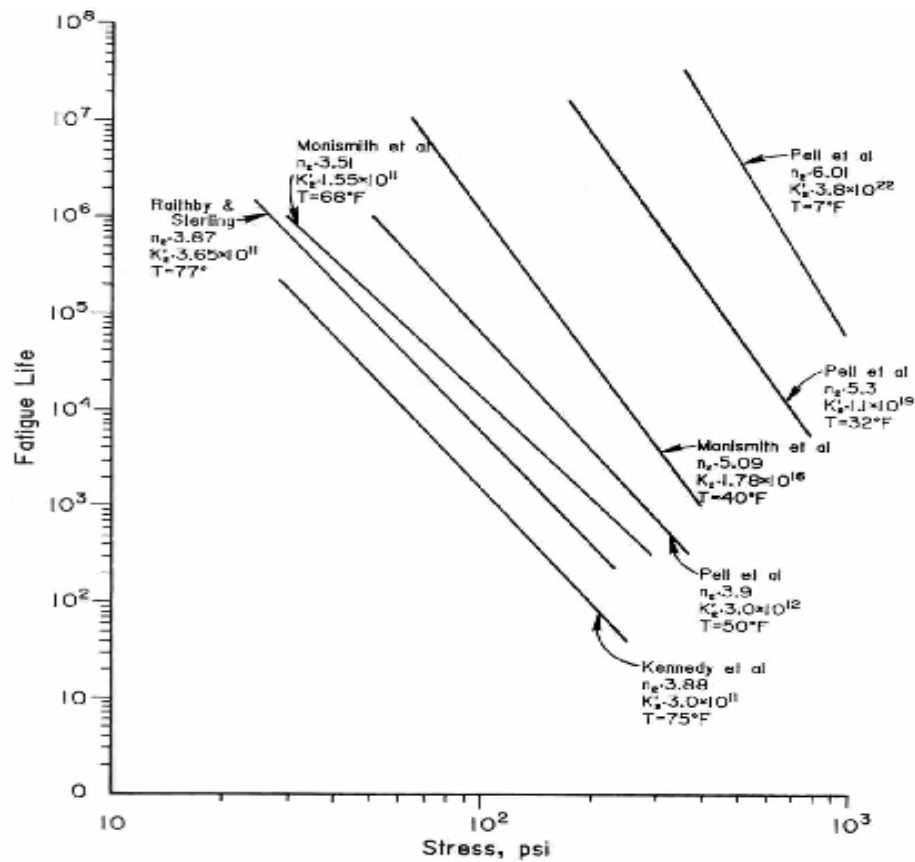
Figure 2.1 Typical Fatigue Life Relationships (Matthews et al, 1993)

The third-point flexure tests (Figure 2.2) is preferred to the center-point flexure tests because the bending moment is uniform between the sections where the bending forces are applied (Roberts et al., 1996). The applied load is typically sinusoidal and is applied at a rate of one to ten cycles per second. The stress and strain at the outer fibers, and mix stiffness at about 200 load applications are computed using the following equations:

$$\Phi = (3 \cong P \cong a) / (b \cong h^2) ; \qquad , = (12 \cong h \cong *) / (3 \cong L^2 - 4 \cong a^2); \qquad S = \Phi / n \qquad (2.2)$$

Where:

Φ - the tensile stress in the outer fiber (maximum axial stress);

n - the tensile strain in the outer fiber (maximum axial strain);

$*$ - dynamic deflection at the center of the beam;

6

S - flexural stiffness of the mix;

P - maximum dynamic load (with half of the force applied at third points);

a - the distance between the support and the first applied load;

L - reaction span length;

b and h - width and height of the specimen.

The size of the beam may vary. For example, in the study conducted at University of California, Berkley, (Matthews et al, 1993) specimens with the following dimensions have been used: 38.1mm x 38.1mm x 381mm (1.5in x 1.5in x 15in). The Asphalt Institute (Asphalt Institute, 1982) recommends using larger specimens with the dimensions of: 76.2mm x 76.2mm x 381mm (3in x 3in x 15in).

KEY

1. Reaction Clamp
2. Restrainer
3. End Plates
4. Specimen
5. Loading Rod
6. Stop Nuts
7. Load Bar
8. Piston Rod
9. Thompson Ball Bushing
10. LVDT Holder
11. LVDT

REPEATED FLEXURE APPARATUS
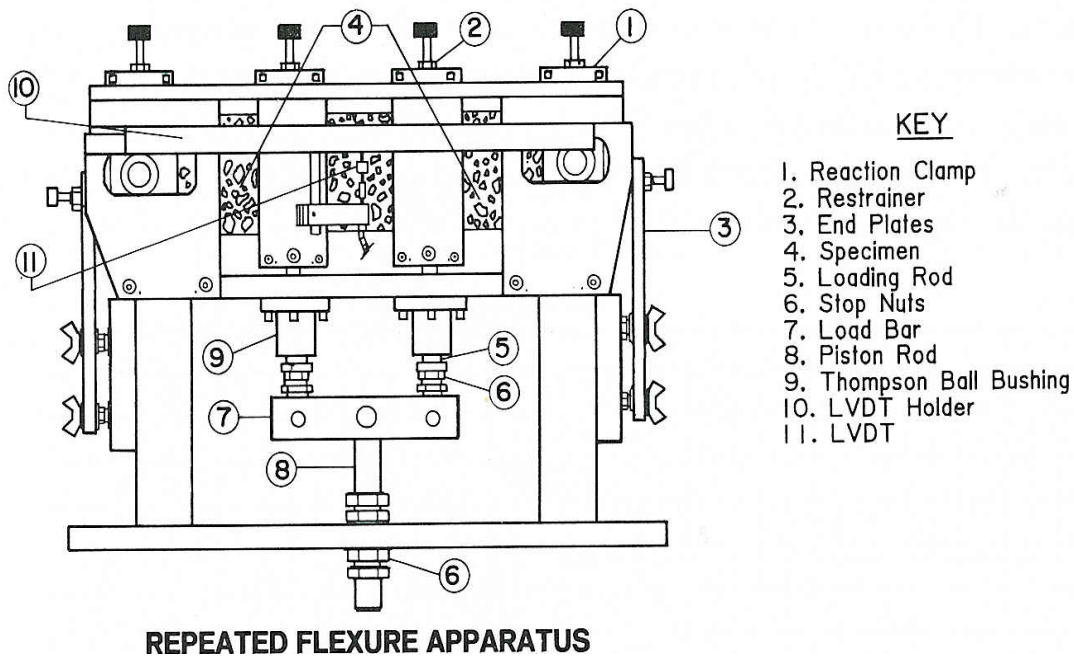
Figure 2.2 Repeated Flexure Apparatus (Matthews et al., 1993)

In stress controlled tests, the failure of the specimen is considered as the number of load repetitions, N_f, when the beam actually breaks. In strain controlled tests, the failure of the

specimen is considered as the number of load repetitions, N_f, when the bending stiffness reaches

half of the initial stiffness. The log of number of cycles to failure, $\log(N_f)$, is plotted against the

log of the applied stress, $\log(\Phi)$, or strain $\log(,)$, and regression analysis is used to determine a

linear relationship between these values, as shown in Figure 2.3. Then, the fatigue relationship,

which expresses the resistance to cyclic loading of the asphalt concrete, has the following form:

$$N_f = K_1 \cong (1 / \Phi)^{n1} \quad \text{or} \quad N_f = K_2 \cong (1 / m)^{n2} \quad\quad (2.3)$$

Where:

Φ and m - the tensile stress and strain in the outer fiber due to the applied load;
N_f - number of load applications to failure;
K_1, K_2, n1, n2 - material parameters (regression coefficients).

The beam fatigue test can be performed in either constant stress or constant strain mode.

For the constant stress mode, the same load P is applied repeatedly until failure occurs. The

logarithm of the number of cycles to failure is plotted against the number of applied stress as

shown in Figure 2.3. The stiffness decreases to half of the initial stiffness with the increasing in

the displacement amplitude, which becomes twice the initial value. In this case the material with

higher initial stiffness generally performs better than materials with low stiffness values

(Baburamani, 2001).
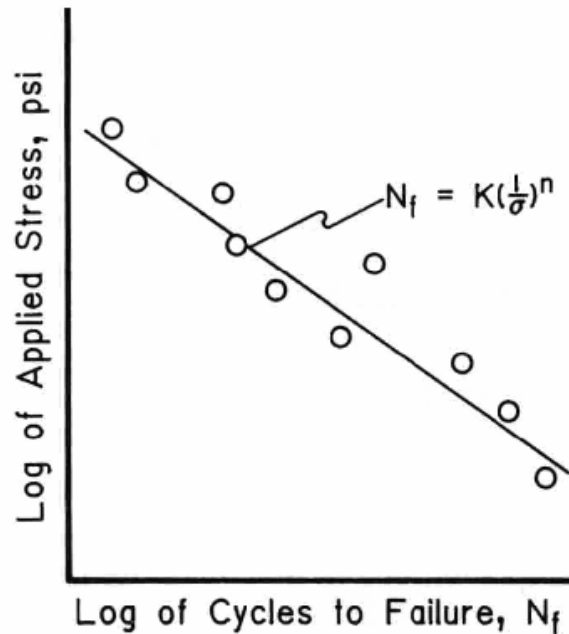
**Figure 2.3: Typical Plot of Fatigue Data using Constant Stress Loading
(Roberts et al., 1996)**

In the constant strain mode tests, the deflection is maintained constant and the applied

load is allowed to decrease gradually with increasing cycles. Failure is usually considered at the

point where the applied load required inducing the desired level of maximum strain reaches some

pre-selected percent of the original load (generally 50%).

Usually, the stress controlled test is used to characterize the fatigue life of thick asphalt

layers (thickness >100 mm); the failure of the specimen occurs at the end of the test and the

number of specimens required for the test is generally small. For these tests the aging of asphalt

or an increased stiffness of the analyzed mix is leading to an increase in the fatigue life.

The tests done under the controlled strain are used to establish the fatigue life for thin

asphalt layers (thickness < 100 mm) because the response of this type of pavement depends

merely of the underlying support (Khalid, 2000). In this case, the failure is accepted to be the

reduction in layer stiffness, usually half of the original stiffness. For these tests, the lower the stiffness of the analyzed mix, the lower is the fatigue life. Usually, the number of specimens required for the test is generally large because of the large variability of the test results.

Khalid (2000) conducted controlled stress fatigue tests on prismatic asphalt specimens, using five different mixes. The tests were conducted at 20^0C, using a sinusoidal loading pattern and a frequency of 5 Hz. The results showed that the mixes containing polymer and fibers performed better that those without polymer and fibers, and concluded that the polymers can improve the fatigue cracking performance of asphalt mixes.

It was also observed that the mixes with low content of air void experience a longer fatigue life. The temperature influenced the behavior of mixes the fatigue life is increasing with the air void content for controlled stress test at low temperature and decreasing with the air void content for controlled strain test at high temperature (SHRP, 1994). A typical strain fatigue relationship is shown in Figure 2.4.

Some other observed differences between the results of the controlled strain and controlled stress tests were:

- the fatigue life is lower in the controlled stress test when compared to that measured in the controlled strain test;
- the stiffness is higher for the controlled stress test when compared to that measured in the controlled strain test and;
- the failure of the specimen is evident for the controlled stress test and unclear for the controlled strain test where, typically, the stiffness reduction is the failure criterion.
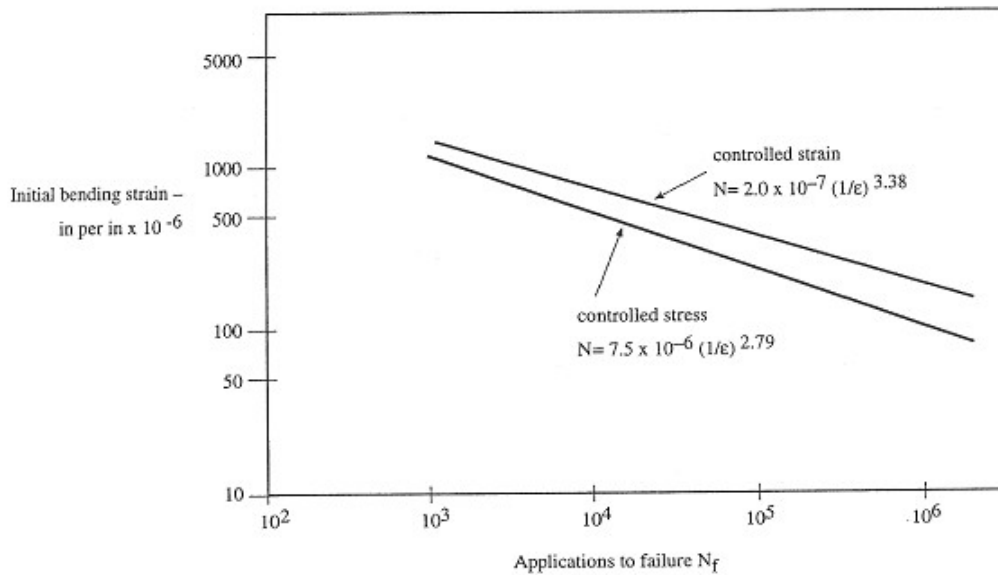
Figure 2.4 Strain Fatigue Relationship for Controlled-Stress and Controlled-Strain Laboratory Tests (Baburamani, 2001)

Kallas et al (1972) tested beam specimens in stress mode using third-point loading system, with haversine form waves and at only one temperature (70^0F) and their fatigue life relationships were similar to the fatigue life prediction model regression equation as follows:

For strain-fatigue life relationship:

$$N_f = K_1 (1/e_t)^n{}_2 \tag{2.4}$$

For stress-fatigue life relationship:

$$N_f = K_2 (1/S_t)^n{}_1 \tag{2.5}$$

Where:

e_t and S_t => the magnitudes of the tensile strain and stress applied repeatedly;

11

K_1, n_1, K_2, n_2 => material coefficients associated with the laboratory test methodology;

N_f => number of load applications to failure obtained in the laboratory

During the life of a pavement aging affects the concrete asphalt layer stiffness. In time, mostly due to the oxidation, the binder from the asphalt layer hardens and becomes brittle and consequently the stiffness modulus changes. In thick pavements a higher stiffness means a higher fatigue life, but for the thin pavements it might lead to fatigue cracking (Baburamani, 2001). Raad et al. (2001) studied the effects of field aging on the fatigue behavior of two mixes by determining the stiffness and fatigue properties using controlled-strain fatigue beam tests performed at 22^0C and -2^0C. They showed that the aging increased the mixtures stiffness at high temperatures, but decreased it at low temperatures.

2.1.2 Uni-Axial Fatigue Tests

The Transport and Road Research Laboratory (TRRL) of the UK performed uniaxial tensile tests without stress reversal using a loading frequency of 25 Hz, duration of 40ms and the rest period varied from 0 to 1 sec. (Matthews et al 1993). These tests were conducted in the controlled stress mode. The effects of rest periods, shape of waveform and sequence of load application (compression/tension, tension/compression, compression only, tension only) were evaluated. The experiments led to the following conclusions:

- Short rest periods (which simulates the field condition) showed an increasing in the fatigue life;
- The fatigue life depends largely on the test temperature;
- The effect of load form (sinusoidal, or triangular) has reduced effects on the fatigue life;
- Pure compressive cycling loading gives the largest fatigue life.

2.1.3   Diametral Fatigue Test

This test uses a cylindrical specimen that has applied a compressive load along the vertical diametral plane and develops tensile stress perpendicular to the direction of the applied load (Khalid, 2000). The specimen will fail by splitting along the vertical diameter as can be seen in Figure 2.5.
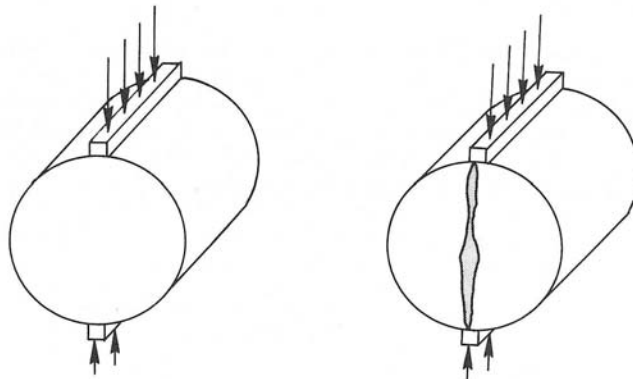
Figure 2.5 Indirect Diametral Test at Loading and Failure (Roberts et al, 1996)

The loading configuration for this test is relatively simple and loads can be easily applied. Usually a haversine load pulse is normally employed. Kennedy et al, (1983) used a loading time of 0.4s and a rest interval of 0.6s. Khosla et al, (1985) used a loading time of 0.05s and a frequency of 20 repetitions per minute. Test specimens are usually 101.6mm (4in) in diameter and 63.5mm (2.5in) high. Load is transmitted to the sides of the right circular cylinder through a 12.7mm (0.5in) wide loading strip. Under a single load of sufficient magnitude, failure of diametral specimen would be governed by the very large stresses beneath the load or near the specimen surface. These stresses are greatly reduced by distributing the load through a loading strip as can be seen in Figure 2.6.
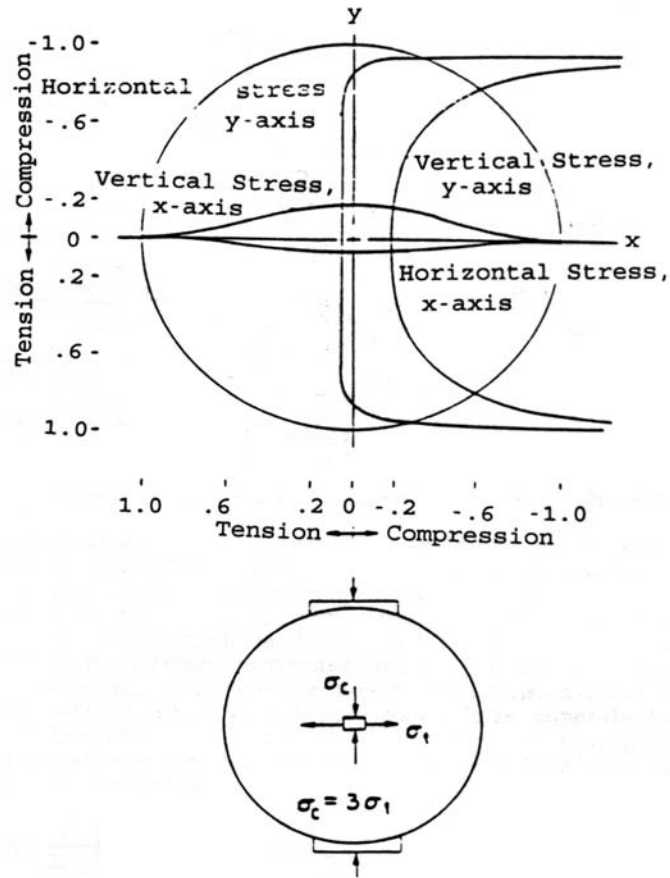
Figure 2.6 Relative Stress Distribution in Diametral Test (Matthews et al., 1993)

Stresses at the center of the specimen under a strip load can be determined as follows:

$$S_t = (2P / \pi ah) \text{ x } (\sin 2\alpha - a / 2R) \tag{2.6}$$

$$S_c = (-6P / \pi ah) \text{ x } (\sin 2\alpha - a / 2R) \tag{2.7}$$

Where,

P	= applied load
a	= width of loading strip
h	= height of the specimen
R	= radius of the specimen
2α	= the angle at the origin subtended by the width of the loading strip
S_t	= indirect tensile stress (horizontal) at the center of the specimen
S_c	= indirect compressive stress (vertical) at the center of the specimen

14

Some differences between the diametral test and the flexural beam test are:

- the state of stress in the diametral test is biaxial;
- permanent deformation is usually prohibited in flexural tests but it's permitted in diametral tests;
- stress reversal is impractical in the diametral test

The effect of these differences results in a smaller fatigue life under diametral testing than under flexural testing (Matthews et al, 1993).

Khalid (2001) conducted a study to evaluate the fatigue properties of five different asphalt mixes in the laboratory. He used for comparison diametral tests performed at 12^oC and at a frequency of 0.67 Hz and three-point flexural tests performed at 20^oC and at a frequency of 5 Hz. The temperatures and frequencies were different in order to match the binder stiffness of the five mixes tested. The findings showed that, for the same tensile strain, the fatigue lives obtained by diametral test were approximately ten times lower than those obtained in the three-point flexural test.

2.1.4 Laboratory Wheel-Track Fatigue Tests

In this testing configuration a loaded wheel with a pneumatic tire is rolled back and forth over a slab of asphalt concrete supported by a rubber mat. The wheel has a diameter of 0.25m and its path is 0.6m long with a width in the range of 0.05-0.07m. Changing either the inflation pressure or the load can vary the tire contact area. The strains at the bottom of the slab, the crack initiation and propagation can be periodically monitored. Results can be expressed in terms of three fatigue stages associated with the:

- development of hairline cracks (N_1)
- real cracks (N_2)
- failure of the slab (N_3)

Fatigue data obtained with this test have been presented by Van Dijk (1977). His results suggested that controlled-strain data might be more appropriate to define pavement cracking than controlled-stress data, which provide more conservative results.

2.2 Fatigue Shift Factors

The difference between the fatigue life test results observed in the field and those obtained in the laboratory may be explained by differences in loading conditions, temperature and moisture, failure type, structural models, level of cracking in the pavement considered as failure, and micro-damage healing. To account for this difference, shift factors are applied to predict the performance under service condition using the following equation.

$$N_{field} = N_{lab} \text{ x } SF \tag{2.8}$$

Where:

N_{field} = Number of cycles to failure in the field, to a specified cracking level

N_{lab} = Number of cycles to failure in the laboratory

SF = Shift factor

The values for these shift factors range between 10 and 20 and are related to the environmental conditions, thickness of asphalt layer, rest periods, tensile strain and the conditions used in the laboratory to develop the fatigue models (Baburamani, 2001). In the case of in-service pavements, the loads are not applied as continuously or as rapidly as in the laboratory condition. Therefore, the in-service pavement has rest periods in which the material is relaxing and partially regains its properties (Tseng et al, 1990). Many researchers consider that, during these rest periods, especially at high temperature, the asphalt heals, the material recovers and some micro-cracks and even cracks close and disappear. The result is an increased cracking life (Kim et al, 1994).

For the in-service pavements the compressive or tensile stresses can remain in the asphalt layer, so when another load is applied it can cause more or less fatigue damage depending on the accumulation of the residual stress. In this case shift factors take into consideration the residual stress and the healing during the rest periods (Tseng et al, 1990).

Shift factors were obtained from laboratory tests at different temperatures and it was observed that for laboratory fatigue life (N_f) greater than 1 million cycles, the shift factor is independent of temperature (Baburamani, 2001).

2.3   Fatigue Life Models Asphalt Concrete

The asphalt concrete fatigue models best known in the literature, such as the Shell, Asphalt Institute and the Strategic Highway Research Program models, are based on relationships between the fatigue life (number of cycles to failure) and stress or strain. These relationships were obtained from the laboratory tests performed in either controlled stress or controlled strain mode.

2.3.1   Shell Model

The Shell fatigue model was developed based on the results obtained on laboratory-controlled strain sinusoidal loading fatigue tests on several typical asphalt mixes used in various countries. The model is incorporated as a nomograph in the Shell fatigue prediction model (Baburamani, 2001).

The permissible strain was calculated function of strain repetitions and asphalt stiffness modulus of various mixes.

The relationship developed between strain, volume of binder, mix stiffness and fatigue life:

$$N_f = [6918 \, (0.856 * V_b + 1.08) \, / \, S_{mix}^{0.36} * me]^5 \qquad (2.9)$$

17

Where:

N_f = number of load applications to failure

S_{mix} = mix stiffness   psi (MPa)

V_b = binder volume   (%)

me = tensile strain produced by the load

2.3.2   Asphalt Institute Model

The same assumptions were used in the developing of the Asphalt Institute model as in the Shell model. The visco-elastic nature of asphalt was taken into consideration by using different stiffness values corresponding to different temperatures and times of loading (Claessen et al., 1977).

This fatigue model was based on controlled stress applied on asphalt beams with a loading form of a sinusoidal load wave (Baburamani, 2001). The design criteria take into consideration the horizontal tensile strain ε_t underneath the asphalt layer and the vertical compressive strain e_c on top of the subgrade layer. Under these criteria, if the horizontal tensile strain e_t is excessive, then the asphalt pavement will exhibit fatigue cracking. The fatigue data is generally expressed as follows:

$$N = a \, (1 \, / \, e_t)^b \tag{2.10}$$

where:

N = number of load applications to cracking

e_t = tensile strain repeatedly applied

a, b   = coefficients resulted from fatigue tests

Pell and Cooper and Epps (1975) developed a regression curve establishing the influence of the binder volume, V_b, and air voids content, V_a, on the fatigue relationship. The laboratory tests they performed led to the following relationship:

18

$$N_f = 18.4 * 10^M * [4.325 * 10^{-3} * (e_t)^{-3.291} * E^{-0.854}] \qquad (2.11)$$

where:

N_f = number of load applications to fatigue failure

$M = 4.84 (VFB - 0.69)$

$VFB = V_b / (V_b + V_a)$ = voids filled with bitumen

The equation may be reduced as follows for $V_b = 11\%$ and $V_a = 5\%$.

$$N_f = 0.0796 * (e_t)^{-3.291} * E^{-0.854} \qquad (2.12)$$

The relationship developed from extensive laboratory fatigue data was related to an approximate fatigue cracking extent of 20% of the loaded area section of the AASHO Road Test (Ali et al, 1998).

Li et al. (1999) performed full-scale fatigue tests on two different soil-cement base pavements (with and without a stone interlayer). The data obtained was used to evaluate the AI model and Jameson model (based on Australian full-scale tests). The following equation describes the Jameson model.

$$\ln (N) = 55.87 - 5.04 \ln (e_t) - 1.8 \ln (E) \qquad (2.13)$$

Where:

N   = number of load applications

e_t = asphalt tensile strain

E   = asphalt modulus (MPa)

Both models predicted well the fatigue life for the soil-cement base layer and confirmed that the major cracks may start from the bottom of asphalt layer and propagate up to the surface (Li et al, 1999).

The temperatures used in developing of the AI model design charts were representative for most of the asphalts used in USA. The temperatures selected ($\leq 7^0$C, 15.5^0C and $\geq 24^0$C) were considered to be representative for every environment condition applicable in the USA. Consequently the asphalt stiffnesses were correlated with these temperatures.

2.3.3   *Strategic Highway Research Program (SHRP) Model*

The Strategic Highway Research Program (SHRP) Model was based on extensive studies and the results of laboratory tests performed on 44 mixes, covered a variety of asphalt mixes, tested under different combinations of temperature, stiffness, air voids, asphalt type and binder content, etc.

The main goal of the SHRP was to determine a proper methodology to test the fatigue response of mixes and to develop a model that might substitute the laboratory testing. This model considered the initial strain, the stiffness loss and the voids filled with binder as the main variables affecting the fatigue life. The fatigue tests were performed on asphalt beams subjected to third-point bending based on controlled strain loading, with a sinusoidal loading at a frequency of 10 Hz. The following equation was developed (Baburamani, 2001, SHRP Manual, 1994):

$$N_f = 2.738 * 10^5 * \exp^{0.077 VBF} * (e_0)^{-3.624} * (S_0)^{-2.72} \tag{2.15}$$

Where:

   N_f = laboratory fatigue life
   e_0 = initial strain
   VBF = % voids filled with binder
   S_0 = initial loss stiffness

CHAPTER 3

METHODOLOGY

The objective of this research is to determine the dynamic modulus, the bending stiffness and the fatigue properties of four representative Superpave HMA mixtures used in the asphalt road construction in Kansas. The findings will allow the development of correlations between the dynamic modulus, stiffness and the fatigue characteristics of typical Superpave Kansas asphalt concrete mixtures. This chapter presents the equipment and the methodology used in the laboratory testing.

3.1 Test Equipment

A Universal Testing Machine (UTM) produced by Industrial Process Controls Ltd. (IPC), Melbourne, Australia, was used to perform the flexural fatigue and dynamic resilient modulus tests. The UTM system has four main components (Figure 3.1): the Computer Data Acquisition System (CDAS), the Hydraulic System, the PC and the Environmental Chamber. The CDAS captures and digitizes analog signals from the transducers and then transfers these data to the PC for further processing. Also, it provides control and data acquisition functions for the testing frame and transducers and adjusts and applies the load through the actuator. The hydraulic pressure system provides a precise control of the loading (force displacement) and thus, a precise control of the stresses or strains induced in the specimens. The actuator is connected with the hydraulic system through an electrically controlled hydraulic servo valve. A strain gauge force transducer, mounted in line with the loading shaft, measures the force applied to the specimen. Displacement transducers attached to the specimen permit the measurement of the deflections during loading (Feeley, 1999).

In this research, the flexural fatigue testing was performed under controlled strain mode. In this testing configuration, the UTM applies through the actuator the force required to reach the desired displacement. The CDAS unit is reading continuously the force applied by the actuator and increases its value until the asphalt beam bends to the required maximum strain.

The Environmental Chamber encases partially the hydraulic testing frame. It ensures the maintaining and controlling of the temperature in the bottom two thirds of the hydraulic testing frame, where the specimens are placed when tested. The temperature in the environmental chamber can be maintained between -15^0 to 60^0 degrees Celsius, with a precision of $\pm0.5^0$C. The UTM system connections are shown in Figure 3.2.
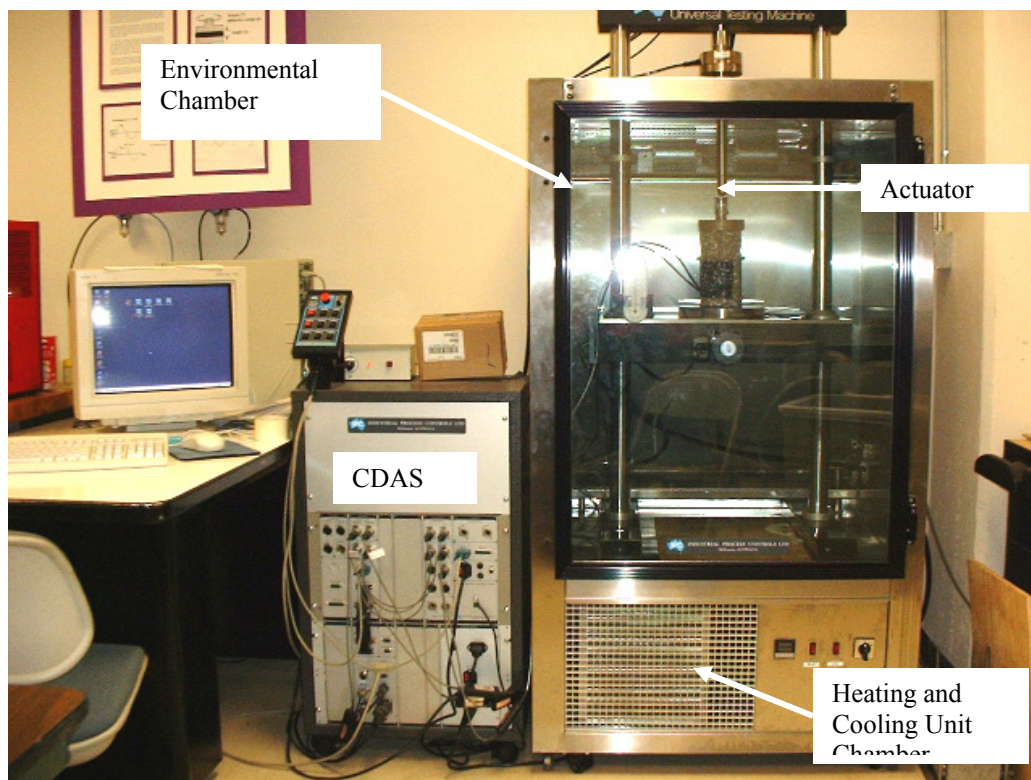
Figure 3.1 Environmental Chamber, PC and CDAS
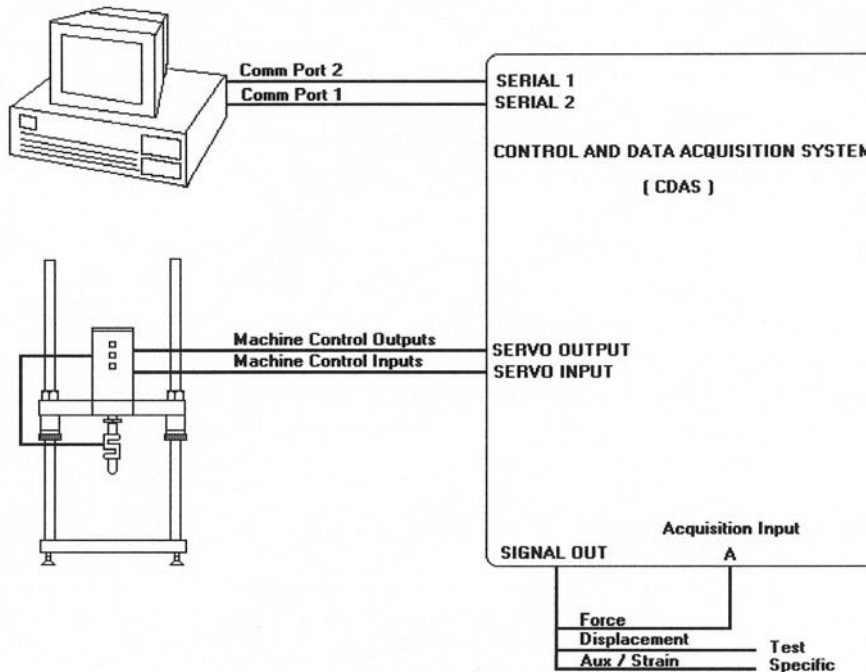
Figure 3.2 System Cnnections (Feeley, 1999)

3.2 Materials

3.2.1 Hot Asphalt Mixes

The laboratory tests were performed on asphalt concrete specimens manufactured from four mixtures type typically used in the construction of Kansas flexible pavements, named here Mix A, B, C and D.

The asphalt mixes to be used in the study were selected and provided by KDOT. Mix A was collected from a major modification project on State Highway 50, near Florence, Kansas, in Marion County. Mixes B and C were manufactured by KDOT using a different aggregate blend and a different binder source than those used in Mix A. The asphalt content and the aggregate blend were the same for mixes B and C but the binder grade and source were different. The binder from mixture C contained styrene-butadiene-styrene polymer (SBS), which usually increases the binder viscosity at high temperatures and, improves the cohesion between the

aggregates and the binder and the cracking resistance at low temperatures. Mix D was collected from a major modification project on State Highway 27, in Morton County, Kansas. The characteristics of the four mixtures are presented in the Table 3.1 and Figures 3.3 to 3.5.

The four mixtures represent well mixes typically used in Kansas for the bottom lift of the asphalt concrete layer. All four mixtures (SM 19A) had the nominal maximum aggregate size of 19 mm. Figures 3.3 and 3.4 show that the aggregate gradation curves for the first three mixes pass through the restricted zone, while the gradation curve for Mix D passes above the restricted zone.

Table 3.1 Volumetric Parameters of the Four HMA Mixes

	Mix A	Mix B	Mix C	Mix D
Binder Grade	PG 64-22	PG 64-22	PG 70-28 (SBS polymer modified)	PG 64-22
Asphalt Content (%)	5.20	6.25	6.25	5.1
Gmm	2.445	2.407	2.414	2.561
AV (%) on Beams	5.8 – 9.7	5.2 – 9.4	4.4 – 7.9	
AV (%) on Cores	6.5 – 7.3	6.6 – 7.5	6.6 – 7.6	

Table 3.2 Aggregate Gradation for the four Kansas HMA Mixes

Sieve #	Sieve Size (mm)	Mix A	Mixes B and C	Mix D	Tolerance
		Percent Passing (%)			
1"	25.4	100	100	100	100 – 100
3/4"	19.0	98	100	91	90 – 100
1/2"	12.5	89	78	73	– 90
3/8"	9.5	84	71	63	
#4	4.75	66	66	56	
#8	2.36	44	45	41	35 - 49
#16	1.18	30	36	32	28 -
#30	0.60	19	15	24	16 -
#50	0.30	10	8	16	9 -
#100	0.15	6	5	8	
#200	0.075	5	2.9	5.1	2 - 8
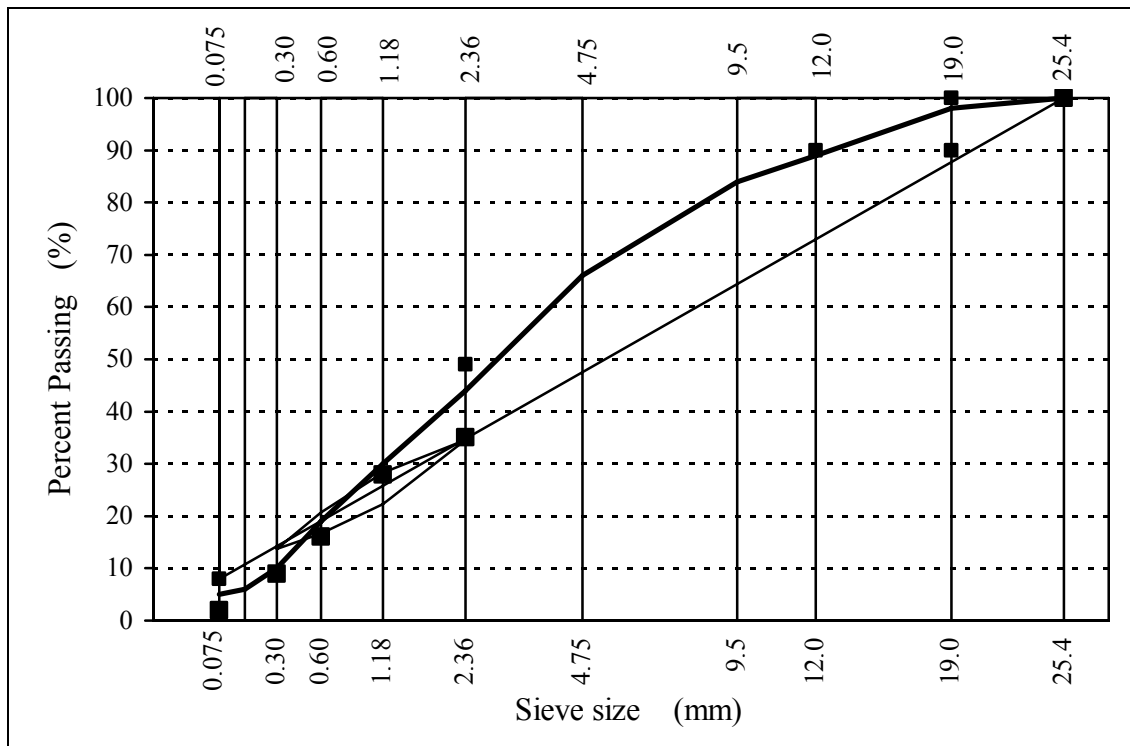
Figure 3.3 Aggregate Gradation Chart for Mix A
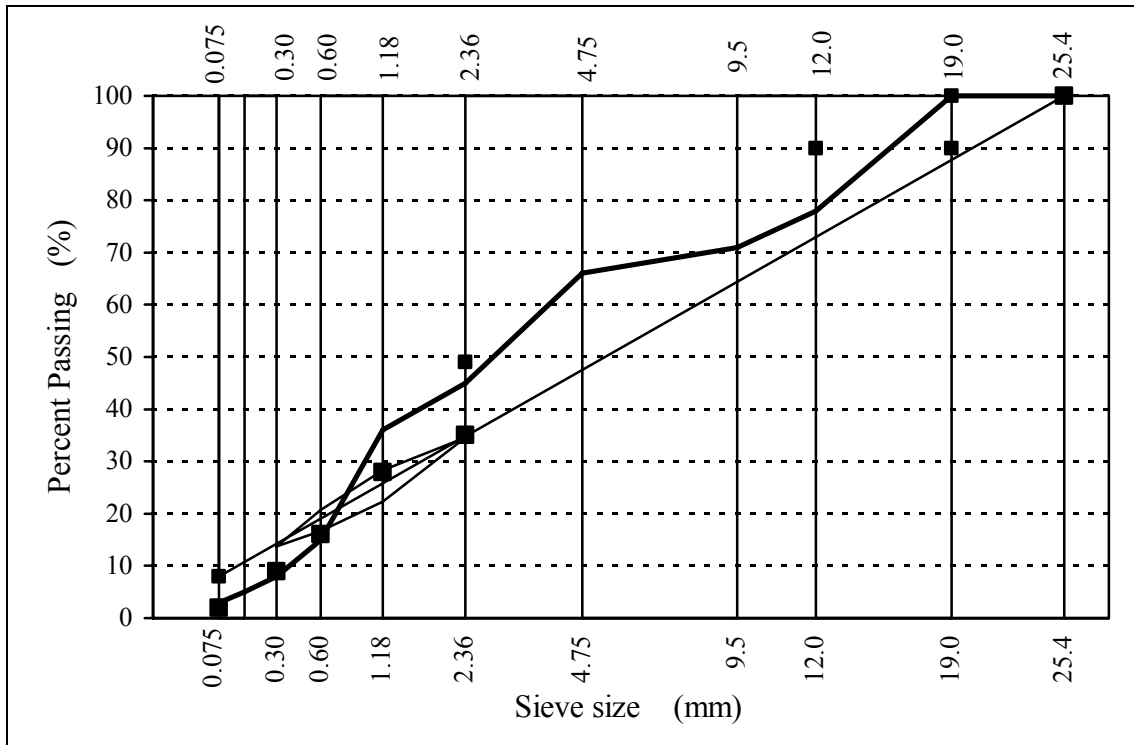
Figure 3.4 Aggregate Gradation Chart for Mixes B and C
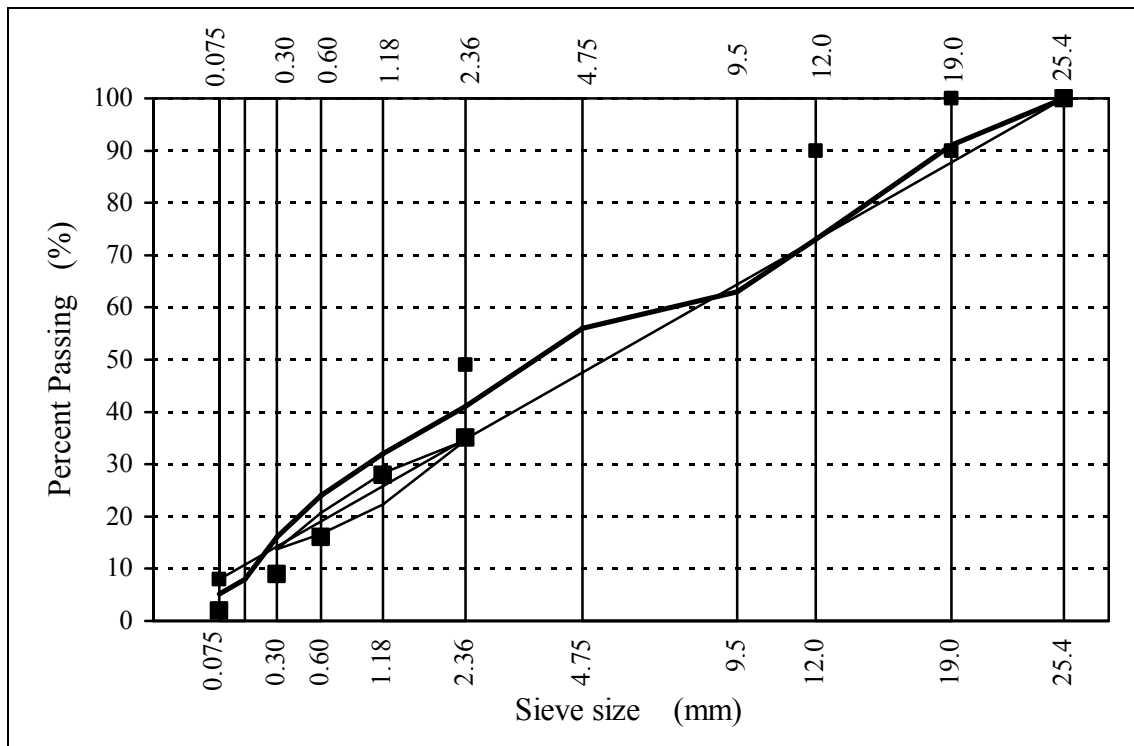
Figure 3.5 Aggregate Gradation Chart for Mix D

3.2.2 Asphalt Beam Fabrication

The asphalt beams were sawed from asphalt slabs which were fabricated using the Linear Kneading Compactor, in the Asphalt Laboratory at KSU. The quantity of mixture necessary for a slab (approximately 2,300 kg) was placed into pans, then heated in the oven to 270 ^{0}F and compacted at a pressure of 400 – 500 psi. The quantity of mixture to be placed in the linear compactor was estimated from the volume of the slab (measured in the mold of the linear compactor) and the desired air void content in the compacted mix. The heated mixture was poured evenly into the mold and steel plates were placed vertically over the loose mixture, as seen in Figure 3.5.

Figure 3.6 Steel Plates over a Slab of Compacted HMA Mix

The mold is fixed, while a steel cylinder rolls on the top of the steel plates. The plates are slowly pushed downward and compact the mixture placed in the mold. Through the kneading

movement, the mixture is compacted without fracturing the aggregates. A compacted mix slab is shown in Figure 3.6.

The dimensions of each beam were first measured with the caliper in five points (edges, middle and the middle third points) because some small deviations can occur during the sawing process. These dimensions were inputted in the UTM software at the beginning of each test. The dimensions, air voids and other mixtures characteristics are presented in Appendix A for each sample tested. Nuts and screws were glued with epoxy on the sawed sides of the beam in the middle third (Figure 3.7), to support the instrumentation.

Figure 3.7 Slab of Compacted HMA Mix

3.2.3 Fatigue Testing Configuration

The beam specimens of 51 mm height, 76 mm width and 406 mm length (2 x 3 x 16 inch – approximate dimensions), obtained from the compacted slabs, were tested in bending using the UTM machine. A LVDT was used to measure the differential deflection in the neutral axis of the specimen. The load applied by the actuator is controlled by CDAS; such as the strain at the extreme fiber of the beam is constant and equal to the desired strain. The screws were glued in the middle third of the beam where the moment is constant and the distance between the exterior screws (A and A') was 4.5 in, or 1/3 of the beam span.

The testing configuration used was different from that recommended by the AASHTO Provisional Standard and the UTM software. The AASHTO Provisional Standard TP8-94 (1994) estimates the maximum tensile strain at the middle third of the beam from the measured deflection at the center of the beam. For convenience, the UTM testing protocols measure the deflection at 1/6 L (beam span) because it is equal to half the deflection in the middle of the beam, when the stiffness of the material is uniform along the beam. Both testing configurations do not take into consideration the variation of the stiffness along the beam, which changes with the applied cycles and with the distance from the supports, because the bending moment is not constant along the beam. After the fatigue test is started the stiffness is uniform only in the middle third because the bending moment and the maximum tensile strains are uniform only in this region (Figure 3.8).
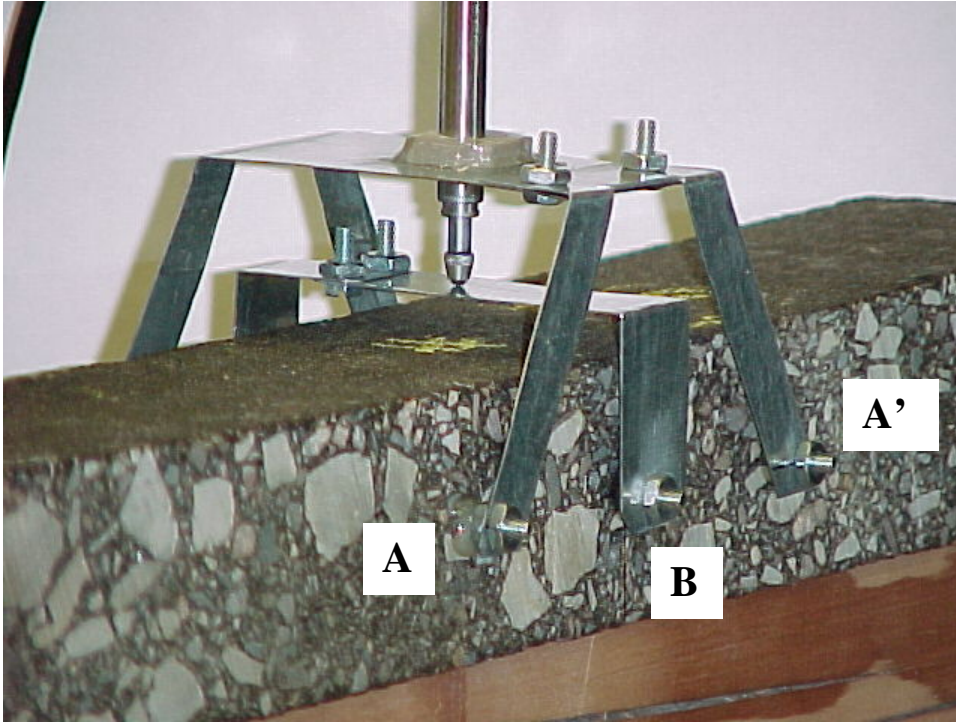
Figure 3.8 Positioning of LVDT
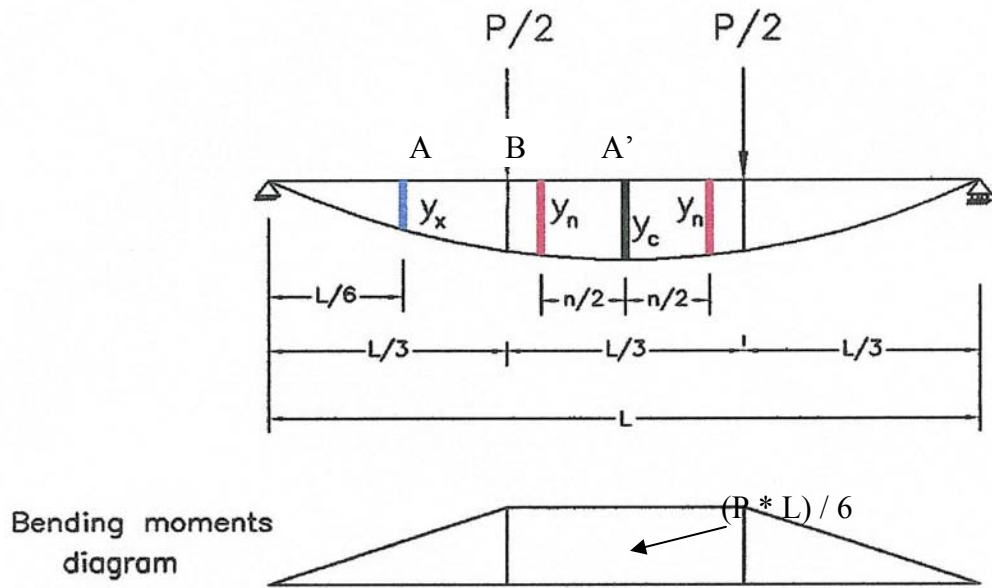
Figure 3.9 Deflection Measurement

The testing configuration used in this research measured the differential deflection in the middle third, in order to estimate the maximum strain in the beam, because the difference in deflection at the points A and B depends only on the stiffness in that region.

An aluminum plate supporting the LVDT was fixed between points A and A'. The LVDT was then fixed to measure the difference in deflection between points A and B (Figures 3.7 and 3.8). The deflection between the points A where the LVDT is fixed and the middle of the beam B can be computed as:

$$d_{A-B} = y_B - y_A = (P * L * n^2) / (4 * S * b * h^3) \qquad (3.1)$$

where:

d_{A-B} = deflection in meters

y_B = deflection measured in the middle of the beam, in meters

y_A = deflection measured in the middle third of the beam, in meters

P = load applied through the actuator, in Newtons

L = span of beam, in meters

n = distance between the screws, in meters

S = stiffness (flexural modulus), in N/m^2, assumed to be uniform in the middle third of the beam

b = width of the beam, in meters

h = height of the beam, in meters

The maximum tensile strain e, can be computed as:

$$e = (M * h/2) / SI = (P * L / 6) * (h/2) / (S * b * h^3 / 12) = (P * L) / (S * b * h^2) \qquad (3.2)$$

The deflection d can be related with the maximum tensile strain as follows:

$$e = (4 * h * d_{A-B}) / n^2 \qquad (3.3)$$

Consequently the stiffness can be backcalculated from the measured deflection as:

$$S = (P * L * n^2) / (4 * d_{A-B} * b * h^3) \qquad (3.4)$$

31

Because the LVDT measures the deflection in the middle of the beam and in the UTM Protocol the LVDT measures the deflection at L/6, the relationship between the deflection measured by the external LVDT and the maximum tensile strain changes for the new position of the LVDT, from:

$$e_{UTM} = (P * L / 6) / [(b * h^2) / 6 * S] = (216 * d_{1/6} * h) / (23 * L^2) \qquad (3.5)$$

$$\text{to:} \quad e = (4 * d_{A-B} * h) / n^2 \qquad (3.6)$$

Since the LVDT measures d_{A-B} instead of $d_{1/6}$, the input value of the strain to be specified on the UTM setup screen to have $d_{1/6} = d_{A-B}$ in equations (3.5) and (3.6), must be:

$$e_{UTM} / e = (54 / 23) * (n^2 / L^2) = 6 / 23 \qquad (3.7)$$

$$\text{For} \quad n = L / 3 \quad => \quad e_{input} = e_{UTM} = (6 / 23) * e \qquad (3.8)$$

Therefore, to reach a maximum tensile strain of 250 microstrain, the value to be typed on the UTM start up screen must be $e_{input} = (6 / 23) * 250 = 65$ microstrain.

From equation (3.5) the UTM software computes the stiffness with the formula:

$$S_{UTM} = (23 * P * L^3) / (216 * d_{1/6} * b * h^3) \qquad (3.9)$$

Because the LVDT measures the difference in deflection between points A and B, d_{A-B}, and not the deflection at 1/6 of the length of the beam, $d_{1/6}$, the flexural modulus computed by the UTM software needs to be corrected with the correction factor of 6 / 23 as follows:

$$S = (6 / 23) E_{UTM} \qquad (3.10)$$

In all the calculations, the correction coefficient of 6/23 was multiplied with the flexural stiffness values given in the UTM output file in order to estimate the real flexural stiffness.

3.2.4 Asphalt Beam Fatigue Testing

Before testing, the specimens were placed in the environmental chamber for at least 2 hours at the desired testing temperature. The temperature was controlled by the heating and

cooling unit. The temperature of the tested specimen was measured by a thermocouple mounted at the center of a dummy specimen placed near the tested beam.

The asphalt specimen was placed into the UTM machine, fixed in position with the clamps, and the LVDT was attached onto the steel plates fixed to points A and A' (Figure 3.7). After the input parameters were selected (dimensions of the beam, microstrain level) and all the readings were zeroed, the fatigue test was started. Figure 3.9 shows the screen with the loading input data and Figure 3.10 shows the screen where the beam dimensions are inputted. After the test is initialized, the UTM displays the initial stiffness, measured after 200 cycles and computes the termination stiffness as half of the initial stiffness.

The applied cyclic load used was sinusoidal, with a frequency of 10 Hz and with no rest periods. The peak-to-peak load amplitude was recorded. The specimens were tested under controlled strain mode at four different strain levels: 125, 250, 375 and 500 microstrain (10^{-6} in/in). These values were corrected with the correlation coefficient of 6/32 when the desired strain was typed in the UTM screen. Thus the corresponding typed values were 33, 65, 98 and 130 microstrain (10^{-6} in/in).
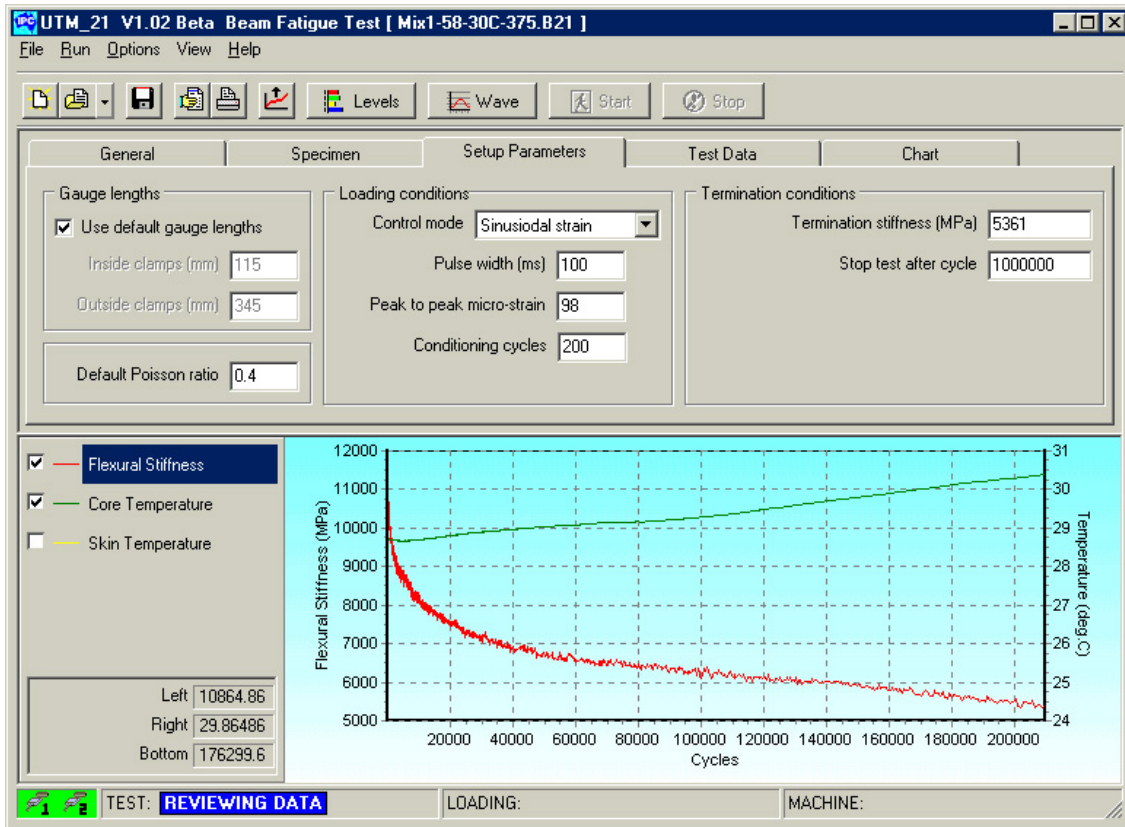
Figure 3.10 Input Parameters, Loading Conditions
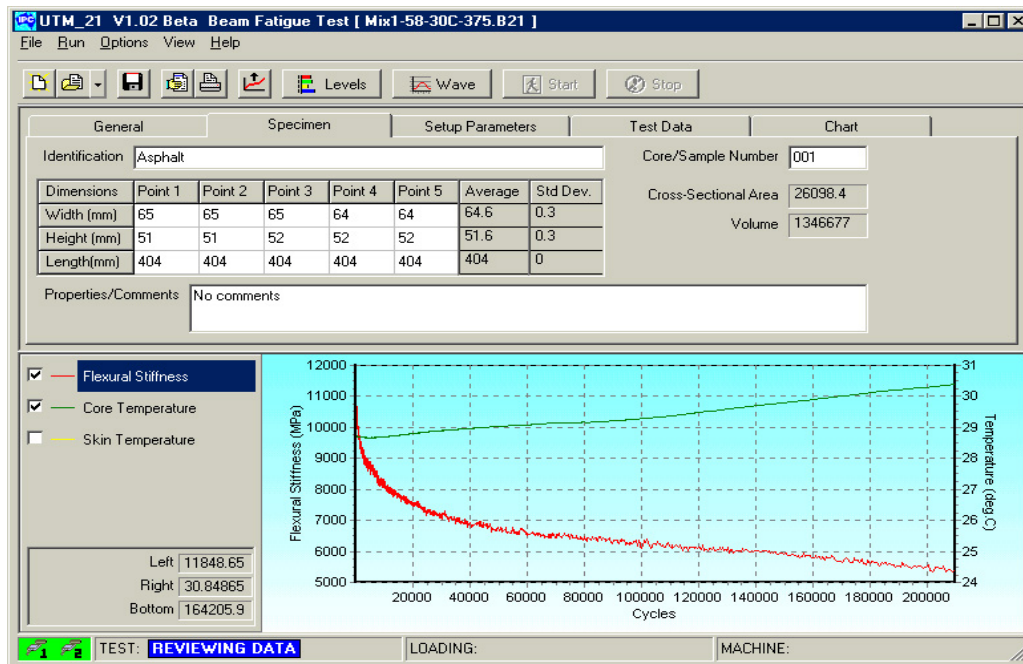
Figure 3.11 Input Parameters, Specimen Dimensions

The testing temperatures used for the fatigue tests were 4°C, 10°C, 20°C and 30°C for mixes A and B and 4°C, 20°C and 30°C for mixes C and D. Four beams were tested for each condition, with a total of 64 beams each for mixes A and B and 48 beams each for mixes C and D. The failure of the specimen was considered when the beam reached 50% of the initial stiffness. Because the mix C contained binder with SBS polymer, the termination stiffness didn't reach 50% of the initial stiffness at any of the strain levels used for Mixes A, B and C. Therefore, the four strain levels used were: 250, 375, 500 and 625 microstrain (10^{-6} in/in) for 4°C; 500, 625, 750 and 875 microstrain (10^{-6} in/in) for 20°C; and 750, 875, 1000 and 1125 microstrain (10^{-6} in/in) for 30°C. In this case, the corresponding typed values were 130, 163, 196, 229, 262 and 295 microstrain (10^{-6} in/in).

The following data was recorded periodically during the test: test loading time, cycle number, maximum and minimum applied load and deflection, tensile stress, strain, phase angle, flexural stiffness, modulus of elasticity and the dissipated energy. The data for each fatigue test was saved in a binary file format and then in ASCII text files. The text files were then imported into Microsoft Excel for further numerical analysis. The typical output (Figure 3.11) shows that the flexural stiffness is decreasing with the increasing of number of loading cycles. This trend was observed for all beams tested in this experiment.

Some asphalt specimens didn't reach the termination stiffness of 50% of the initial stiffness after the maximum number of cycles of 2 million, especially the specimens tested at 250 and 125 microstrain. For time considerations, the tests were stopped after 2 million loading cycles. This limited cycle number was imputed in the UTM software, because it was considered that the stiffness data collected in the first 2 million cycles allowed the estimation of the number

of cycles to failure, considered as the number of cycles where the stiffness reaches half of the

initial values
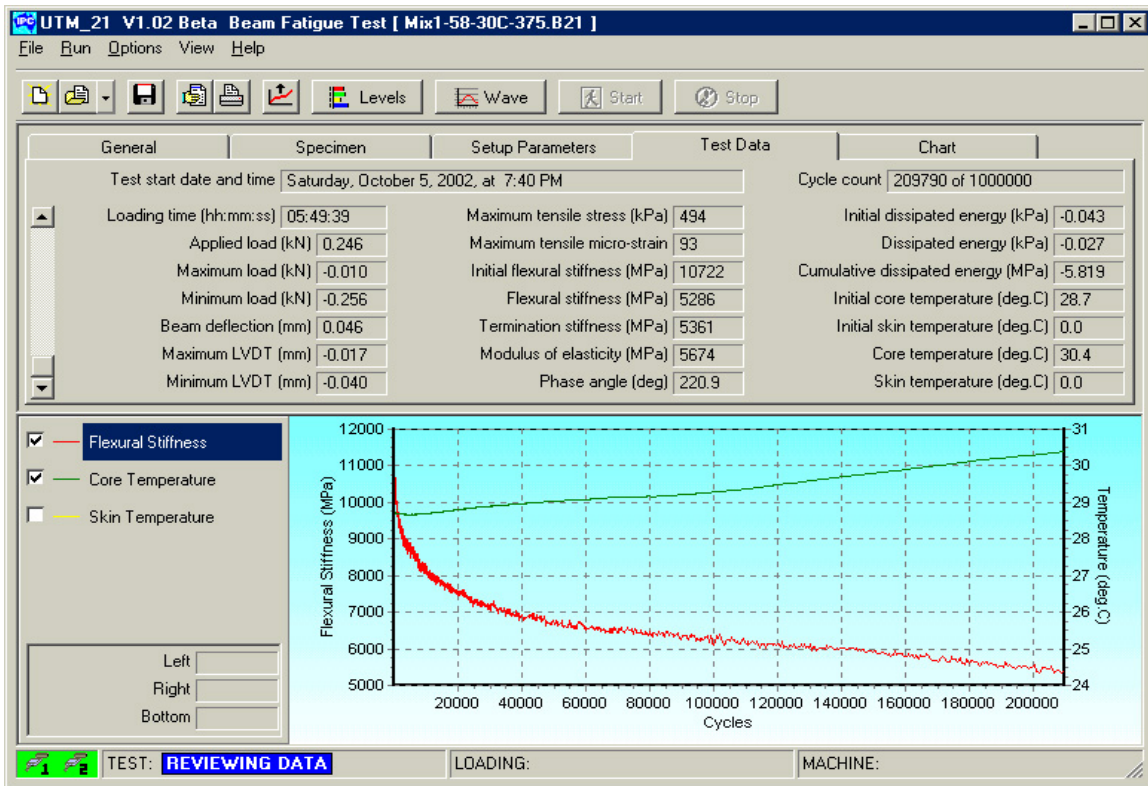
Figure 3.12 Typical Output

3.2.5   Temperature Correction

The flexural stiffness is very sensitive to even small change in temperature. It was

observed during the fatigue tests that a deviation in the temperature during the testing of $\pm 2^0 C$

leads to a significant change in the flexural stiffness, as seen in Figure 3.12. A correction

procedure was developed in order to correct the flexural stiffness to the desired temperature.

The procedure was based on the assumption that, for short testing time (less than 20

minutes) and the strain level of 125 microstrain, the flexural stiffness is not affected by the

applied number of loading cycles. For each mix, four asphalt specimens with a varying air void

content were subjected to short bending tests, at 125 microstrain, with a fast change in the

36

temperature. Near each of the testing temperatures of 4^0C, 10^0C, 20^0C and 30^0C, a variation of ±2 ^{0}C was applied in order to observe the change of the flexural stiffness with the temperature. A typical variation of the stiffness with the temperature is shown in Figure 3.12. The variation of the flexural stiffness was then approximated with a linear relationship to obtain the temperature correction model:

$$S = a_0 + a_1 T_0 \tag{3.11}$$

Where:

a_0 = is the intercept of the Y axis and a_1 is the slope

S = is the flexural stiffness in MPa and,

T_0 = is the reference temperature (4^0C, 10^0C, 20^0C, 30^0C)
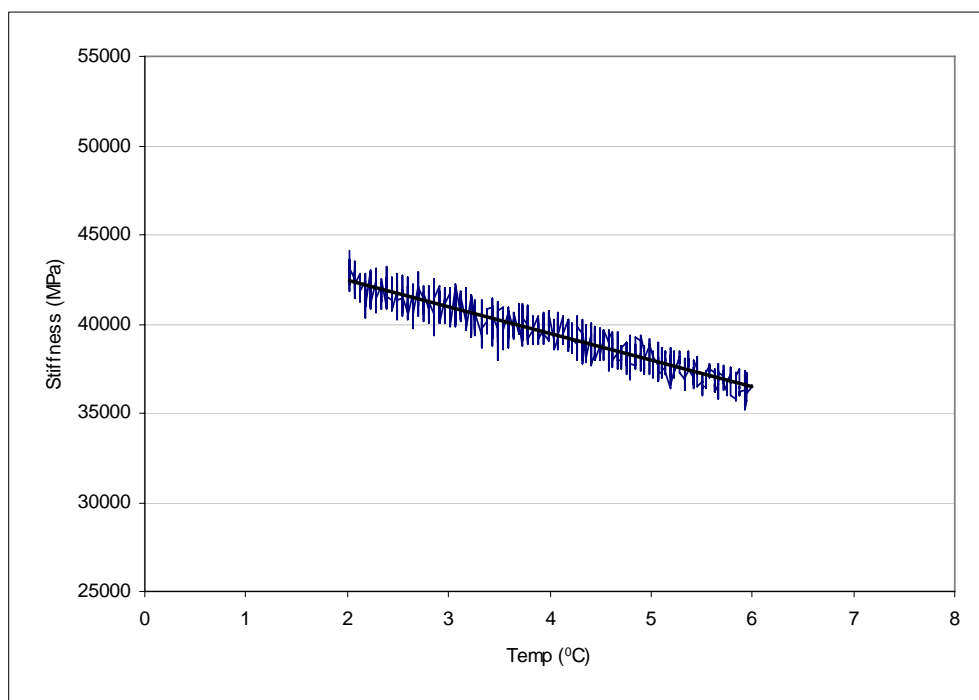
Figure 3.13 Variation of Stiffness with Temperature

This temperature correction procedure was used for all the three mixes, at all the four testing temperatures. The results for the regression analysis are given in Tables 3.2, 3.3 and 3.4.

From equation (3.11) the flexural stiffness at 4^0C was corrected for the stiffness measured at temperature T, close to 4^0C with the following equation.

$$S_4 = S + a_1 (4^0 - T) \qquad (3.12)$$

Figure 3.13 shows an example of original and temperature corrected flexural modulus.
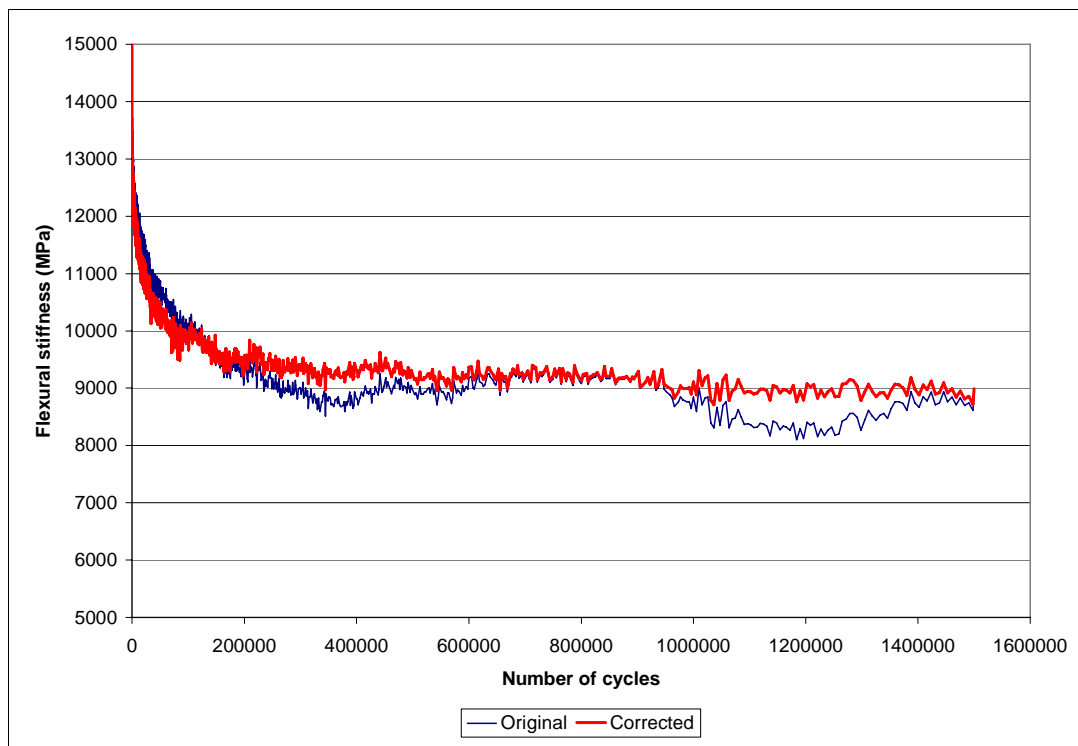
Figure 3.14 Temperature Correction

Table 3.3 Temperature Correction Coefficients for Mix A

Temp. (^{o}C)	Specimen #	Air Voids (%)	Intercept (a_0)	Slope (a_1)
4	86	6.4	9,443	-231
	90	6.7	9,825	-412
	89	7.6	7,788	-434
	85	8	9,394	-397
10	86	6.4	5,204	-499
	90	6.7	13,023	-621
	89	7.6	4,910	-533
	85	8	8,035	-582
20	86	6.4	3,807	-364
	90	6.7	10,924	-368
	89	7.6	3,037	-310
	85	8	3,400	-293
30	86	6.4	1,921	-129
	90	6.7	2,170	-128
	89	7.6	1,793	-133
	85	8	2,478	-149

Table 3.4 Temperature Correction Coefficients for Mix B

Temperature (°C)	Specimen #	Air Voids (%)	Intercept (a_0)	Slope (a_1)
4	65	6.9	14,871	-653
	66	5.8	14,112	-686
	97	6.4	12,835	-507
	103	7.2	16,133	-836
10	65	6.9	13,817	-545
	66	5.8	13,089	-538
	97	6.4	13,647	-577
	103	7.2	14,898	-579
20	65	6.9	9,826	-307
	66	5.8	10,178	-319
	97	6.4	10,229	-322
	103	7.2	12,024	-367
30	65	6.9	6,182	-153
	66	5.8	6,257	-156
	97	6.4	5,785	-147
	103	7.2	7,927	-197

Table 3.5 Temperature Correction Coefficients for Mix C

Temperature (°C)	Specimen #	Air Voids (%)	Intercept (a_0)	Slope (a_1)
4	2	4.8	10,856	-515
	8	5.7	10,449	-560
	17	7.3	9,474	-2039
	18	6.5	10,804	-532
20	2	4.8	6,328	-203
	8	5.7	7,320	-247
	17	7.3	6,377	-214
	18	6.5	7,668	-255
30	2	4.8	3,592	-88
	8	5.7	4,045	-107
	17	7.3	3,031	-78
	18	6.5	4,047	-106

Table 3.6 Temperature Correction Coefficients for Mix D

Temperature (°C)	Intercept (a_0)	Slope (a_1)
4	53,426	-2,120
20	36,430	-1,100
30	23,253	-508

3.2.6 Estimation of Number of Cycles to Failure

During the testing, not all specimens exhibited failure before 2 million cycles. For these specimens the assumption made was that, after 500,000 load cycles, the flexural stiffness decreases linearly with the number of applied cycles:

$$S = b_0 + b_1 N \qquad (3.13)$$

where

S = stiffness (MPa),

N = is the number of cycles,

b_0 = is the intercept of the Y axis and b_1 is the slope

The final modulus, which is half of the initial modulus, has the following equation:

$$S_{fin} = b_0 + b_1 N_{fin} = 0.5 * S_{initial} \qquad (3.14)$$

Therefore, the fatigue life N_{fin} was determined as follows:

$$N_{fin} = (S_{fin} - b_0) / b_1 \qquad (3.15)$$

The coefficients b_0, b_1, R^2 and N_{fin} were computed using the Microsoft Excel for both original and corrected values of temperature and stiffness. The results are tabulated in Appendix B. A graphical example of the use of linear regression to estimate the number of cycles to failure for the specimens that did not fail up to 2 million cycles is shown in the Figure 3.14.
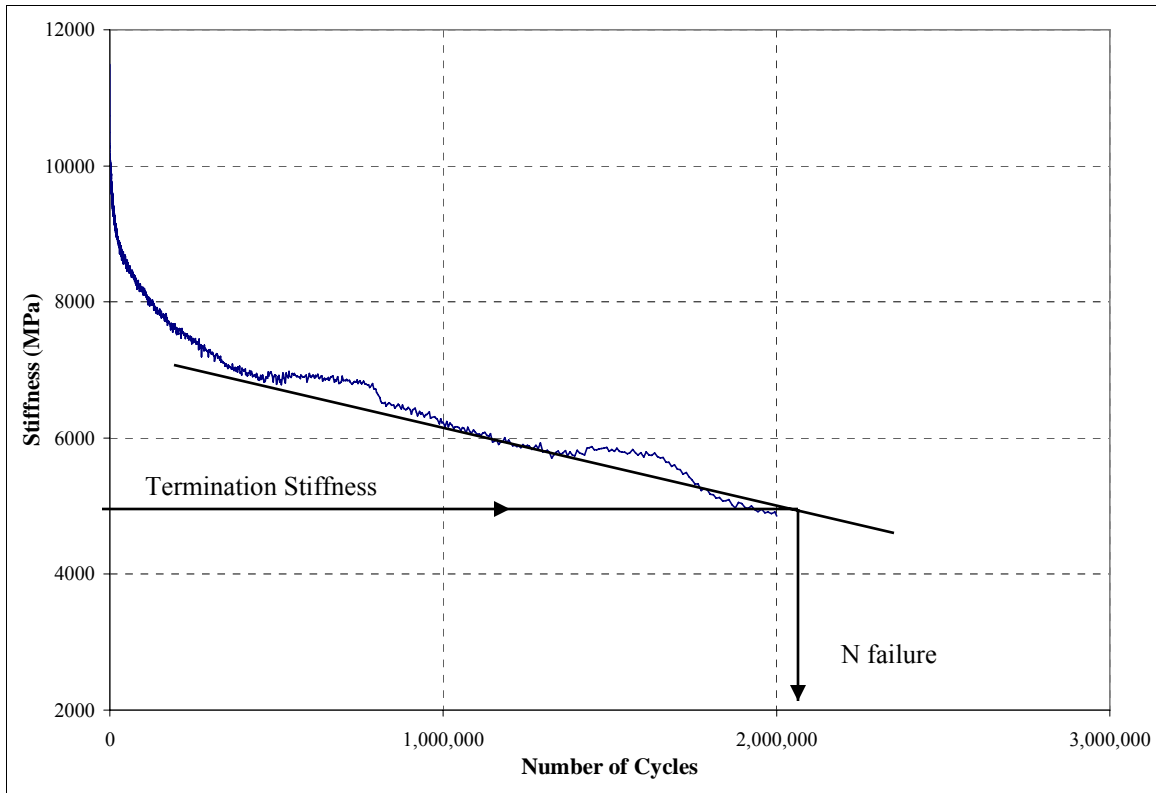
Figure 3.15 Estimation of Loading Cycles to Failure

3.3 Dynamic Resilient Modulus Testing

The dynamic resilient modulus testing is a cyclic compressive test performed on cylindrical asphalt specimens with the dimensions of 100 mm diameter (4 in) and 150 mm height (6 in). The test was performed according to "Simple Performance Test for Permanent Deformation Based upon Dynamic Modulus of Asphalt Concrete Mixtures", (NCHRP, 2001).

In this test a sinusoidal axial compressive load is applied to the cylindrical specimen at a sweep of loading frequencies. During testing, the UTM system measures the vertical stress and the resulting vertical compression strain. The dynamic resilient modulus is calculated by dividing the peak to peak vertical compressive stress to the peak-to-peak vertical strain.

3.3.1   Specimen Preparation

The cylinders were cored from samples with 150 mm diameter (6 in) fabricated in the Superpave Gyratory Compactor (Figure 3.15) and sawed at the ends, at the Kansas Department of Transportation (KDOT), Materials and Research Center. The compacted samples need to be cored and sawed on the plane surfaces in order to obtain a cylinder with a smooth surface, free from ridges or grooves. The air void content, determined for each sample; the values are given in Appendix C.

Figure 3.16 Sample Obtained from Superpave Gyratory Compactor

Two LVDTs are mounted on the side of the specimen using a system of screws and nuts glued with epoxy to the specimen (Figure 3.16). The axial deformation of the central region of the specimen is computed by averaging the deformation recorded by the two LVDTs. The distance between the centerline of the glued screws was 100 mm and was considered as the gage length.

3.3.2   Dynamic Resilient Modulus Test

The asphalt specimens were tested at five temperatures 4°C, 10°C, 20°C, 30°C and 35°C and five load frequencies (10 Hz, 5 Hz, 1 Hz, 0.5 Hz and 0.1 Hz). The specimens were conditioned in the environmental chamber for at least two hours before testing. In this testing configuration, the specimen is placed centered on the steel platen. The LVDTs are fixed to the glued nuts and, the top steel plate is centered on the specimen to ensure centric loading. The actuator is gradually lowered until it touches slightly the top plate.

Once the preparation and mounting of the asphalt cylinder specimen is finished the test is controlled entirely by the CDAS. The cyclic load is applied by the actuator through the steel plate placed on the top of the specimen. The cycling loading is applied at a succession of five load frequencies in the following order: 10 Hz (100 cycles), 5 Hz (50 cycles), 1 Hz (25 cycles), 0.5 Hz (6 cycles) and 0.1 Hz (6 cycles).

Figure 3.17 The Configuration of the Dynamic Resilient Modulus Test

The following data were recorded periodically during the test: dynamic load and stress, microstrain, dynamic modulus, Poisson's ratio, maximum and minimum load displacement, temperature, duration of test, phase angle. The data for each test were saved in a binary file format and ASCII text files. The text files were then imported into Microsoft Excel for further numerical analysis.

Figures 3.17 and 3.18 show the typical stress-strain relationship at 10 Hz and 0.1 Hz. It can be observed that absolute value of the total compressive strain is increasing with time, indicating an accumulation of plastic deformation during the cyclic compression test.

The dynamic resilient modulus E* is calculated by dividing the peak-to-peak stress to the recoverable strain under a repeated sinusoidal waveform loading. For each load cycle, the final value is averaged and the dynamic resilient modulus is computed for each load frequency as:

$$E^* = S_o \, / \, e_o \qquad\qquad\qquad (3.16)$$

where:

E^* = dynamic resilient modulus (MPa)
S_o = applied stress (kN); e_o = strain

The recoverable strain e_o is calculated as follows:

$$e_o = d \, / \, GL \qquad\qquad\qquad (3.17)$$

where:

d = average deformation amplitude (mm)
GL = gage length = 100 mm for all samples
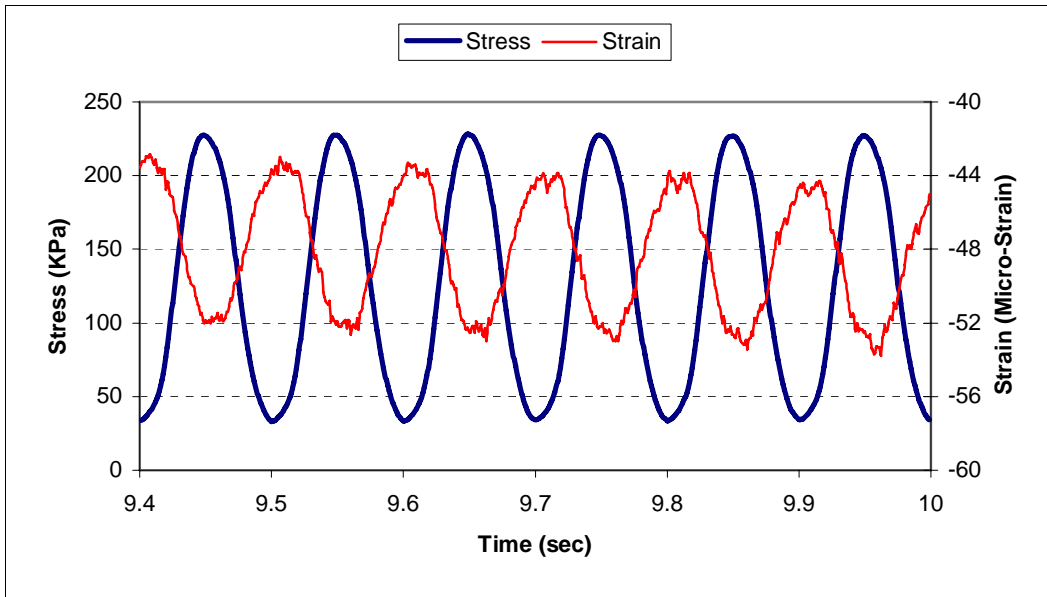
Figure 3.18 Typical Output at 10 Hz
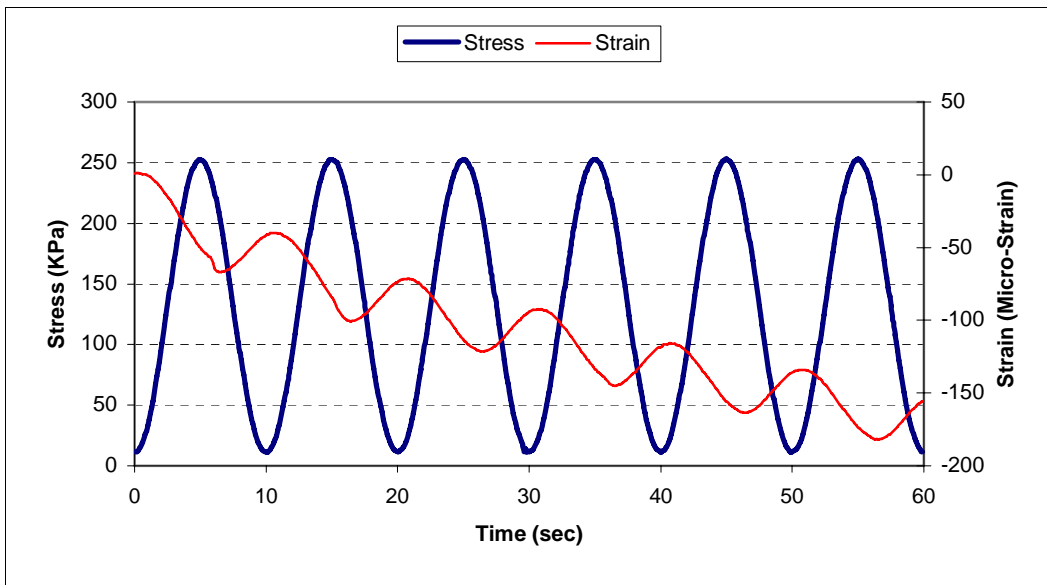
Figure 3.19 Typical Output at 0.1 Hz

CHAPTER 4

RESULTS AND ANALYSIS OF RESULTS

4.1   Summarized Results

The goal of this research was to determine the stiffness properties and the fatigue life of the Superpave Kansas HMA mixes. Also, another objective was to develop a relationship between the fatigue properties and the bending stiffness. The findings presented herein were collected on experiments performed over almost 2 years on asphalt beams and asphalt cylindrical samples.

The previous chapter presented the methodology of testing the asphalt beams and cylinders. Also, the temperature correction procedure for all the three mixes was described.

4.1.1   Beam Fatigue Test

The uncorrected and corrected values for stiffness and temperature for asphalt beams were summarized in Tables 4.1 to 4.8 for mixes A to D. The data reported in the table indicate that, as expected, all mixes had a longer fatigue life at lower levels of strain, (125 and 250 microstrain) for mixes A, B and D, and (250 microstrain at 4^0C, 500 microstrain at 20^0C, and 750 microstrain at 30^0C) for mix C. The temperature played an important role in the behavior of asphalt specimens during the test. The beams tested at 4^0C and 10^0C had a longer fatigue life than those tested at 20^0C and 30^0C. Mix C, which contained SBS polymer in the binder composition, had the longest fatigue life among the mixes tested in this project.

The log of number of cycles to failure versus the microstrain was plotted at every tested temperature for every mix tested as can be seen in Figures 4.1, to 4.4. From these figures it can be observed that, for all three mixes, the fatigue life was longer for the asphalt beams tested at low values of strain than for those tested at high values of strain.

Also, charts showing the fatigue life of asphalt beams versus air void content are presented in Figures 4.5 – 4.18. No strong conclusion regarding the effect of percent air voids can be drawn from these charts. For mix A the general trend was a decreasing of the fatigue life with the increasing of the percent of air void content. For mixes B and C no conclusion can be drawn, because the trend of the number of cycles to failure was either increasing or decreasing regardless of air void content.

Table 4.1 Number of Cycles to Failure for Mix A, for Uncorrected Stiffness

Temperature (°C)	Strain (microstrain)			
	125	250	375	500
4	4,091,394	690,897	91,978	85,477
	15,746,282	856,391	57,434	19,970
	31,003,136	2,235,798	101,644	11,415
	22,629,279	2,126,817	63,710	15,559
Average N_f	18,367,523	1,477,476	78,692	35,429
Coeff. of Variation (%)	61.96	55.28	27.25	96.60
10	8,230,155	2,978,133	306,499	44,905
	18,324,552	3,095,123	114,993	49,204
	8,294,908	843,168	101,201	22,083
	10,914,917	3,225,877	116,742	37,780
Average N_f	20,085,034	2,535,575	159,859	38,493
Coeff. of Variation (%)	72.95	44.68	61.31	30.94
20	2,436,025	2,460,754	572,478	50,004
	1,287,998	806,348	611,324	177,897
	2,957,291	1,469,716	229,977	122,106
	10,189,251	2,469,898	1,413,938	41,628
Average N_f	4,217,641	1,801,679	706,929	97,908
Coeff. of Variation (%)	95.83	45.11	70.94	65.79
30	2,699,254	242,619	997,936	245,228
	14,604,975	238,314	376,757	126,117
	12,047,443	772,255	550,050	300,714
	3,342,622	1,515,842	197,277	134,788
Average N_f	8,173,574	692,258	530,505	201,712
Coeff. of Variation (%)	73.97	87.19	64.71	42.35

Table 4.2 Number of Cycles to Failure for Mix A, for Temperature Corrected Stiffness

Temperature (°C)	Strain (microstrain)			
	125	**250**	**375**	**500**
4	4,654,410	642,561	81,195	70,561
	14,191,910	607,129	55,080	19,396
	28,098,740	823,624	100,294	12,255
	22,289,642	1,985,918	62,295	16,236
Average N$_f$	**17,308,676**	**1,014,808**	**74,716**	**29,612**
Coeff. of Variation (%)	**58.83**	**64.48**	**27.17**	**92.72**
10	10,617,833	1,937,552	396,666	43,852
	17,611,689	2,141,900	97,080	50,040
	7,277,840	722,667	89,551	22,347
	15,368,420	3,768,604	96,545	40,979
Average N$_f$	**12,718,946**	**2,142,681**	**169,961**	**39,305**
Coeff. of Variation (%)	**36.59**	**58.43**	**88.95**	**30.33**
20	8,286,897	2,380,640	430,420	50,007
	1,082,647	688,214	441,673	263,483
	3,208,223	2,762,175	160,115	74,688
	12,837,241	2,352,435	1,146,761	45,293
Average N$_f$	**6,353,752**	**2,045,866**	**544,742**	**108,368**
Coeff. of Variation (%)	**83.01**	**45.17**	**77.45**	**96.16**
30	2,699,254	260,238	381,482	217,973
	14,058,676	254,494	252,150	118,880
	12,047,443	614,674	481,101	366,554
	3,342,622	1,076,216	259,910	169,605
Average N$_f$	**8,036,999**	**551,406**	**343,661**	**218,253**
Coeff. of Variation (%)	**72.86**	**70.42**	**31.75**	**48.95**

Table 4.3 Number of Cycles to Failure for Mix B, for Uncorrected Stiffness

Temperature (°C)	Strain (microstrain)			
	125	250	375	500
4	10,730,476	1,507,535	138,144	33,421
	7,010,746	689,936	64,121	24,993
	42,463,041	908,576	58,789	33,158
	14,583,788	1,491,426	162,292	22,972
Average N$_f$	**18,697,013**	**1,149,368**	**105,837**	**28,636**
Coeff. of Variation (%)	**86.34**	**36.03**	**49.35**	**18.99**
10	6,637,255	1,425,982	236,618	36,326
	17,057,682	2,234,673	162,083	31,162
	5,624,300	2,044,923	36,326	35,531
	8,077,353	1,110,389	117,285	51,379
Average N$_f$	**9,349,148**	**1,703,992**	**138,078**	**38,599**
Coeff. of Variation (%)	**56.01**	**30.82**	**60.70**	**22.84**
20	6,918,111	1,657,987	197,322	52,293
	3,959,373	420,697	307,413	35,407
	5,246,822	309,847	254,306	57,473
	5,016,012	1,718,670	293,336	39,288
Average N$_f$	**5,285,079**	**1,026,800**	**263,094**	**46,115**
Coeff. of Variation (%)	**23.17**	**74.56**	**18.73**	**22.69**
30	248,539	220,033	47,833	38,284
	841,814	206,535	53,691	42,267
	3,337,204	348,727	294,340	57,829
	596,658	248,052	46,650	126,020
Average N$_f$	**1,256,054**	**255,837**	**110,629**	**66,100**
Coeff. of Variation (%)	**112.15**	**25.13**	**110.74**	**61.77**

Table 4.4 Number of Cycles to Failure for Mix B, for Temperature Corrected Stiffness

Temperature (°C)	Strain (microstrain)			
	125	**250**	**375**	**500**
4	11,325,902	1,221,361	131,233	31,392
	12,552,445	605,760	65,366	24,497
	16,847,955	864,053	54,000	30,527
	16,322,560	1,237,357	138,061	22,330
Average N$_f$	**14,163,448**	**982,133**	**97,165**	**27,186**
Coeff. of Variation (%)	**19.95**	**30.99**	**44.89**	**16.40**
10	8,237,066	1,192,004	212,560	36,088
	16,534,290	1,682,494	150,102	36,934
	6,376,474	2,207,519	36,088	36,324
	6,010,326	1,019,397	117,718	50,576
Average N$_f$	**9,289,539**	**1,525,354**	**129,117**	**39,981**
Coeff. of Variation (%)	**53.04**	**35.04**	**56.89**	**17.69**
20	11,130,141	1,625,837	201,560	42,203
	6,308,757	529,399	345,175	36,367
	5,724,338	263,921	302,023	43,535
	5,352,335	1,871,224	342,293	54,712
Average N$_f$	**7,128,893**	**1,072,595**	**297,763**	**44,204**
Coeff. of Variation (%)	**37.82**	**74.06**	**22.53**	**17.34**
30	329,464	271,187	48,128	36,558
	875,342	261,640	44,239	47,623
	2,840,996	180,741	393,966	50,159
	1,882,117	313,910	40,978	132,554
Average N$_f$	**1,481,980**	**256,869**	**131,828**	**66,723**
Coeff. of Variation (%)	**74.97**	**21.65**	**132.58**	**66.37**

Table 4.5 Number of Cycles to Failure for Mix C, for Uncorrected Stiffness

Temperature (°C)	Strain (microstrain)			
	250	**375**	**500**	**625**
4	3,844,490	1,859,197	67,677	125,882
	16,810,785	441,045	288,853	101,635
	5,193,251	574,447	230,858	208,601
	7,394,860	1,344,035	190,329	42,106
Average N$_f$	**8,310,846**	**1,054,681**	**194,429**	**119,556**
Coefficient of Variation (%)	**70.42**	**63.32**	**48.18**	**57.73**
	Strain (microstrain)			
	500	**625**	**750**	**875**
20	2,554,822	3,149,265	1,016,888	170,877
	2,843,139	2,401,217	984,005	427,050
	241,370	2,338,526	355,129	494,174
	1,235,480	1,524,509	320,527	527,040
Average N$_f$	**1,718,703**	**2,353,379**	**669,137**	**404,785**
Coefficient of Variation (%)	**70.30**	**28.22**	**57.25**	**39.87**
	Strain (microstrain)			
	750	**875**	**1000**	**1125**
30	1,283,099	2,667,966	1,092,600	610,329
	2,578,516	2,919,938	1,914,723	248,908
	2,366,131	2,391,010	754,593	620,897
	2,732,944	1,179,052	2,320,847	906,656
Average N$_f$	**2,240,173**	**2,289,491**	**1,520,691**	**596,698**
Coefficient of Variation (%)	**29.26**	**33.68**	**47.51**	**45.16**

Table 4.6 Number of Cycles to Failure for Mix C, for Temperature Corrected Stiffness

Temperature (°C)	Strain (microstrain)			
	250	**375**	**500**	**625**
4	4,078,603	1,664,041	70,122	116,935
	24,490,792	465,417	258,125	108,420
	4,360,000	547,021	138,565	173,770
	7,047,723	1,303,217	139,116	41,606
Average N_f	**9,994,279**	**994,924**	**151,482**	**110,183**
Coefficient of Variation (%)	**97.62**	**58.71**	**51.58**	**49.14**
	Strain (microstrain)			
	500	**625**	**750**	**875**
20	2,158,772	2,935,977	943,631	167,757
	1,730,317	2,306,225	869,545	358,258
	409,151	2,601,255	442,364	430,084
	1,063,251	1,725,218	303,132	528,275
Average N_f	**1,340,373**	**2,392,169**	**639,668**	**371,093**
Coefficient of Variation (%)	**57.24**	**21.47**	**49.22**	**41.07**
	Strain (microstrain)			
	750	**875**	**1000**	**1125**
30	1,708,703	2,634,202	1,513,988	982,182
	2,508,549	3,340,890	1,528,215	249,820
	2,577,497	3,236,043	964,465	1,040,490
	3,547,810	1,178,308	2,248,515	1,373,204
Average N_f	**2,585,640**	**2,597,361**	**1,563,796**	**911,424**
Coefficient of Variation (%)	**29.12**	**38.35**	**33.67**	**51.95**

Table 4.7 Number of Cycles to Failure for Mix D, Uncorrected Stiffness

Temperature (°C)	Strain (microstrain)			
	125	250	375	500
4	21,060,315	2,342,100	1,019,857	9,375
	10,635,859	2,845,751	116,658	28,457
	32,087,269	2,321,108	128,867	49,159
	47,093,465	2,828,543	104,114	20,036
Average N_f	**27,719,227**	**2,584,375**	**342,374**	**26,757**
Coeff. of Variation (%)	**56.30**	**11.30**	**131.95**	**62.98**
20	7,741,386	2,818,036	103,929	23,876
	32,168,981	3,968,284	164,344	74,254
	14,000,317	3,052,363	285,578	117,120
	19,449,526	1,517,955	490,697	91,855
Average N_f	**18,340,053**	**2,839,160**	**261,137**	**76,776**
Coeff. of Variation (%)	**56.63**	**35.61**	**65.35**	**51.33**
30	22,719,494	5,620,689	769,767	197,172
	12,161,701	3,959,191	229,853	103,772
	6,459,335	2,440,882	1,274,945	118,308
	11,708,908	2,548,283	329,534	141,155
Average N_f	**13,780,177**	**4,006,921**	**758,188**	**139,751**
Coeff. of Variation (%)	**59.87**	**39.69**	**68.93**	**35.96**

Table 4.8 Number of Cycles to Failure for Mix D, Temperature Corrected Stiffness

Temperature (°C)	Strain (microstrain)			
	125	250	375	500
4	14,443,006	2,386,818	1,107,977	9,394
	14,820,904	2,840,947	118,866	27,971
	122,251,683	2,341,403	131,429	45,655
	33,537,712	3,064,742	94,449	19,881
Average N_f	**46,263,326**	**2,658,478**	**363,180**	**25,725**
Coeff. of Variation (%)	**111.18**	**13.26**	**136.78**	**59.51**
20	10,664,770	2,279,073	111,829	18,353
	16,822,496	3,511,588	150,592	75,457
	11,815,680	2,491,914	291,634	142,729
	13,906,724	1,432,645	484,710	77,210
Average N_f	**13,302,418**	**2,428,805**	**259,691**	**78,437**
Coeff. of Variation (%)	**20.32**	**35.19**	**64.98**	**64.82**
30	8,686,167	3,131,634	858,796	216,109
	12,072,023	3,497,127	914,579	112,046
	7,230,640	2,613,403	1,874,678	159,180
	7,223,624	3,177,658	558,310	279,206
Average N_f	**9,329,610**	**3,080,721**	**1,216,018**	**162,445**
Coeff. of Variation (%)	**26.62**	**14.41**	**46.96**	**32.08**
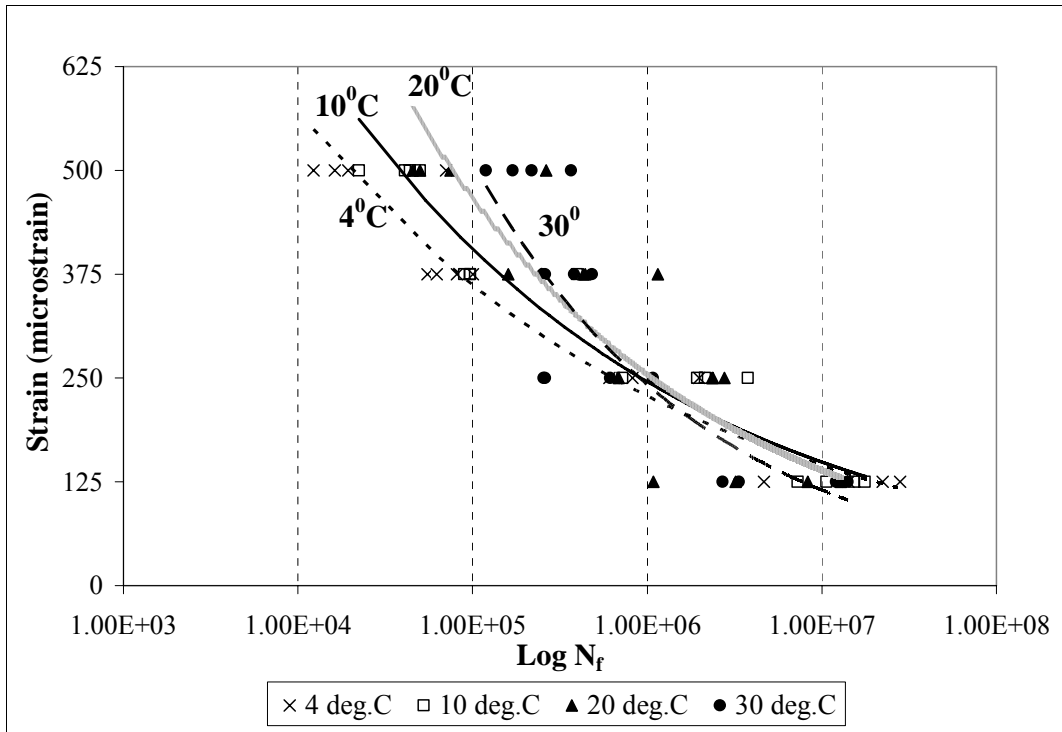
Figure 4.1 N_f vs. Strain for Temperature Corrected Stiffness for Mix A
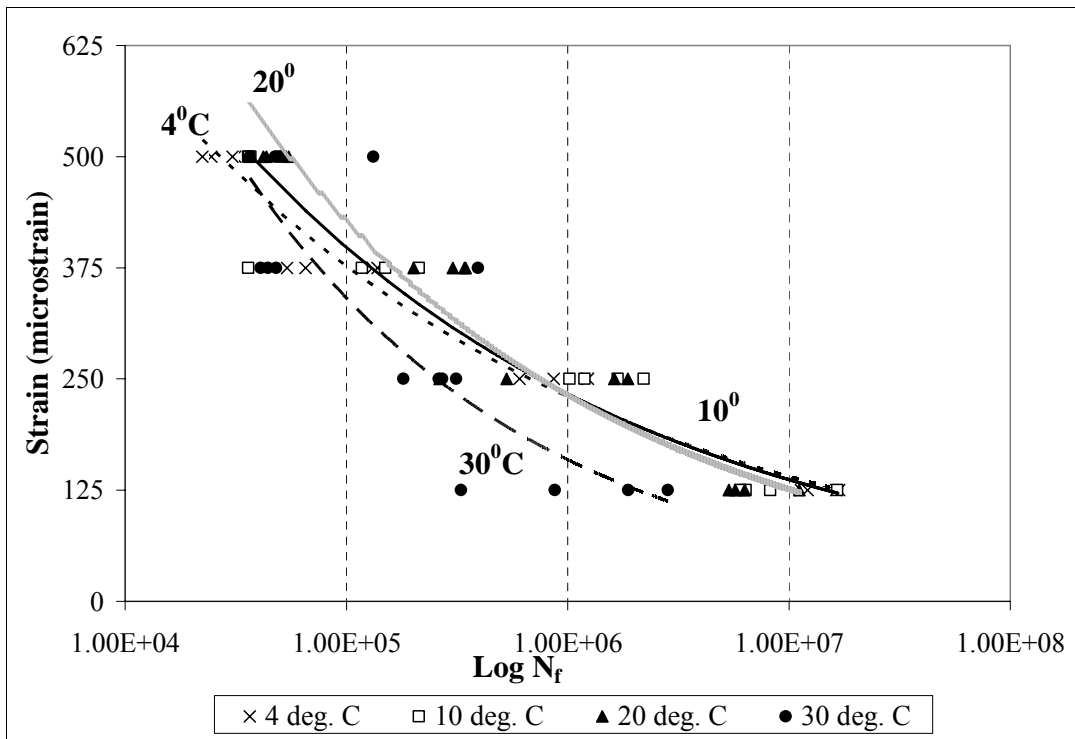
Figure 4.2 N_f vs. Strain for Temperature Corrected Stiffness for Mix B
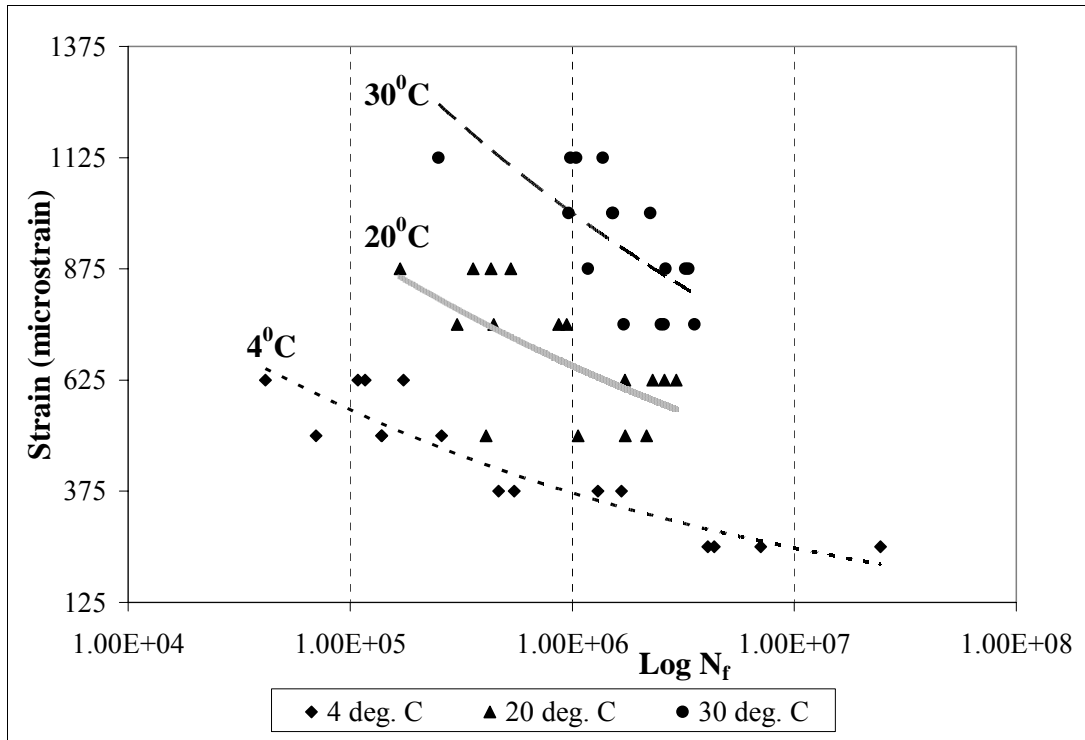
Figure 4.3 N_f vs. Strain for Temperature Corrected Stiffness for Mix C
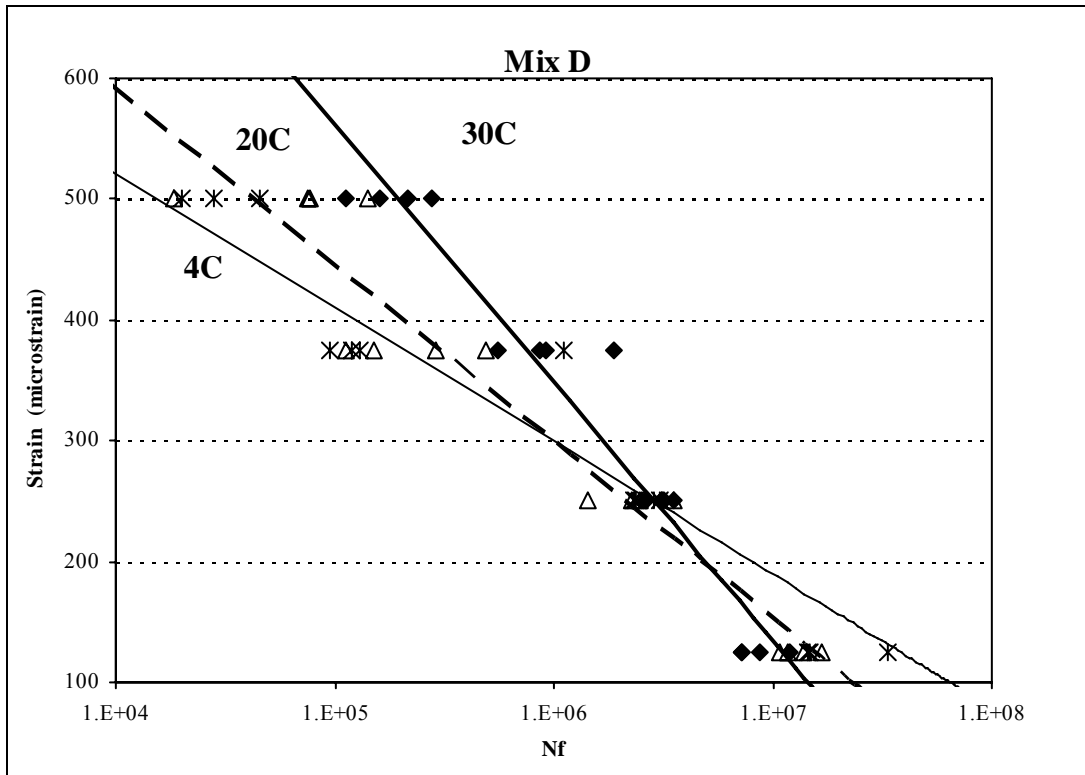
Figure 4.4 N_f vs. Strain for Temperature Corrected Stiffness for Mix D
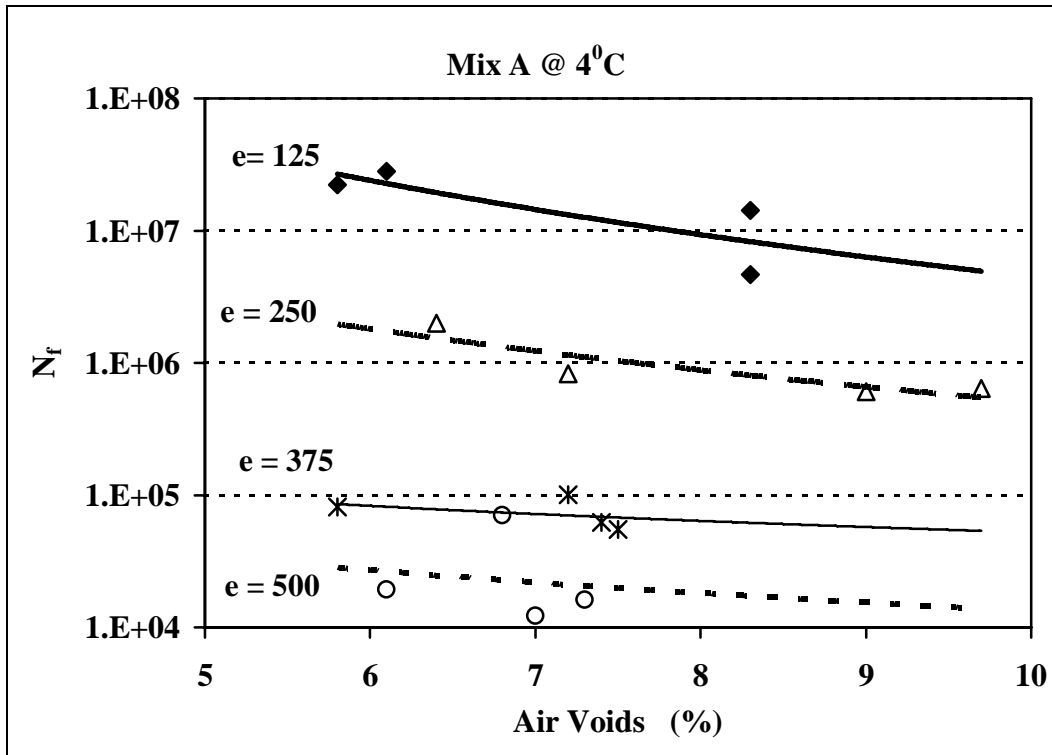
Figure 4.5 N_f vs. Air Voids for Temperature (4^0C) Corrected Stiffness for Mix A
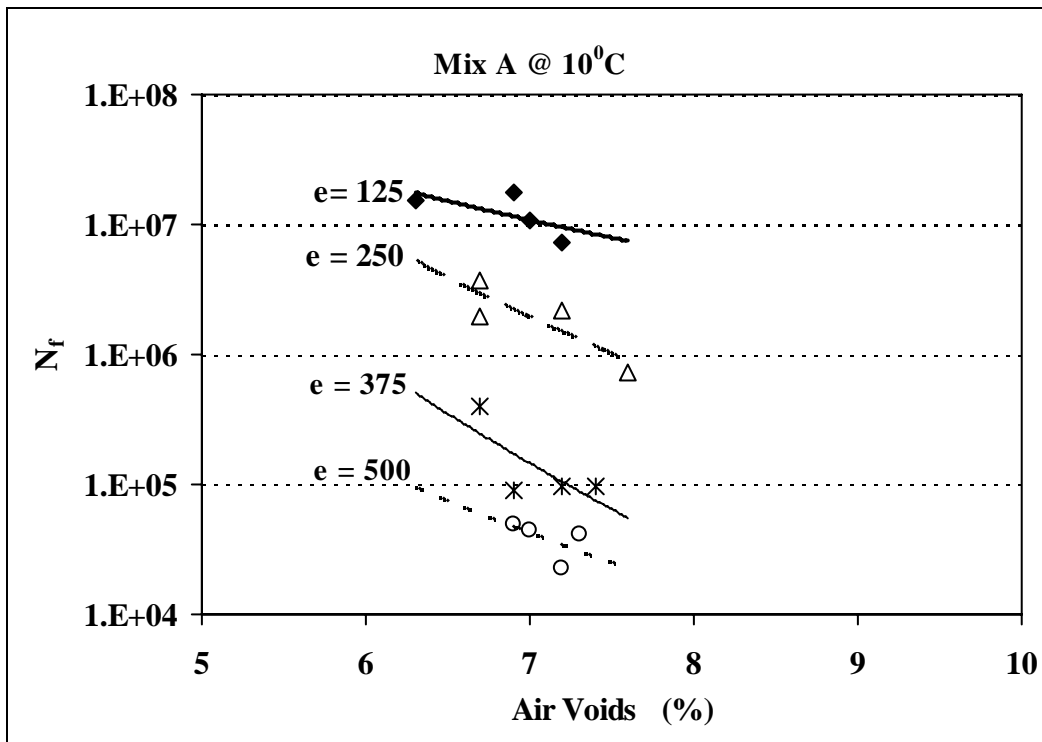
Figure 4.6 N_f vs. Air Voids for Temperature (10^0C) Corrected Stiffness for Mix A
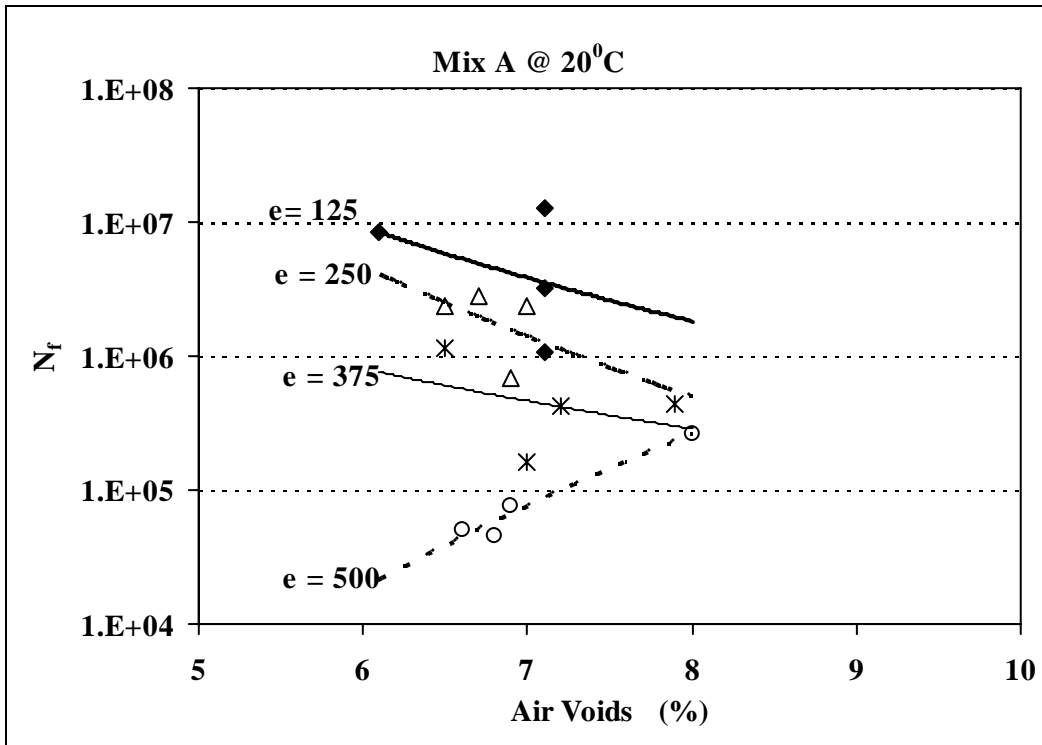
Figure 4.7 N_f vs. Air Voids for Temperature (20^0C) Corrected Stiffness for Mix A
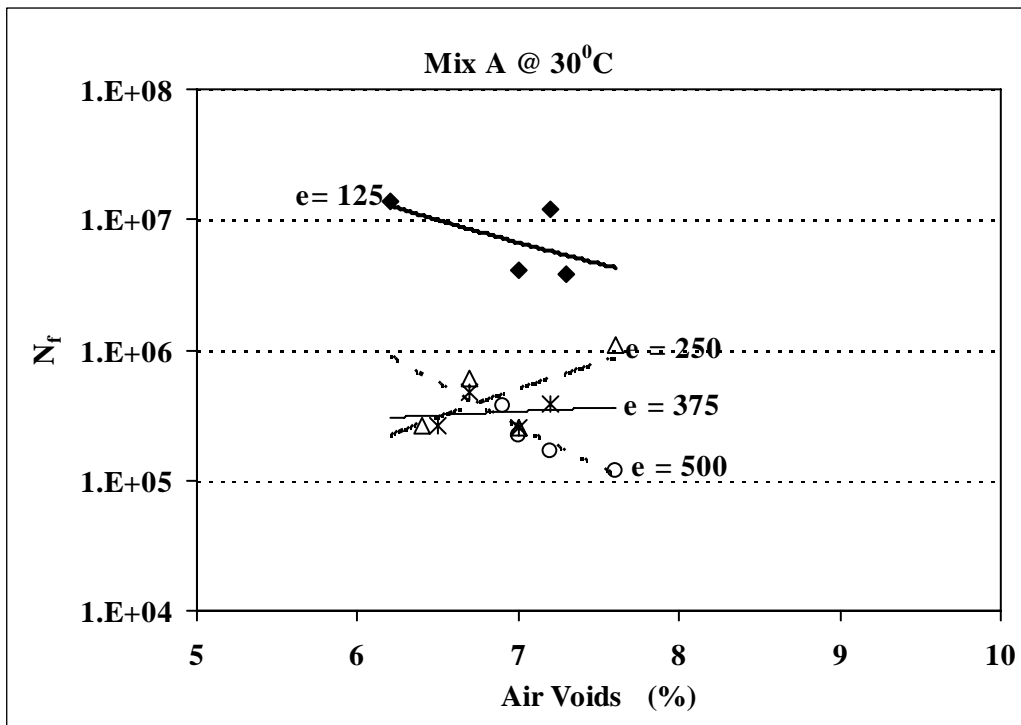
Figure 4.8 N_f vs. Air Voids for Temperature (30^0C) Corrected Stiffness for Mix A
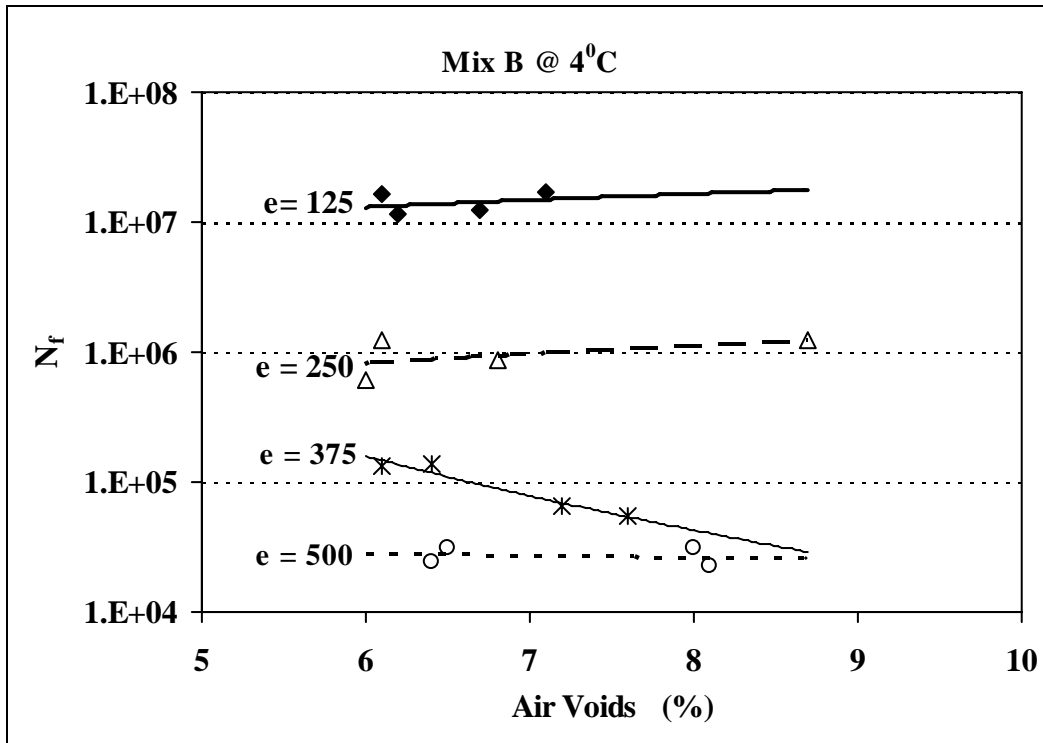
Figure 4.9 N_f vs. Air Voids for Temperature (4^0C) Corrected Stiffness for Mix B
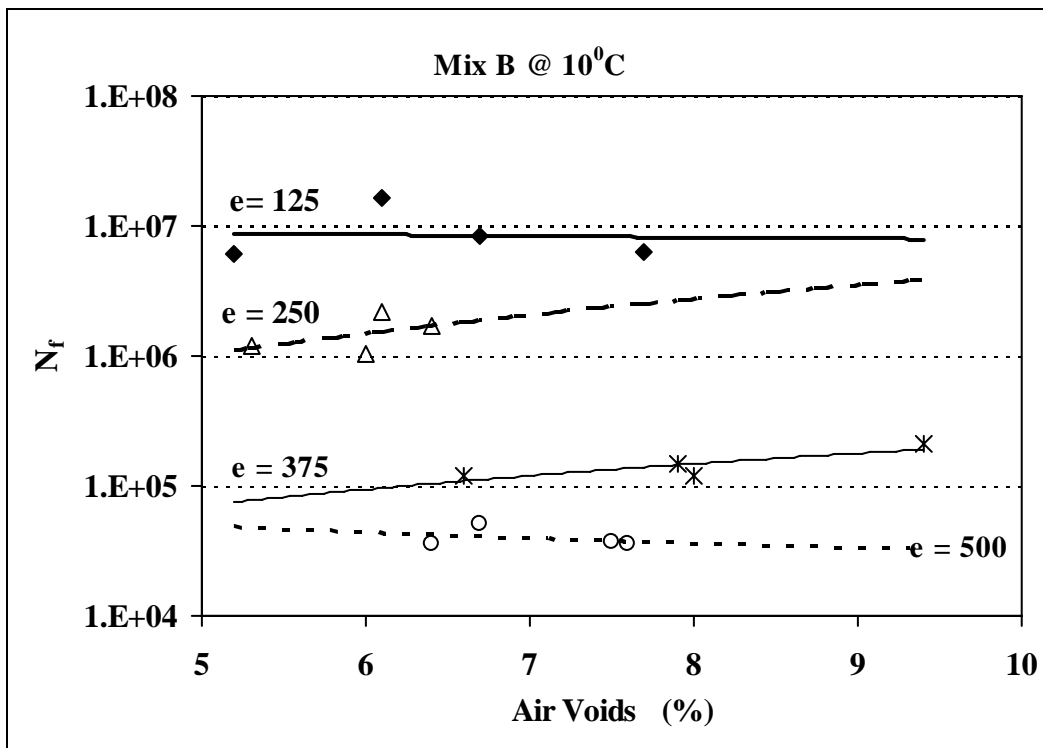
Figure 4.10 N_f vs. Air Voids for Temperature (10^0C) Corrected Stiffness for Mix B
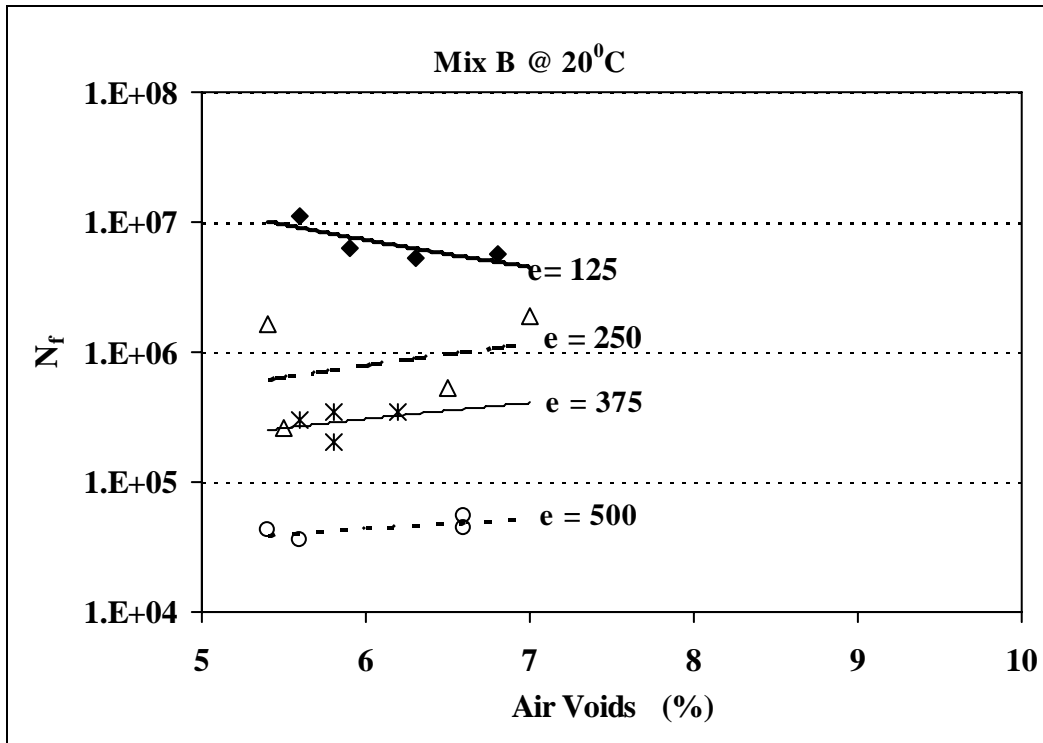
Figure 4.11 N_f vs. Air Voids for Temperature (20^0C) Corrected Stiffness for Mix B
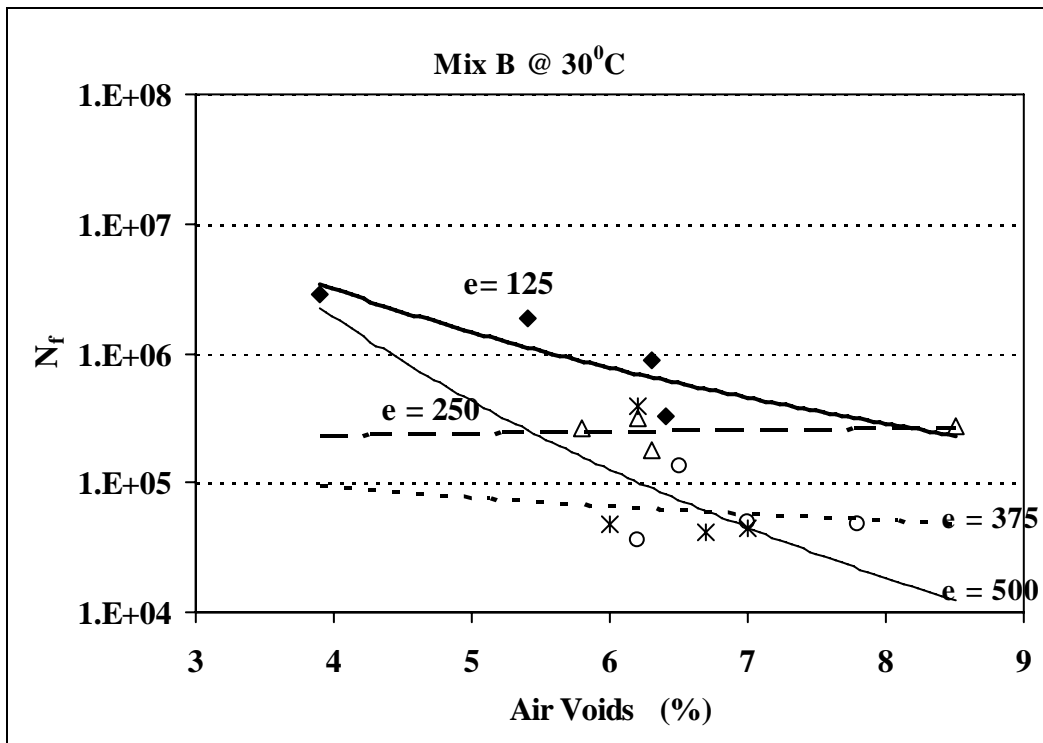
Figure 4.12 N_f vs. Air Voids for Temperature (30^0C) Corrected Stiffness for Mix B
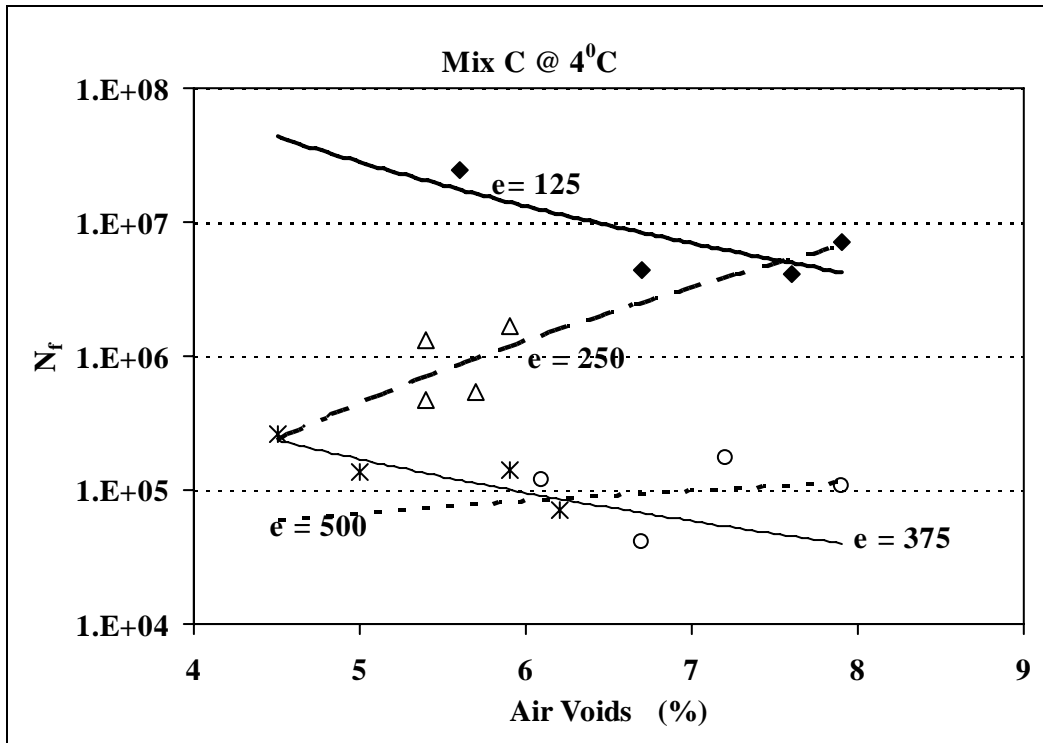
Figure 4.13 N_f vs. Air Voids for Temperature (4^0C) Corrected Stiffness for Mix C
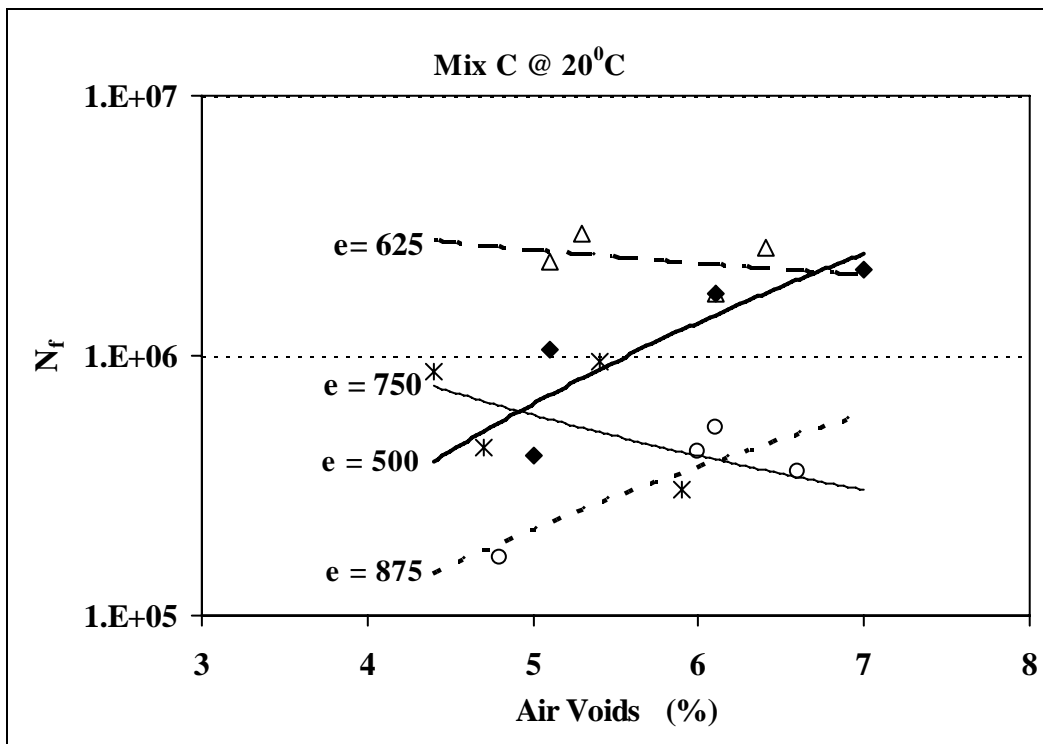
Figure 4.14 N_f vs. Air Voids for Temperature (20^0C) Corrected Stiffness for Mix C
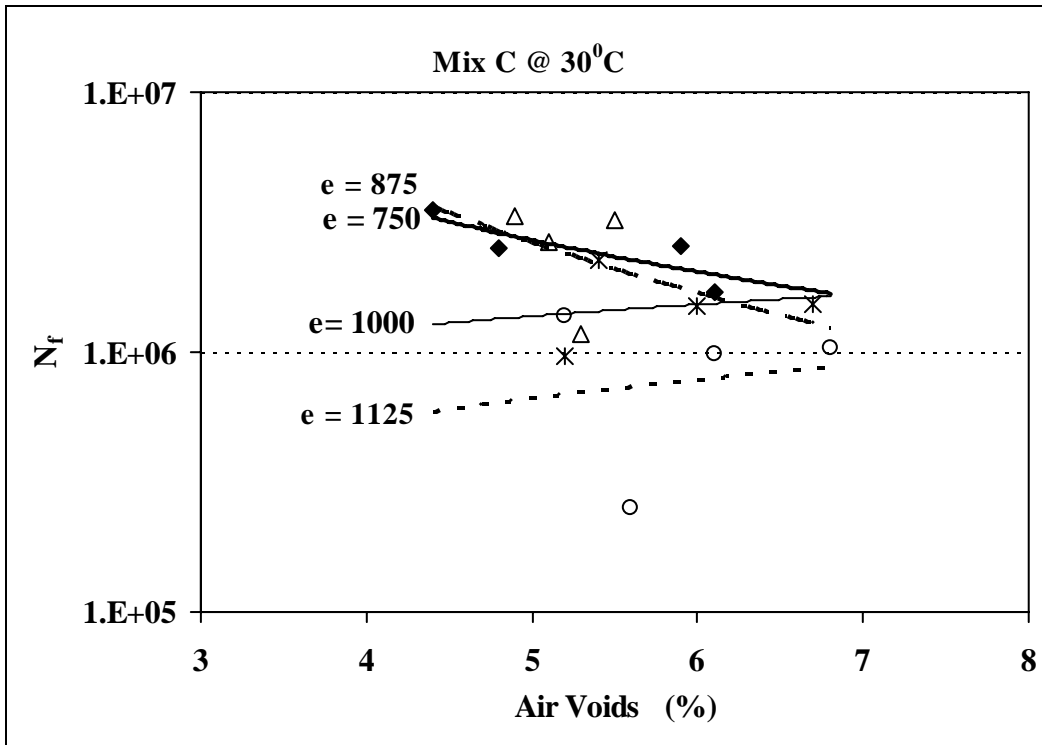
Figure 4.15 N_f vs. Air Voids for Temperature (30^0C) Corrected Stiffness for Mix C
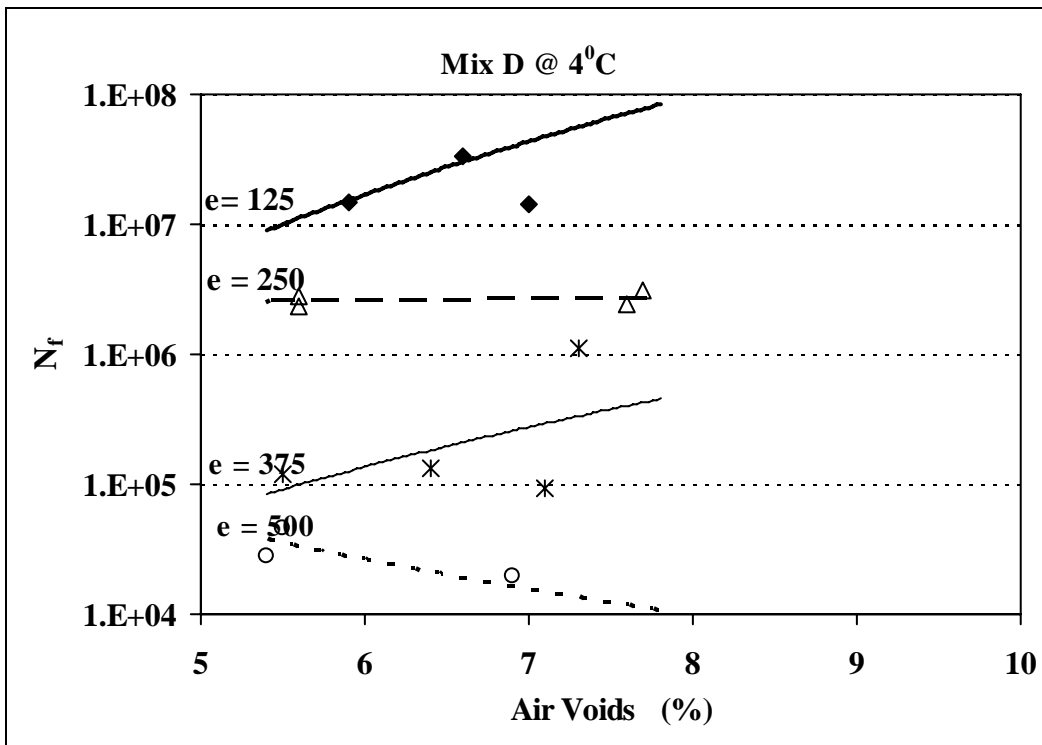
Figure 4.16 N_f vs. Air Voids for Temperature (4^0C) Corrected Stiffness for Mix D
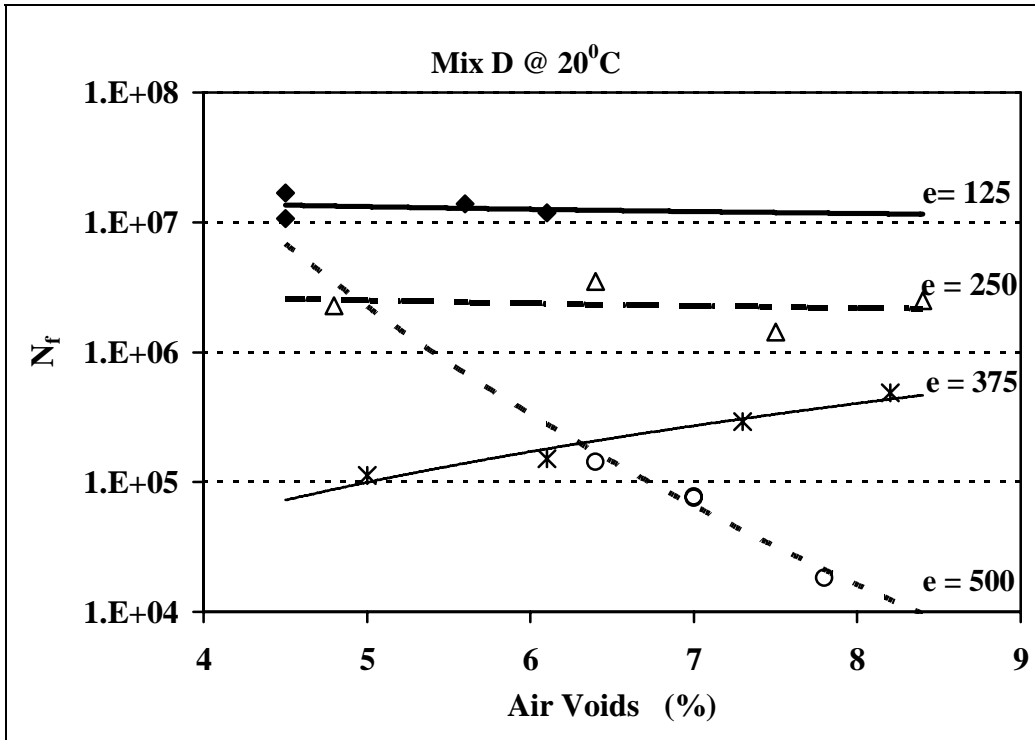
Figure 4.17 N_f vs. Air Voids for Temperature (20^0C) Corrected Stiffness for Mix D
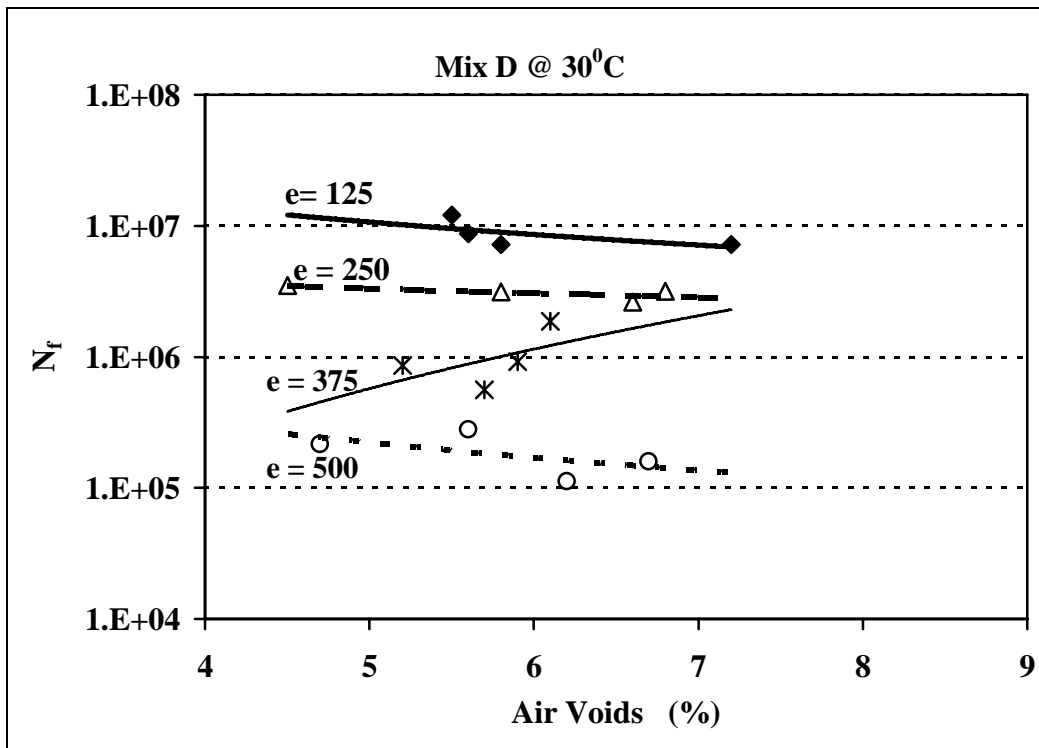
Figure 4.18 N_f vs. Air Voids for Temperature (30^0C) Corrected Stiffness for Mix D

4.1.2 Dynamic Resilient Modulus Test Results

The results are given in Appendix C for the dynamic modulus test, for each sample, load cycle and frequency. The average values of the dynamic resilient modulus at each temperature and loading frequency are summarized in Table 4.9. Figures 4.19 to 4.22 show, for all four mixes, the average dynamic resilient modulus versus temperature, at each frequency. The following conclusions can be drawn from Figures 4.19 to 4.22:

- Mix A had the highest dynamic modulus, followed by mix D and then by Mixes C and B.

- Mix A had a higher dynamic modulus than mix B, proving that the aggregate gradation and binder content affect the dynamic modulus value. This is true because, Mix A had different aggregate structure and binder content but the same binder grade as Mix B.

- Mixes B and C had the lowest and quite similar values for the dynamic modulus at all the frequencies. These two mixes had the same aggregate blend, the same binder content but different binder grade: PG 64-22 (Mix B) and PG70-28 (Mix D). Mix C contained polymer modified binder. Because of these factors it can be concluded that the higher binder grade and the presence of the polymer in the binder does not influence the dynamic modulus values. This may indicate that the gradation of the aggregate blend has a major influence on the dynamic modulus of asphalt concrete, while the binder grade, and thus binder viscosity, influence the modulus in lesser extend.

- For all four mixes and for the range of temperatures used, the loading variable that influenced the most the dynamic modulus was the temperature. A small variation in the testing temperature led to a significant change of the mixes characteristics. In the range of the loading frequency used, the loading frequency was the second most influential factor, followed by the percent air voids in the compacted mix.

Table 4.9 Average Dynamic Resilient Modulus

Frequency (Hz)	Temperature (°C)	Average Dynamic Modulus (MPa)			
		Mix A	Mix B	Mix C	Mix D
0.1	4	22,816	14,426	13,755	19,681
0.1	10	13,787	8,931	6,538	15,239
0.1	20	6,651	4,125	4,855	7,505
0.1	30	1,771	1,311	1,628	4,575
0.1	35	993	1,262	886	2,330
0.5	4	23,797	17,499	17,886	22,965
0.5	10	17,294	11,493	9,619	18,473
0.5	20	9,341	6,347	7,101	10,170
0.5	30	2,952	2,077	2,275	6,503
0.5	35	1,588	1,903	1,174	3,157
1	4	24,925	18,261	19,157	23,650
1	10	18,423	12,359	10,571	19,284
1	20	10,167	7,237	8,249	11,035
1	30	3,554	2,579	2,777	7,542
1	35	2,059	2,423	1,433	3,700
5	4	27,854	20,658	22,442	26,266
5	10	21,122	14,882	13,998	22,000
5	20	13,192	10,104	11,808	13,900
5	30	5,631	4,274	4,141	10,447
5	35	3,833	4,017	2,167	5,292
10	4	28,612	21,747	23,981	26,340
10	10	21,785	15,914	15,934	23,854
10	20	14,516	11,409	14,111	16,119
10	30	6,880	5,443	5,216	12,018
10	35	5,068	4,975	2,723	6,372
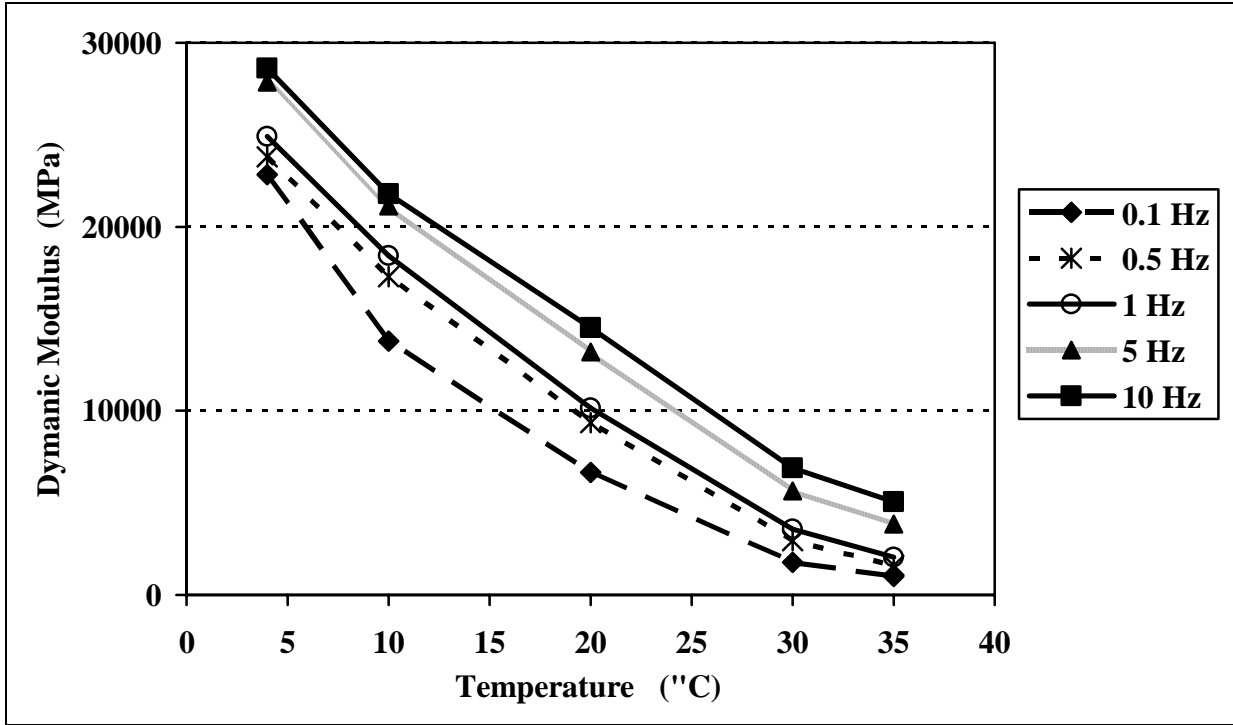
Figure 4.19 Average Dynamic Modulus for Mix A
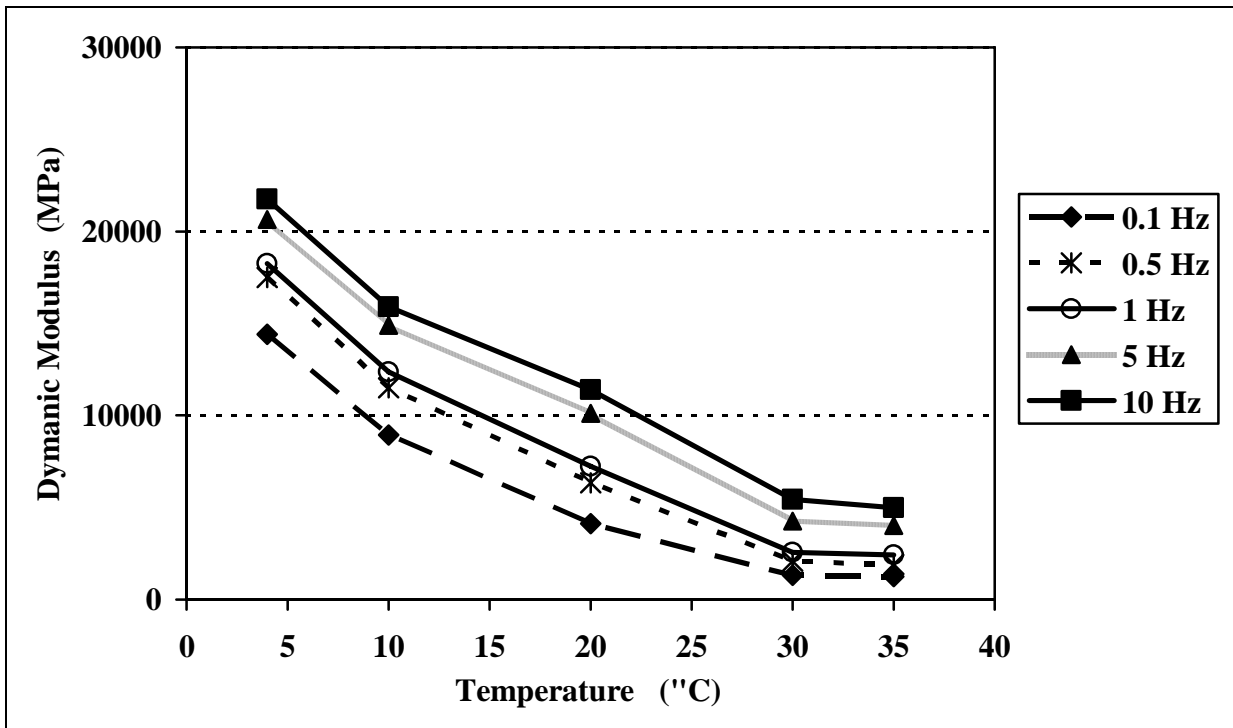
Figure 4.20 Average Dynamic Modulus for Mix B
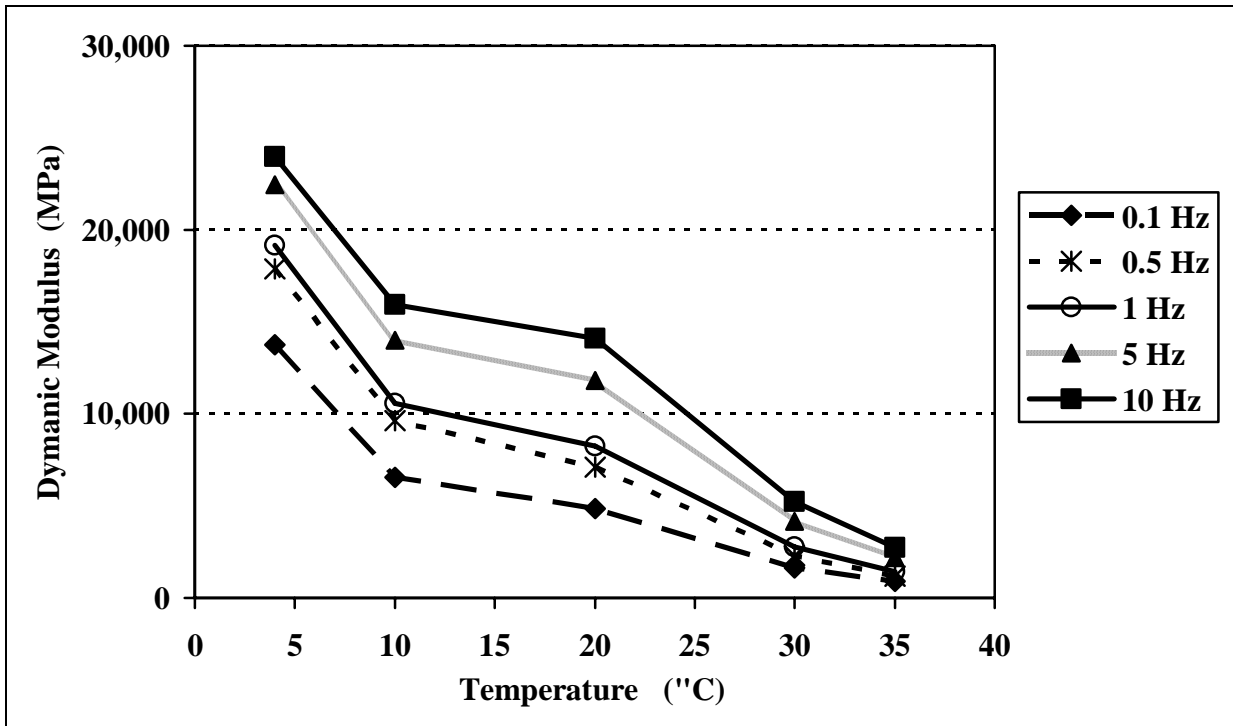
Figure 4.21 Average Dynamic Modulus for Mix C
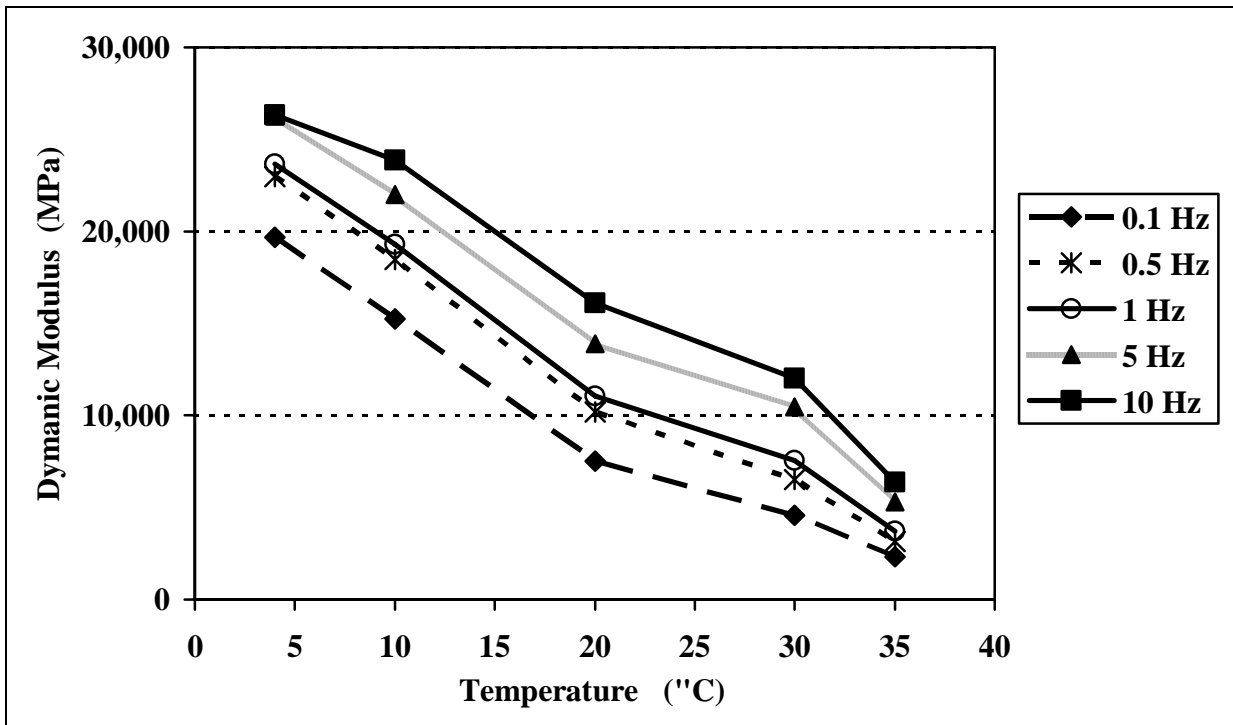
Figure 4.22 Average Dynamic Modulus for Mix D

4.2   Models Development and Validation

A multiple linear regression analysis was performed in order to identify the factors affecting the fatigue life, the bending stiffness of the asphalt beams and the dynamic modulus of the asphalt cylinders. The program used for the statistical analysis was SAS (Statistical Analysis System). The outputs of the analyzed data are presented in Appendix C.

In a multiple linear regression model, the dependent variable is related to a set of independent variables. The result is an equation that determines the best model by describing and explaining the existing data (Ott, 2001). In this research, for both the beam fatigue and dynamic modulus data, the parameters of the linear regression were calculated using a multiple regression analysis. The regression models were evaluated based on the following criteria:

- R^2 value: This value indicates the effectiveness of a regression model and how much of the variability of the dependent variable is explained by the independent variables (Ott, 2001).
- P-value or the level of significance for regression coefficients: It's an indication if the dependent variable corresponding to that regression coefficient has a significant effect on the independent variable. If the p-value is smaller than 0.05 it can assumed that the independent variable has a significant effect on the dependent variables. Independent variables with p-values (>0.1) may not be significant and may be removed from the linear model.

4.2.1   Beam Fatigue Model

A regression model of the following form (equation 4.1), relating the fatigue life expressed by the number of cycles to failure to the tensile strain and the initial stiffness was developed. It was considered that the number of cycles to failure, N_f, depends on percent air voids and asphalt content and it can be expressed with the following relationship:

$$\log N_f = a + b * (1 / e) + c * (1 / S) + d * (1 / AV) \tag{4.1}$$

where:

N_f = number of cycles to failure for temperature corrected (drop in the bending stiffness to 50% of the initial stiffness)

e = tensile strain (microstrain)

S = initial bending stiffness (MPa) for asphalt beams after temperature correction

AV = percent of air voids (%)

a, b, c, d = experimentally determined coefficients function of temperature

Individual relationships were developed for each of the three mixes at each test temperature. The coefficients a, b, c and d resulted from the regression analysis; p-values and the R^2 are presented in Table 4.10. From Table 4.10 the following can be inferred:

- The strain had a significant effect on the fatigue life for all mixes at all testing temperatures and with a slightly lower significant effect for Mix C at 20^0C.
- The initial stiffness had a significant effect for Mix A at 10^0C, Mix B at 10^0C and 30^0C, and Mix C at 4^0C.
- The air void content had a significant effect only for Mix B at 10^0C and 30^0C.
- At for Mix A at 10°C it was found that the fatigue life increases with the mix stiffness. This contradicts the common knowledge, that stiffer the mix, the lower the fatigue life.

Table 4.10 Regression Coefficients for the Beam Fatigue Model

Mix	4⁰C Coeff.	4⁰C p-value	10⁰C Coeff.	10⁰C p-value	20⁰C Coeff.	20⁰C p-value	30⁰C Coeff.	30⁰C p-value
A	a = 3.185 b = 444.2 c = 3591 d = 1.522	0.0126 <0.0001 0.6745 0.7684	a = 5.1 b = 306.7 c = -28873 d = 16.7	0.0310 <0.0001 0.0041 0.2096	a = -0.111 b = 307.9 c = 8.514 d = 21.5	0.9704 0.0003 0.0895 0.1903	a = 4.233 b = 273 c = 672 d = 1.4	0.0027 <0.0001 0.2834 0.8593
	$R^2 = 0.8966$		$R^2 = 0.9289$		$R^2 = 0.7016$		$R^2 = 0.8875$	
B	a = 2.18 b = 434.8 c = 10117 d = 3.93	0.2851 <0.0001 0.4837 0.4956	a = 0.32 b = 427 c = 14841 d = 10.9	0.7818 <0.0001 0.0087 0.0140	a = 2.1 b = 343.3 c = 6685 d = 1.86	0.2257 <0.0001 0.0866 0.7676	a = 1.889 b = 279.5 c = 2005 d = 6.5	0.0346 0.0001 0.0218 0.0354
	$R^2 = 0.9305$		$R^2 = 0.9304$		$R^2 = 0.8769$		$R^2 = 0.8501$	
C	a = 2.046 b = 947.3 c = 1362 d = 5.97	0.011 <0.0001 0.038 0.059	Not tested at 10°C		a = 4.88 b = 717.3 c = 391 d = -1.54	0.0551 0.0757 0.7729 0.8137	a = 2.922 b = 1375 c = 744 d = 3.94	0.0184 0.0051 0.0786 0.2109
	$R^2 = 0.9261$				$R^2 = 0.3712$		$R^2 = 0.5796$	
D	a = 4.772 b = 468 c = -5121 d = -2.31	0.145 <0.0001 0.840 0.778	Not tested at 10°C		a = 4.954 b = 376.4 c = -652 d = -2.51	<0.0001 <0.0001 0.490 0.548	a = 4.702 b = 246.8 c = 203.3 d = 1.96	0.001 0.001 0.840 0.664
	$R^2 = 0.8169$				$R^2 = 0.8355$		$R^2 = 0.7556$	

The model developed above can be further simplified if the temperature is not explicitly considered as an independent variable, but reflected thru its effects on bending stiffness. Also, the air voids can be eliminated as an independent variable. As indicated in Table 4.10, the air voids has no significant statistical effect on fatigue life, for most temperature and mix combinations.

The simplified fatigue model has the following form:

- linear model : $\log N_f = a + b * (1 / e) + c * (1 / S)$ (4.2)

- non-linear model : $N_f = a * (1 / e)^b * (1 / S)^c$ (4.3)

where:

N_f = number of cycles to failure for temperature corrected (drop in the bending stiffness to 50% of the initial stiffness)

e = tensile strain (mm/mm or in/in)

S = initial bending stiffness (MPa) for asphalt beams after temperature correction

a, b, c = experimentally determined coefficients

For each mix, separate linear and non-linear models were developed. The coefficients of the non-linear regression model were determined using the Microsoft Excel Solve algorithm. As expected, different coefficients were obtained for the linear and non-linear model. The coefficients are given in Table 4.11. Coefficient a changes if the bending stiffness, S, is measured in MPa or in psi.

Table 4.11 Regression Coefficients for the Simplified Beam Fatigue Model

	Mix A	Mix B	Mix C	Mix D
Non-Linear Model (Equation 4.3)				
If S is in MPa	$a = 7.362 \ 10^{-5}$ $b = 2.39$ $c = -0.477$ $R^2 = 0.6578$	$a = 1.987 \ 10^{-2}$ $b = 1.705$ $c = -0.511$ $R^2 = 0.734$	$a = 2.972 \ 10^{-7}$ $b = 6.6$ $c = 2.6876$ $R^2 = 0.904$	$a = 3.403 \ 10^{-2}$ $b = 1.623$ $c = -0.661$ $R^2 = 0.408$
If S is in psi	$a = 6.842 \ 10^{-6}$	$a = 1.562 \ 10^{-3}$	$a = 1.908 \ 10^{-1}$	$a = 1.268 \ 10^{-3}$
Linear Model (Equation 4.2)				
If S is in MPa	$a = -5.401$ $b = 3.641$ $c = 0.4721$ $R^2 = 0.821$	$a = -7.945$ $b = 3.474$ $c = -0.3182$ $R^2 = 0.849$	$a = -2.138$ $b = 4.684$ $c = 2.096$ $R^2 = 0.646$	$a = -6.808$ $b = 3.951$ $c = 0.3486$ $R^2 = 0.840$
If S is in psi	$a = -4.381$	$a = -8.633$	$a = 2.392$	$a = -6.055$

4.2.2 Dynamic Modulus Model

A simple linear model was developed for predicting dynamic modulus test. In the development of this model, the average dynamic modulus for the five cycles of loading at each frequency was computed. The linear regression model has the following form:

$$E = a + b * Frequency + c * Temp + d * AV \qquad (4.3)$$

where:

    E   = average dynamic modulus (MPa)

    Frequency   = testing frequencies (10, 5, 1, 0.5, 0.1 Hz)

    Temp   = testing temperature (4°, 10°, 20°, 30°, 35°C)

    AV   = percent of air voids (%)

The coefficients a, b and c resulted from the regression analysis, p-values and the R^2 are presented in Table 4.12.

Table 4.12 Results of the Dynamic Modulus Regression Model

Mix	Regression Coefficients	p-values	R^2
A	a = 47,503.8 b = 543.6 c = -758.5 d = -3,129.8	<0.0001 <0.0001 <0.0001 0.0404	0.859
B	a = 11,249.7 b = 508.5 c = -496.1 d = 828.4	0.2214 <0.0001 <0.0001 0.5152	0.759
C	a = -55,713.1 b = 594 c = -474.2 d = -5,610.6	<0.0001 <0.0001 <0.0001 <0.0001	0.771
D	a = -39866 b = 45,338.7 c = -530.9 d = -3,764.7	<0.0001 <0.0001 <0.0001 <0.0001	0.727

From Table 4.12 the following can be inferred:

- The temperature and the load frequency have a significant effect on all mixes tested.

- The air void content has a significant effect on dynamic modulus for all mixes except for Mix B.

CHAPTER 5

RELATIONS TO THE NCHRP PAVEMENT DESIGN MODEL

The *AASHTO Guide for the Design of Pavement Structures* is the primary document used currently by state highway agencies to design new and rehabilitated highway pavements. The Federal Highway Administration's 1995-97 National Pavement Design Review found that some 80% of the States make use of either the 1972, 1986, or 1993 AASHTO Pavement Design Guide. All those design guide versions employ empirical performance equations developed using AASHO Road Test data from the 1950's. The 1986 and 1993 guides contained some state-of-the-practice refinements in material input parameters and design procedures for rehabilitation design. In recognition of the limitations of earlier Guides, the AASHTO Joint Task Force on Pavements (JTFP) initiated an effort in the late 1990's to develop an improved Guide by the year 2002. The major long-term goal identified by the JTFP was the development of a design guide based as fully as possible on mechanistic principles.

The National Academy of Science through its NCHRP Program (specifically NCHRP Project 1-37A) has dedicated significant resources provided by the AASHTO member states to develop a user-friendly procedure capable of executing mechanistic-empirical design while accounting for local environmental conditions, local highway materials, and actual highway traffic distribution by means of axle load spectra. Since the resulting procedure is very sound and flexible and it considerably surpasses any currently available pavement design and analysis tools, it is expected it will be adopted by AASHTO as the new AASHTO design method for pavement structures. It is also expected that, in the future, the Kansas Department of Transportation will

adopt the new Mechanistic-Empirical design method to replace the 1993 AASHTO design method currently in use.

The products of the NCHRP Project 1-37A are the design software and the documentation supporting the design guide (NCHRP, 2004). They were released to the pavement engineering community in June 2004. For successful application of the new AASHTO design method to local conditions, this specific calibration strategy should address all main aspects of pavement performance and economic analysis: (1) characterization of pavement materials and soil, (2) traffic loading, (3) environment conditions, (4) field calibration, (5) design reliability, (6) alternative surface type consideration and (7) life cycle cost (LCC) analysis.

5.1   The NCHRP 1-37A Design Guide and Models for Flexible Pavements

5.1.1   General Framework of the Guide

The design approach followed by the Guide is divided into three major parts:

Part 1 consists of the development of input values for the analysis. A key step of this process is the foundation analysis. For new pavements, the foundation analysis consists of strength and stiffness determination and, where appropriate, the evaluation of volume change, frost heave, thaw weakening, and drainage concerns. As part of the foundation analysis, subgrade improvements such as strengthening and drainage are considered.

The foundation analysis for rehabilitation projects also includes a subgrade analysis. However, the most important part of the foundation analysis for rehabilitation projects is the investigation of distress types occurring in the existing pavements and the underlying causes of those distresses. The overall strength/stiffness of the existing pavement is evaluated using deflection testing and back-calculation procedures.

Also during the first stage, pavement materials characterization and traffic input data are

developed. The FHWA Integrated Climate Model is used to develop climatic inputs for the foundation and materials analysis and the pavement response analysis in Part 2.

In the NCHRP 1-37A model, traffic is considered in terms of axle load spectra. The full spectra for single, tandem, tridem, and quad axles is considered.

Part 2 of the design process is the structural/performance analysis. After the pavement structure or rehabilitation alternative is selected, a structural model that employs the input data prepared in Part 1 is used to estimate pavement response. The structural model for flexible pavement design is the JULEA linear elastic pavement model.

The pavement response computed in critical locations in the pavement structure is then used to estimate pavement performance. The performance is expressed by the evolution of major distresses in time. The distresses considered for new flexible pavement structures are: rutting, load associated cracking, temperature associated cracking and roughness of the longitudinal profile. Roughness is considered as a derivative distress; it is computed from the magnitude of rutting and cracking and not directly from pavement response data. The concept of reliability is introduced when the evolution of distresses are estimated. They are computed based on probabilistic reliability levels and typical standard deviations for each distress type.

The final version of the Guide does not allow automatic iterative adjustments of the design alternative if the performance criteria are not satisfactory. The user needs to modify the design pavement structural alternative and to rerun the software.

Part 3 of the process was planned to contain those activities required to evaluate the technically viable alternatives: an engineering analysis and life cycle cost analysis of the alternatives. Unfortunately, this part is not included in the final version of the NCHRP1-37A design software, even though in the initial stages of the development of the Guide, it was

intended to do so. The user needs to successively select technical viable alternatives and to compute pavement performance for each alternative. The pavement performance data obtained from the runs on different alternatives need to be fed in a life cycle coast analysis. This will lead to the final selection of the optimum design solution.

5.1.2 The Hierarchical Design Approach

The NCHRP 1-37A design model uses a hierarchical design approach. Such an approach provides the designer with several levels of "design efficiency" that can be related to the class of highway under consideration or to the level of reliability of design desired. A chosen higher level of design output implies that the inputs also will be of a higher level. The hierarchical approach is employed with regard to traffic, materials, and environmental inputs and in some cases to the types of analyses used.

While there are many variations throughout the guide where as few as two levels or as many as four are available, the general approach is to provide for three levels. Within the three levels there also are variations, but generally the features of each level are (McGhee, 2004):

Level 1 - Level 1 is a "first class" or advanced design procedure and provides for the highest practically achievable level of reliability. It typically would be used for design in the heaviest traffic corridors or wherever there are dire safety or economic consequences of early failure. The design inputs also are of the highest practically achievable level and generally require site specific data collection and/or testing. Examples are dynamic modulus testing of asphalt concrete and site specific axle load spectra.

Level 2 - Level 2 is the standard design procedure expected to be used for routine design. Level 2 inputs typically would be user selected possibly from an agency database, would be derived from a less than optimum testing program, or would be estimated empirically. Examples would be dynamic modulus estimated from binder, aggregate, and mix properties or site-specific traffic volume and

classification data used in conjunction with agency specific axle load spectra.

Level 3 - Level 3 typically is the lowest class of design and would be used where there are minimal consequences of early failure and on lower volume roads. Inputs typically would be user selected default values.   Examples would be default dynamic modulus values for given mix classes or default axle load spectra for functional highway classes.

5.1.3 *Pavement Materials Characterization*

Materials characterization guidelines are provided so the designer can develop appropriate materials property inputs for use in the analysis portion of the design process. The materials parameters needed for the design process may be classified in one of three major groups:

- Pavement response model materials inputs
- Materials related pavement distress criteria
- Other materials properties.

Pavement response model material inputs related to the moduli and Poisson's ratio used to characterize layer behavior within the specific model. Bound materials such as AC, PCC, and high-strength stabilized bases generally display a linear or nearly linear stress-strain relationship. Unbound materials such as granular materials and fine-grained soils display stress dependent properties. Coarse granular materials generally are "stress hardening" and show an increase in modulus with an increase in stress. Fine-grained soils generally are "stress softening" and display a modulus decrease with increased stress. Modulus-stress state relations have been developed for granular materials and for fine-grained soils. In practice, assumed Poisson's ratio values are acceptable for routine mechanistic-empirical pavement design based on isotropic elastic structural analysis models. This is true because the parameter has well defined limits for specific

77

materials types and because the stress, strain, and displacement outputs of the response model are not particularly sensitive to the parameter.

Materials parameters associated with pavement distress criteria normally are linked to some measure of material strength (shear strength, compressive strength, modulus of rupture, etc.). The "other" category of materials properties constitutes those associated with special properties required for the design solution. Examples of this category are the thermal expansion and contraction coefficients of both Portland cement concrete and asphalt mixtures.

5.1.4   Classes of Materials and Levels of Materials Characterization

In the NCHRP 1-37A design model, all flexible pavement materials have been classified in one of the following categories:

- Hot mix asphalt - dense graded (HMAC)
- Open graded asphalt treated materials (ATPB)
- Cold mix asphalt (CMA)
- Cementitious Stabilized Materials (CTB,CSB,CTPB)
- Non-Stabilized Granular Base/Subbase (AB,GAB,CA)
- Subgrade Soils
- Bedrock

In keeping with the hierarchical approach materials characterization is comprised of three levels with Level 1 indicative of a design approach philosophy of the highest practically achievable reliability and Levels 2 and 3 of successively lower reliability. The details of hierarchical characterization are given in the materials characterization section of the NCHRP 1-37A model (NCHRP, 2004). However, a general tabulation of elastic modulus characterization methods is given in Table 5.1.

Table 5.1 Characterization of Materials Modulus of Elasticity

Material	Level 1	Level 2	Level 3
Asphalt Concrete	Measured Dynamic Modulus	Estimated Dynamic Modulus from binder viscosity and gradation data	Default Dynamic Modulus
Stabilized Materials	Measured Elastic Modulus	Estimated Elastic Modulus from chemical content and soil type	Default Elastic Modulus
Granular Materials	Measured Resilient Modulus	Estimated Resilient Modulus from gradation data	Default Resilient Modulus
Subgrades	Measured Resilient Modulus	Estimated Resilient Modulus from gradation and plasticity data or soil classification data	Default Resilient Modulus

5.1.5   Prediction Model for the Dynamic Modulus of HMA Mixes

The accurate prediction of the dynamic modulus of HMA represents a key factor in the structural design of flexible pavements, since it has a significant influence on the pavement response. The equation for predicting dynamic modulus, popularly known as the Witczak equation is:

$$\log|E*| = -1.249937 + 0.029232 P_{200} - 0.001767 (P_{200})^2 + 0.002841 P_4 - 0.058097 V_a$$

$$-0.802208 \frac{V_{beff}}{(V_{beff}+V_a)} + \frac{[3.871977 - 0.0021 P_4 + 0.003958 P_{38} - 0.000017 (P_{38})^2 + 0.00547 P_{34}]}{1+e^{(-0.603313-0.313351 \log f -0.393532 \log \eta)}} \qquad (5.1)$$

where,

E = Asphalt Mix Dynamic Modulus, in 10^5 psi

η = Bitumen viscosity, in 10^6 poise (at any temperature, degree of aging)

f = Load frequency, in Hz

V_a = percent air voids in the mix, by volume

V_{beff} = effective bitumen content, by volume, in percent

P_{200} = percent passing the No. 200 sieve, by total aggregate weight

P_{34}, P_{38}, P_4 = cumulative percent retained on the ¾ inch sieve, the 3/8 inch sieve and the No. 4   sieve, by total aggregate weight

The equation was derived based on a database of 2,750 dynamic modulus measurements obtained from 205 different asphalt mixtures (Table 5.2).

Table 5.2 Statistic Summary of the Dynamic Modulus Prediction Equation

Statistic	Value
Goodness of fit	$R^2=0.96$ Se / Sy = 0.24
Data Points	2,750
Temperature Range	0 to 130°F
Frequency Range	0.1 to 25Hz
Mixtures	205 (171 with unmodified asphalt binder and 34 with modified binders)
Binders	23(9 unmodified and 14 modified)
Aggregates	39
Compaction Methods	Kneading and Gyratory Compaction
Specimen Sizes	Cylindrical 4x8 in or 2.75x5.5 in

The viscosity of the binder at the temperature for which the dynamic modulus is computed is estimated with the following equation:

$$\log[\log(\eta)] = A + VTS * \log(T) \tag{5.2}$$

where:

η = Bitumen viscosity, in 10^6 poise (at the desired temperature)

T – temperature (in Rankine)

The coefficients of the viscosity model, A and VTS, are determined by regression analysis from binder viscosity data measured at no less than five temperatures. The NCHRP Guide recommends a set of default values of A and VTS for each binder grade.

5.1.6   Structural Response Models for Flexible Pavements

Adequate structural modeling of flexible pavement structures is the heart of a mechanistic-based design procedure. Structural response models are used to compute critical stresses, strains, and displacements in flexible pavement systems due to both traffic loads and climatic factors (temperature and moisture). These responses are then utilized in damage model to accumulate damage, month by month, over the entire design period. The accumulated damage

at any time is related to specific distresses such as fatigue cracking, which is then predicted using a field calibrated cracking model (the main empirical part of a mechanistic-empirical design procedure).

The structural models selected for use in the NCHRP 1-37A design model for flexible pavements include the multi-layer elastic system (JULEA code for linear elasticity). If the user opts to use the Level 1 hierarchical approach to characterize the non-linear moduli response of any unbound layer materials (bases, subbases and/or subgrades), then a 2-D finite element system (non-linear unbound materials) code (DSC2D) can be used. The structural response models require several inputs:

- Traffic loading
- Pavement cross-section
- Poisson's ratio each layer
- Elastic modulus each layer
- Thickness each layer
- Coefficient of thermal expansion (for AC)

Given these inputs the structural models produce stresses, strains, and displacements at critical locations in the pavement and subgrade layers.

This design procedure is the first to include the capability to accumulate damage on a monthly basis over the entire design period. This approach attempts to simulate how pavement damage occurs in nature, incrementally, load by load, over continuous time periods. By accumulating damage monthly, the design procedure becomes very versatile and comprehensive. This approach allows the use of elastic moduli within a given time period, such as a month, that are representative of that time increment. Thus, in the heat of summer, the dynamic modulus of AC is much lower than in the cold of winter. The resilient modulus of an unbound base course

and of the fine-grained subgrade can vary with moisture content. This procedure also allows for the aging of paving materials. For example, AC materials age with time, increasing their stiffness. This is modeled so that the E of the AC is constantly increasing over time. It is believed that the added capabilities that incremental damage gives far outweigh its main disadvantage of computation time and the inclusion of aging models for paving materials.

5.1.7   Models for Load Associated Cracking

The NCHRP 1-37A pavement design model (NCHRP, 2004) contains models for predicting load associated cracking. The repeated vehicle loads induce tensile stresses in the bound layers. Under repeated loadings, fatigue cracks initiate at locations where the largest tensile strains and stresses develop. The location of these critical points depends on many factors like the structural configuration of the pavement, the stiffness of the layers and the configuration of the wheel load (area of distribution, magnitude of stresses at the tire-pavement interface). After the cracking initiation at critical locations, the repeated traffic effect causes the cracks to propagate through the entire layer. These cracks allow water infiltration thereby reducing the overall performance of the pavement.

Most pavement structural models assume that cracks initiate at the bottom of the asphalt concrete surface layer and then propagate upward. These cracks are named bottom-up fatigue cracks. The NCHRP 1-37A Guide considers the alligator cracking as bottom-up fatigue cracking. In addition to the conventional bottom-up type fatigue cracking, top-down cracking is also taken into account. The NCHRP 1-37A Guide considers longitudinal cracks in the wheel path as top-down cracks. Even though there is no consensus on the cause for the formation of top-down cracking, there is extensive evidence for their existence.

82

The NCHRP 1-37A model adopted Miner's law to estimate fatigue damage:

$$D = \sum_{i=1}^{T} \frac{n_i}{N_i}$$

where,

D = damage.

T = total number of periods.

n_i = actual traffic for period i.

N_i = allowable repetitions to failure under conditions prevailing in period i.

The most commonly used model to predict the number of repetitions to fatigue cracking is a function of tensile strain and mix stiffness. The final relationship used for predicting the number of repetitions to fatigue cracking is the Asphalt Institute Model that is based on constant stress criterion. The final fatigue model used in the design guide obtained by numerical optimization and other modes of comparison is as below:

$$N_f = 0.00432 \ * \ k_1^{'} \ * \ C \ (1/\varepsilon_t)^{3.9492} \ (1/E)^{1.281}$$

where:

$C = 10^M$ and $M = 4.84*[V_b / (V_a+V_b) - 0.69]$

V_b = effective binder volumetric content (%).

V_a = air voids (%).

The parameter $k_1^{'}$ was introduced to account for different asphalt layer thicknesses and is given by below for bottom-up cracking. The parameter $k_1^{'}$ is very close to 250 for asphalt layer thicknesses equal or above five inches.

$$k'_1 = \cfrac{1}{0.000398 + \cfrac{0.003602}{1 + e^{(11.02-3.49*h_{ac})}}}$$

(5.5)

For top-down cracking, k'_1 is given by:

$$k'_1 = \frac{1}{0.01 + (12.00/1 + e^{(15.676-2.8186*h_{ac})})}$$

(5.6)

Finally, the transfer functions to estimate fatigue cracking from fatigue damage are expressed as in the equations below for bottom-up and top-down cracking respectively.

Bottom-up cracking

$$F.C. = \left(\frac{6000}{1 + e^{(C_1*C_1+C_2*C'_2*\log10(D*100))}} \right) * \left(\frac{1}{60} \right)$$

(5.7)

Where:

F.C=bottom-up fatigue cracking, percent lane area

D= bottom-up fatigue damage

C1 = 1.0

C2 = 1.0

C'1= -2 * C'2

C'_2= -2.40874-39.748*$(1+h_{ac})^{-2.856}$

Top-down cracking

$$F.C. = \left(\frac{1000}{1 + e^{(7-3.5*\log10(D*100))}} \right) * 10.56$$

(5.8)

where,

FC= top-down fatigue cracking, ft/mile

D= top-down fatigue damage

The fatigue cracking model for asphalt concrete was calibrated based on data from 82 LTPP sections located in 24 states, using 441 observations for alligator cracking and 408 data points for longitudinal cracking. The bottom-up cracking is calculated as a percentage of lane area while the longitudinal cracking is expressed in terms of linear feet per mile of pavement. An important observation made during the calibration process was that for all levels of asphalt thickness the alligator cracking increases with decreasing subgrade modulus. It was also observed that the impact of subgrade support upon alligator cracking is directly dependent on the thickness of HMA layer, and that the greatest potential for damage is observed for asphalt layers with thickness in the range of 3 to 5 inches.

The fatigue damage reduces below the maximum cracking level in the range of 3 to 5 inches because at the bottom of very thin HMA layers little or no tensile stresses or strains develop. Pavements with thin HMA layers exhibit rutting failure in the foundation layers before exhibiting fatigue cracking in the asphalt concrete layers.

5.2. Comparison between the Research Findings and the Models Included in the NCHRP Design Guide

5.2.1   Comparison of Predicted and Measured Dynamic Modulus for HMA

Since the dynamic modulus tests were performed on four representative Kansas Superpave HMA mixes at several temperature and load frequencies, and the composition and volumetric characteristics are known, it is important to compare the measured dynamic moduli with the values predicted by the Witczak equation (Equation 5.1). For Level 3 design of flexible

pavement structures, the Witczak equation is used to predict the dynamic modulus of the asphalt mix, as a function of loading frequency, the viscosity of the binder, gradation of the aggregates and volumetric properties.

Figures 5.1, 5.3, 5.5 and 5.7 plot the predicted dynamic modulus of the four mixes versus the average measured dynamic modulus, for five loading frequencies and five temperatures. The estimation of the binder viscosity was done using the default values recommended by the NCHRP Guide for binders with the same grades as those used in mix preparation. The prediction of the dynamic modulus using the Witczak equation was done using the mix composition (Table 3.1), the aggregate gradation data (Table 3.2) corresponding to each mix. The air voids contents measured on each individual sample was considered in the calculation of predicted dynamic moduli.

Figures 5.2, 5.4, 5.6 and 5.8 plot the predicted dynamic modulus of the four mixes versus the average measured dynamic modulus, for five temperatures and the loading frequency of 10 Hz. This frequency was the highest used in the dynamic modulus testing The moduli measured at this frequency reflect the best the moduli the NCHRP Guide would estimate for the design of a flexible pavement at a design vehicle speed of more than 20mph.

Figures 5.1 to 5.8 suggest the following conclusions regarding the comparison between estimated and predicted dynamic moduli:

- For Mix A, the ratio between the measured and the predicted dynamic modulus is between 1.0 and 4.5, with an average ratio close to 3.0. For the loading frequency of 10Hz, the ratio is between 1.0 and 2.0, with an average ratio close to 1.5.
- For Mix B, the ratio between the measured and the predicted dynamic modulus is between 0.5 and 2.5, with an average ratio close to 1.33. For the loading frequency of 10Hz, the ratio is between 0.9 and 2.6, with an average ratio close to 1.5.

- For Mix C, the ratio between the measured and the predicted dynamic modulus is between 1.0 and 3.0, with an average ratio close to 1.8. For the loading frequency of 10Hz, the ratio is between 1.0 and 3.0, with an average ratio close to 1.8.

- For Mix D, the ratio between the measured and the predicted dynamic modulus is between 1.2 and 3.2, with an average ratio close to 1.5. For the loading frequency of 10Hz, the ratio between the measured and the predicted dynamic modulus is between 1.2 and 3.2, with an average ratio close to 1.5. The moduli values measured on one sample tested at 4°C were much lower than those measured on the other samples (see Table C4). Therefore, the sample was considered an outlier and the values obtained for it were not plotted.

- For all mixes, the range of the ratio between the measured and the predicted dynamic modulus was about the same no matter the testing temperature.

- In the Witczak equation, the standard error for the estimation of $\log(E^*)$ is 0.24 (see Table 5.2). Therefore, from the accuracy of the model itself, there is a 66 percent probability to have the ratio of the real dynamic modulus and the predicted dynamic modulus between 0.575 and 1.738. The ratios for the four Kansas Superpave mixes are in many cases outside of this range; ratios greater than 2.0 were not uncommon. This indicated that the Witczak equation severely under-predicts the dynamic modulus of the four mixes. This leads to significant over-predictions of pavement distresses, when the NCHRP design software is used for the design of pavements structures that have layers built with Kansas Superpave mixes.
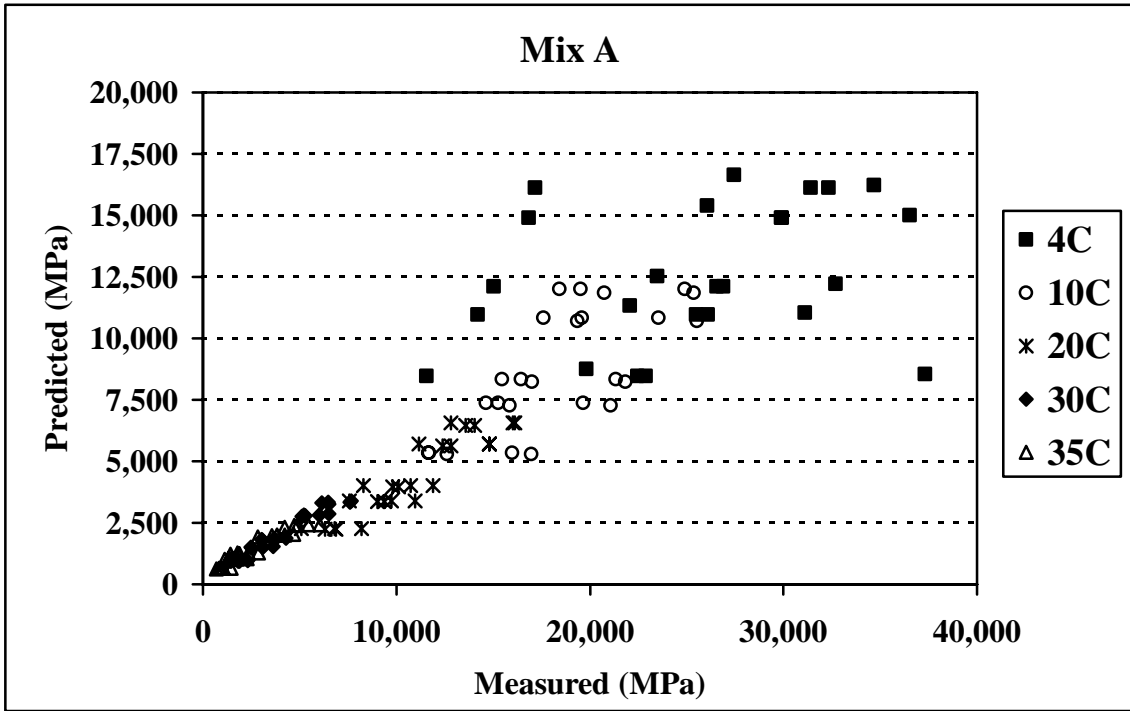
Figure 5.1 Predicted vs. Measured Dynamic Modulus – Mix A
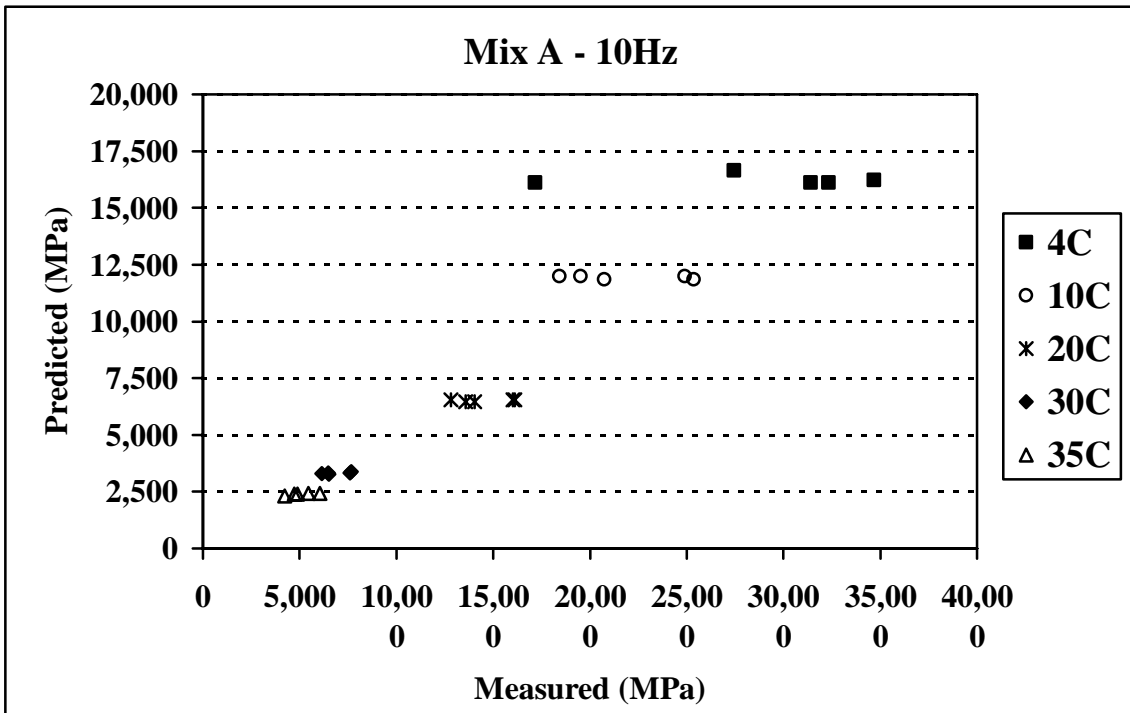
Figure 5.2 Predicted vs. Measured Dynamic Modulus at 10 Hz – Mix A
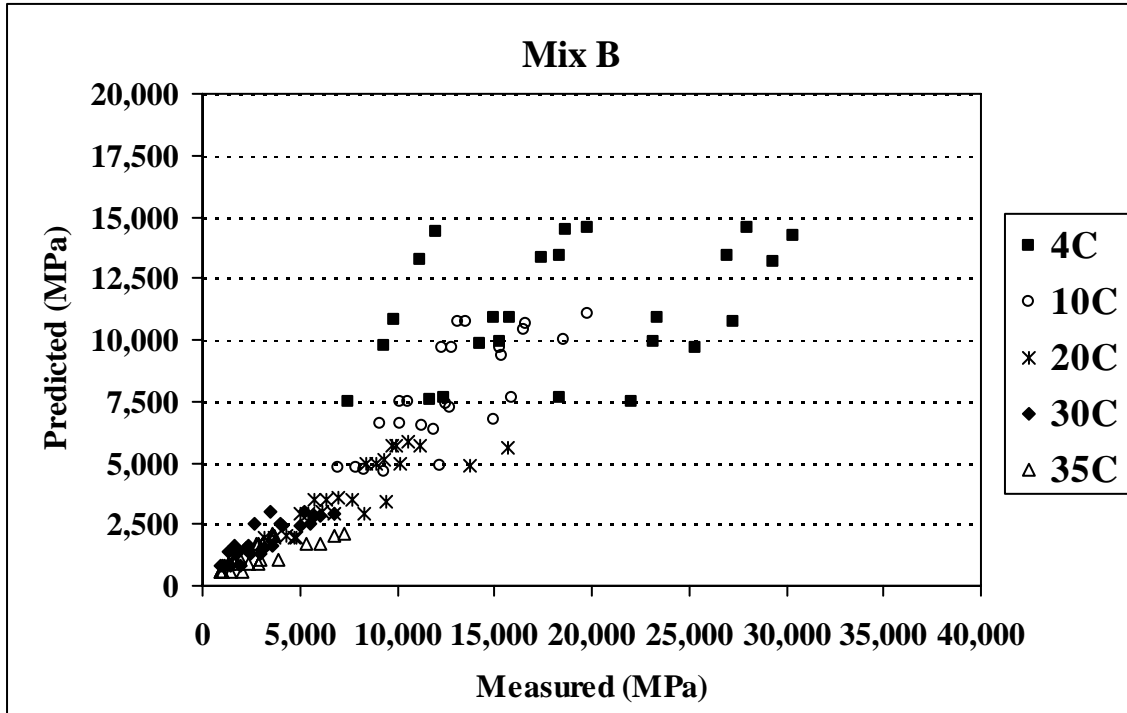
Figure 5.3   Predicted vs. Measured Dynamic Modulus – Mix B
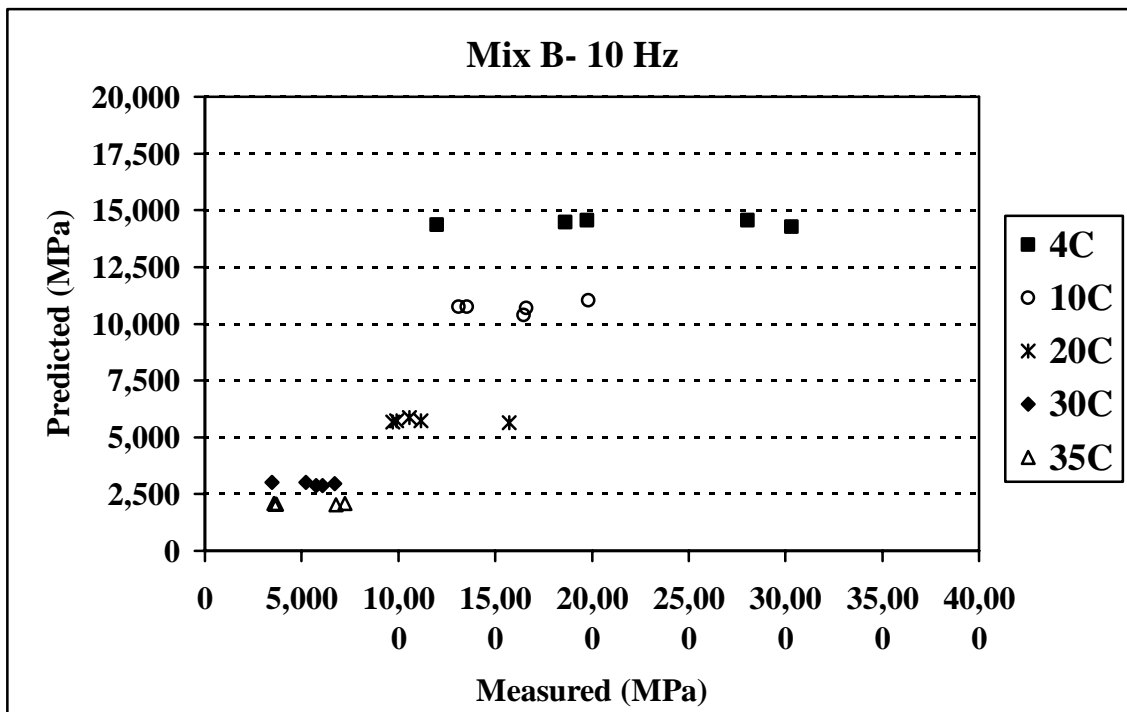
Figure 5.4   Predicted vs. Measured Dynamic Modulus at 10 Hz – Mix B
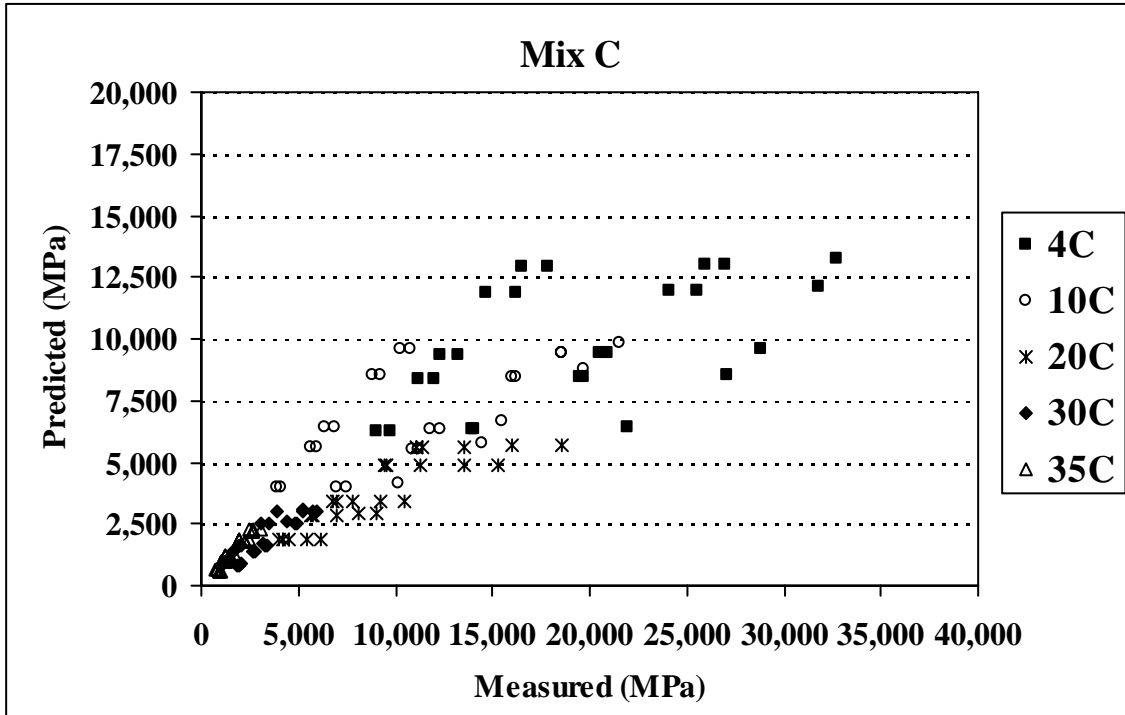
Figure 5.5 Predicted vs. Measured Dynamic Modulus – Mix C
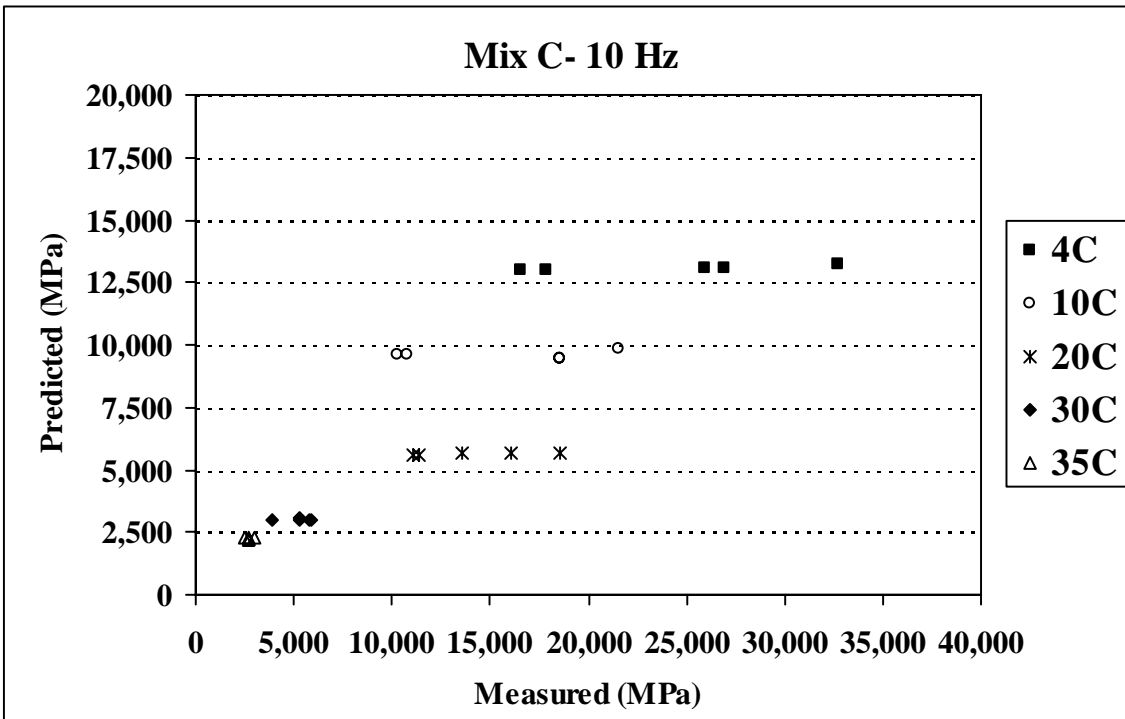
Figure 5.6 Predicted vs. Measured Dynamic Modulus at 10 Hz – Mix C
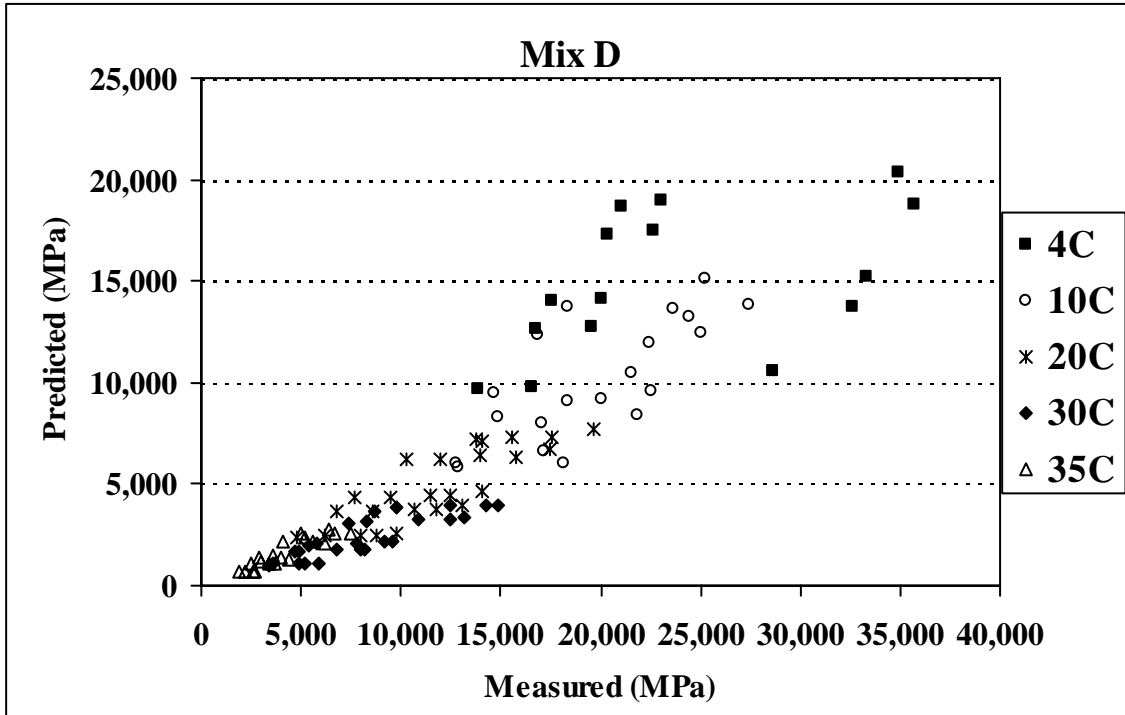
Figure 5.7 Predicted vs. Measured Dynamic Modulus – Mix D
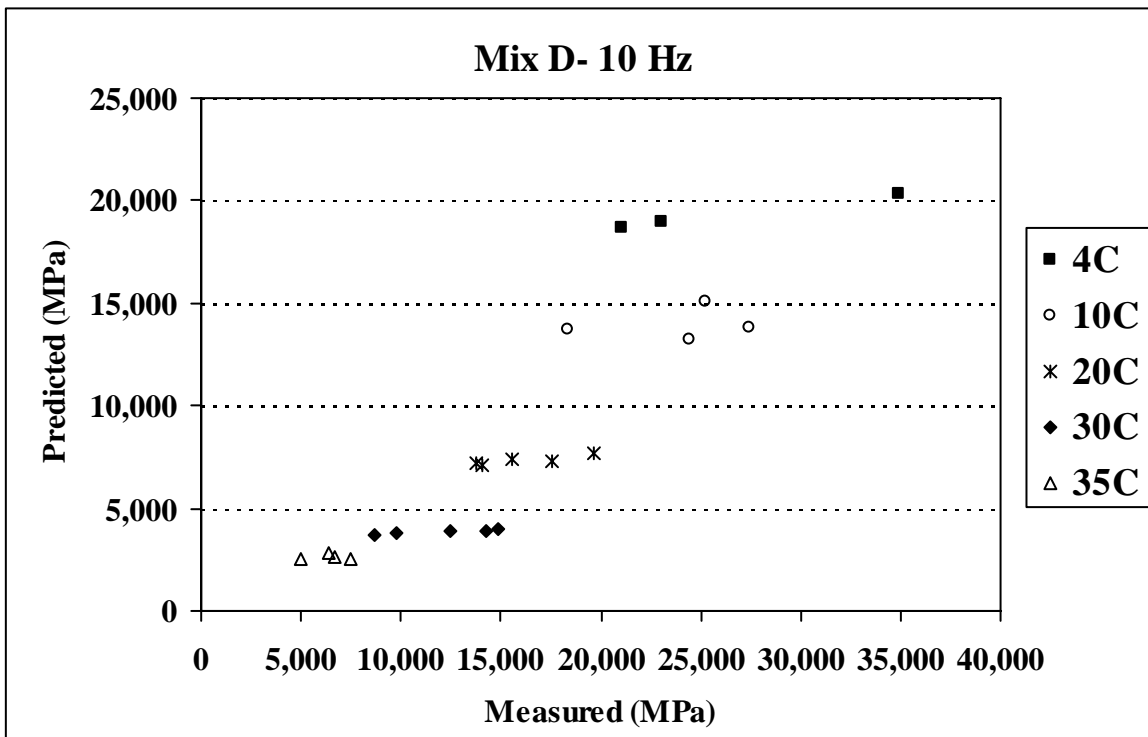
Figure 5.8 Predicted vs. Measured Dynamic Modulus at 10 Hz – Mix D

91

5.2.2 Comparison of Dynamic Modulus and Bending Stiffness of HMA

Since the beam fatigue and dynamic resilient modulus tests were performed on the same mixes, compacted at very similar densities and air void contents and at the same temperatures, it is important to compare their corresponding values, because the NCHRP Design Guide assumed that dynamic modulus and bending stiffness are equal (NCHRP,2004).

Figure 5.9 presents the comparison between the initial bending stiffness computed as average for the four replicates tested at the same strain level, and the average dynamic resilient modulus measured at the corresponding temperature and at 10Hz, the same frequency the beam fatigue tests were performed. The figure indicates that, for all mixes tested, the dynamic modulus values are more than two times higher than the bending stiffness. The ratio was the highest for Mix C, which contained polymer modified binder.
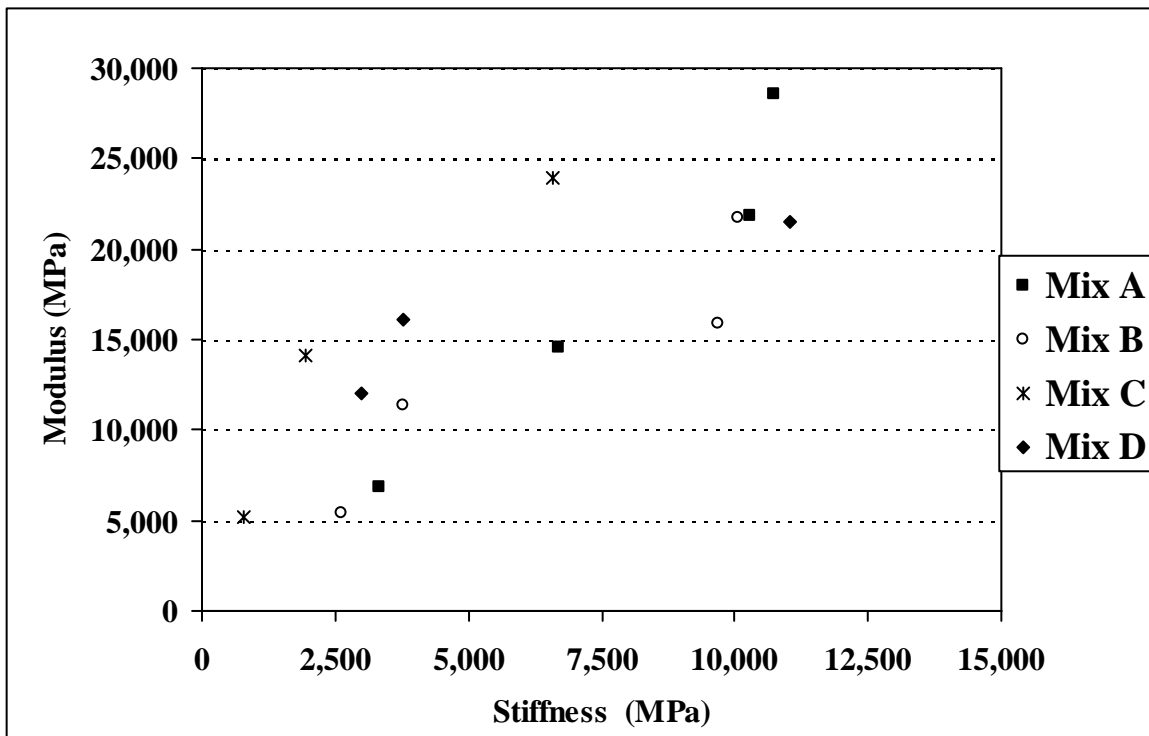
Figure 5.9 Dynamic Modulus vs. Bending Stiffness at 10 Hz

It is important to note that, for each beam fatigue test, the initial bending stiffness is the value recorded after 200 cycles of sinusoidal load applications. The initial bending stiffness is always lower that the stiffness measured for the first load application. The dynamic modulus values are recorded for each sample, at each of the five test frequencies, as the average value for the last five of the first 100 cycles of load application. However, the difference in the number of applications for which the modulus and stiffness are recorded cannot explain the large differences between modulus and stiffness.

5.2.3   *Comparison of Fatigue Life Models*

The beam fatigue tests conducted in this research allowed the derivation of fatigue life models for each of the four Kansas Superpave mixes studied. A comparison between the life predicted by these models (Equations 4.2 and 4.3) and the life predicted by the NCHRP fatigue life model (Equation 5.4) must be done in order to determine if the NCHRP model can accurately predict the life of the studied mixes. The comparison is possible since the models have similar form and, all models, including the NCHRP model, were obtained from the results of strain controlled beam-fatigue tests in which failure was considered as the number of cycles for which the bending stiffness drops to half of its initial value.

Figures 5.10 to 5.13 plot the predicted fatigue life for each mix, in number of cycles to failure, by the NCHRP model (Equation 5.4), the linear model (Equation 4.2) and the non-linear model (Equation 4.3). The prediction is done for the same mix stiffness of 500,000 psi (3,450MPa) and for strains between 75 and 100 microstrain. It is important to note that the fatigue lives predicted by the NCHRP model are different because the C coefficient, which depends on mix volumetric properties, is different for each mix. The k_1' coefficient in the NCHRP model was considered as equal to 250 for all four mixes.

Figures 5.10 to 5.13 suggest the following conclusions regarding the comparison between fatigue lives predicted by the three models:

- For all four mixes, the lines for the NCHRP model and the linear model are close to parallel. This indicates that the ratio between the lives predicted by the NCHRP and linear models is significantly less influenced by the strain level than the ratio between the lives predicted by the NCHRP and the non-linear model

- The ratio between the lives predicted by the NCHRP and linear models is between 1.6 and 2.1 for mix A, between 5.0 and 7.5 for mix B and close to 1.8 for mix D. For these three mixes, the NCHRP model will over-predict the fatigue life. If the fatigue model is not replaced in the NCHRP design software, the design model will under-estimate the extent of fatigue associated cracking.

- For mix C, the life predicted by NCHRP model is between 12 and 63 times lower than the life predicted by the linear model. If the default fatigue model is not replaced in the NCHRP design software, the design model will severely over-estimate the extent of fatigue associated cracking for pavement structures containing Mix C. The possible explanation for the large differences in predicted fatigue lives is that mix C contained a polymer modified binder. Mixes B and C had very similar aggregate gradations and volumetric properties and differed only in the binder grade. The binder used in Mix B was not modified.
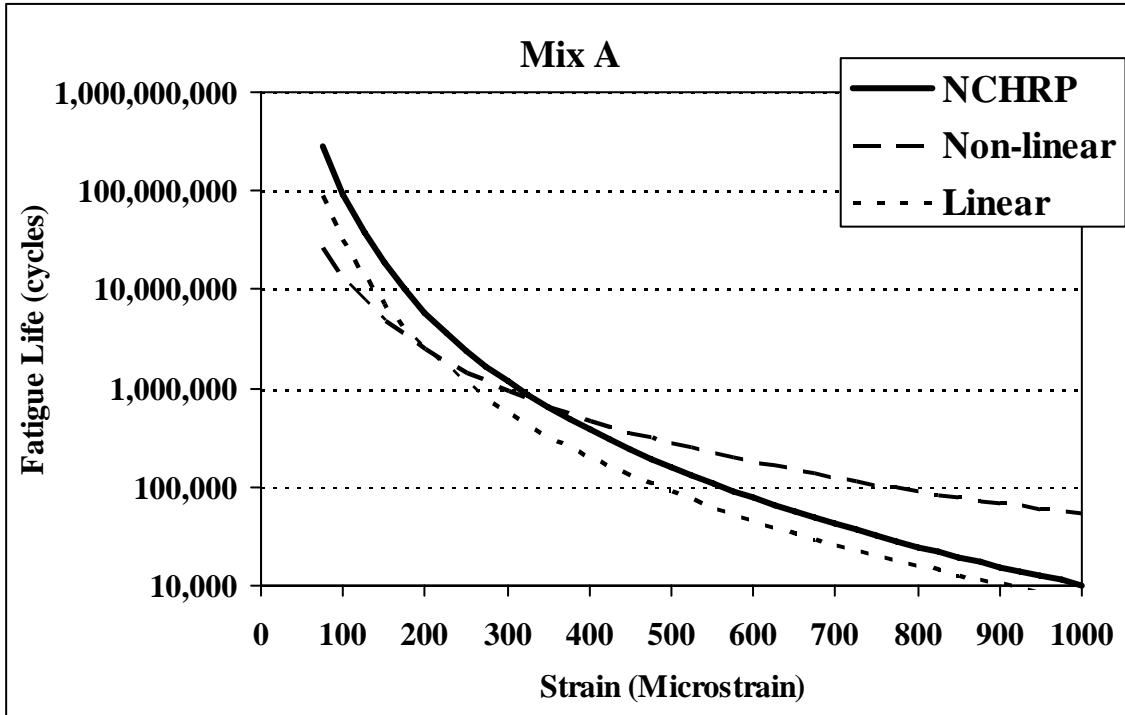
Figure 5.10 Comparison of Fatigue Life Models – Mix A
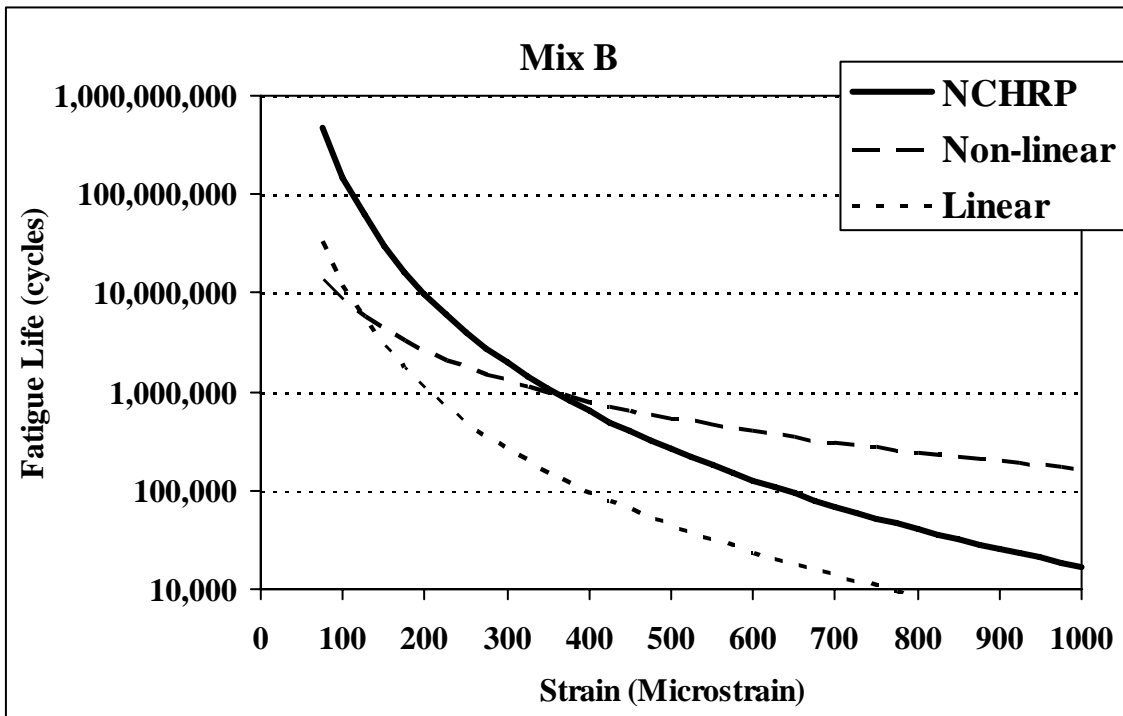
Figure 5.11 Comparison of Fatigue Life Models – Mix B
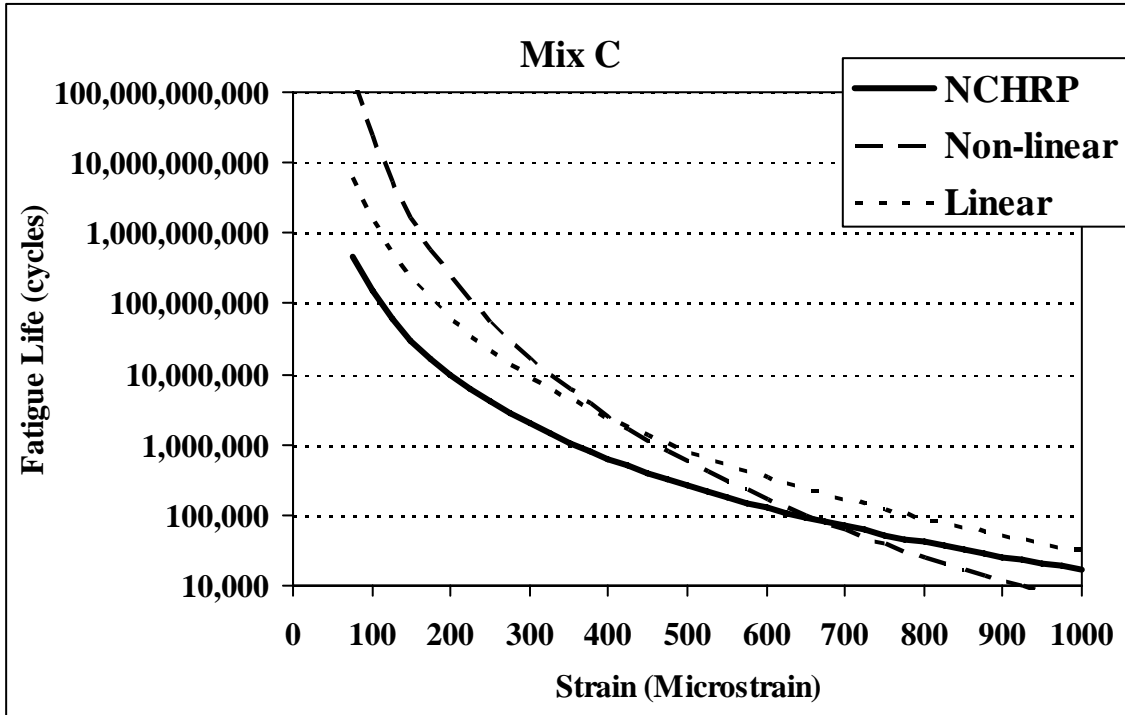
Figure 5.12 Comparison of Fatigue Life Models – Mix C
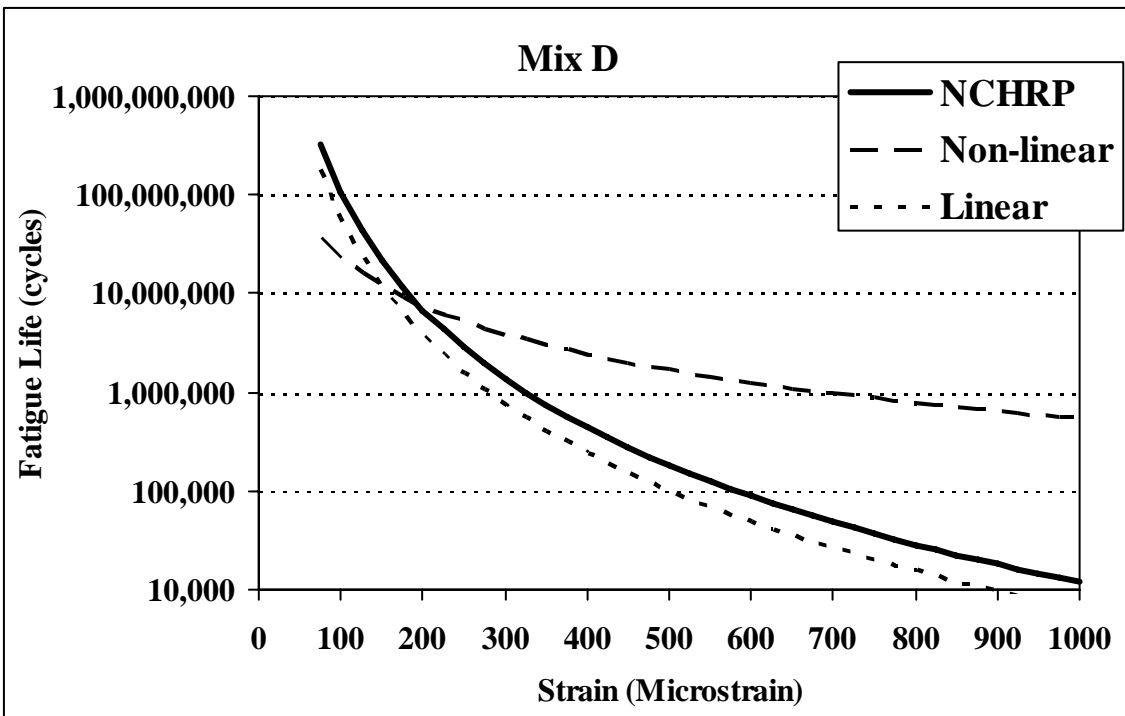
Figure 5.13 Comparison of Fatigue Life Models – Mix D

96

CHAPTER 6

CONCLUSIONS AND RECOMMENDATIONS

The objective of this research is to determine the dynamic modulus, the bending stiffness and the fatigue properties of four representative Kansas Superpave HMA mixtures used in the construction of base layers for flexible pavements, to allow the development of correlations between the dynamic modulus, stiffness and the fatigue characteristics of typical Superpave Kansas mixtures and to compare the measured dynamic moduli and fatigue life models with those predicted by the NCHRP Design Guide.

To achieve these objectives, asphalt concrete beams were tested in third point-bending at constant strain, at four temperatures and four levels of strain. Four replicate samples were tested for each condition. Dynamic resilient modulus tests were performed on asphalt cylindrical specimens at five temperatures and five loading frequencies. Four replicate samples were tested for each condition. Multilinear regression analysis was performed based on the results of the fatigue test and a linear relationship was developed between the bending stiffness and the fatigue life for the asphalt mixes tested. The effects of temperature, loading frequency and air void content on the dynamic resilient modulus were also evaluated with regression analysis.

6.1   Conclusions

The following conclusions can be drawn based on the results of this study:

1.   The testing temperature and the level of strain influence significantly the fatigue life of Superpave asphalt mixes. As expected, the asphalt beams subjected to a low level of strain had a longer fatigue life that those subjected to a high level of strain.

2. The mix (mix C) which contained binder modified with SBS polymer (PG 70-28) had a longer fatigue life (N_f) than the mixes with unmodified binder, at all the tested temperatures and levels of strain. At strain values > 500 microstrain, the asphalt beams from mixes with unmodified binders couldn't be tested because the samples broke before 10,000 load cycles, whereas the mix with polymerized binder lasted more than 2 million cycles at strain levels greater than 500 microstrain. However, the mix with SBS polymer modified binder had very similar dynamic modulus with mix B, that had the same aggregate gradation and volumetric properties but a virgin binder (PG 64-22).

3. In general, the lower the air voids content then the longer the fatigue life, but due to the small number of specimens tested for each condition and the large variability of fatigue test results then no universal conclusion can be drawn. The range of the air voids was between 4.4 and 7.9 %.

4. As expected, all asphalt mixes exhibited a higher dynamic modulus at low temperatures than at high temperatures, and at high loading frequencies than at low frequencies.

5. The statistical analysis proved that, in the dynamic modulus testing of all mixes, the modulus was dependent on frequency and temperature. For three mixes, the analysis proved that the dynamic resilient modulus significantly decreases when the air void content increases.

6. The measured dynamic moduli on all four mixes were, in most cases, more than two times the dynamic moduli predicted by the Witczak equation, the model included in the NCHRP Design Guide. Therefore, the Witczak equation severely under-predicts the dynamic modulus of the four mixes.

7. At the same temperatures and at the same frequency (10 Hz), the measured dynamic moduli were more than two times larger than the corresponding bending stiffnesses.

8. For the mixes containing virgin binder, the laboratory measured fatigue life was between 13 and 60 percent of the life predicted by the fatigue life model included in the NCHRP Design Guide. For the mix containing SBS polymer modified binder, the laboratory measured fatigue life was between 12 and 63 times longer

than the life predicted by the fatigue life model included in the NCHRP Design Guide.

6.2   Recommendations

The following recommendations are made based on the results of this study:

- The dynamic resilient moduli should be determined on several other mixes that may be used in base layer construction. The test is easier to perform and the cylindrical specimens can be fabricated easier. The dynamic moduli change significantly from one mix to another.

- The use of the Witczak equation for prediction of dynamic moduli should be done with caution. More dynamic moduli tests should be performed to determine if the equation can be used for other mixes or to derive a new equation for dynamic moduli prediction.

- Because the fatigue tests are taking a long time and the asphalt specimens are difficult to fabricate, it is not recommended the fatigue tests to be performed on a routine basis. The fatigue regression coefficients developed in this project should be used for other similar mixes. However, it is recommended to perform the tests for on several other mixes that may be used in base layer construction and differ significantly from the mixes studied in this project.

- The use of the NCHRP Design Guide model for prediction of fatigue life should be done with caution. More fatigue tests should be performed to determine if the model can be used for other mixes or to derive a new fatigue life model which can better predict the fatigue life of Kansas Superpave mixes.

REFERENCES

Ali, H., A., Tayabji, S., D., "Evaluation of Mechanistic-Empirical Performance Prediction Models for Flexible Pavements", *Transportation Research Record, no. 1629*, National Research Council, Washington, D.C., pp 169-180, 1998.

American Association of State Highway and Transportation Officials, "Standard Test Method for Determining the Fatigue Life of Compacted HMA Subjected to Repeated Flexural Bending", *AASHTO Provisional Standard TP8-94*, September 1994.

Asphalt Institute "Research and Development of the Asphalt Institute's Design Manual (MS-1)", Ninth Edition, August 1982.

Baburamani, Pud, "Asphalt Fatigue Life Prediction Models", *ARRB no. 334, Transport Research*, 2001.

Claessen, A. I. M., Edwards, J. M., Sommer, P., Uge, P., "Asphalt Pavement Design - The Shell Method", *Proceedings Fourth International Conference on Structural Design of Asphalt Pavements*, Michigan, 1977.

Feeley, A.J., "Universal Testing Machine, UTM 25, Hardware Reference", *Industrial Process Controls Ltd.*, Australia, 1999.

Kallas, B.F.; Puzinauskas, V.P., "Flexure Fatigue Tests on Asphalt Paving Mixtures", *ASTM Special Technical Publications, no. 508*, pp 47-66, 1972.

Kennedy, T.W., Anagnos, J. N., "Procedure for the Static and Repeated Load Indirect Tensile Tests", *Res. Record 183-14, Ctr. For Transp. Res.*, University of Texas at Austin, 1983.

Kim, Y. R., Whitmoyer, S.L., Little, D. N., "Healing in Asphalt Concrete Pavements: Is it real?" *Transportation Research Record 1454*, TRB, National Research Council, Washington D.C., pp. 89-96, 1994.

Khalid, H. A., "Evaluation of Asphalt Fatigue Properties in the Laboratory", *Journals of the Institution of Civil Engineers*, London, 2000.

Khosla, N. P., Omer, M.S., "Characterization of Asphalt Mixtures for Prediction of Pavement Performance", *Transportation Research Record, no. 1034,* TRB, National Research Council, Washington, D.C., pp 47-85, 1985.

Li, Y., Metcalf, J.B., Romanoschi, S.A., Rasoulian, M., "The Performance and Failure Modes of Louisiana Asphalt Pavements with Soil Cement Bases under Full-Scale Accelerated Loading", *Transportation Research Record 1673,* Transportation Research Board, National Research Council, Washington, DC, pp 9-15, 1999.

Matthews, James M., Monismith, C. L., Craus, J., "Investigation of Laboratory Fatigue Testing Procedures for Asphalt Aggregate Mixtures" *Journal of Transportation Engineering, No. 4*, July / August, 1993.

McGee, K.H. *Overview of the AASHTO 2002 Guide.* http://www.2002guide.com/ Accessed May 2004.

Monismith, C.L., Epps J.A., F.N. Finn., "Improved Asphalt Mix Design", *Journal of Association of Asphalt Paving Technologists,* Vol.54, pp 347-406, 1985.

Monismith, C.L., Salam, Y. M., "Proc. of Fracture Characteristics of Asphalt Concrete", *Association of Asphalt Paving Technologists,* 215-255, 1971.

NCHRP Project 9-19 Draft Test Protocol X1: "Simple Performance Test for Permanent Deformation Based Upon Dynamic Modulus of Asphalt Concrete Mixtures", 2001.

NCHRP *Guide for Mechanistic-Empirical Design of New and Rehabilitated Pavement Structures*. Final Report. NCHRP Project 1-37A. Transportation Research Board,

National Research Council, Washington, DC, webdocument: www.trb.org/mepdg/guide.htm Accessed August 2004.

Ott, R.L., Longnecker, M., "An Introduction to Statistical Methods and Data Analysis", Duxbury, Fifth Edition, 2001.

Pell, P. S., Cooper, K. E., "The Effect of Testing and Mix Variables on the Fatigue Performance of Bituminous Materials", *Journal of the Association of Asphalt Paving Technologists, Vol. 44,* pp. 1-37, 1975.

Raad, L., Saboundjian, S., Minassian, G., "Field Aging Effects on the Fatigue of Asphalt Concrete and Asphalt-Rubber Concrete", *Transportation Research Record, no. 1767,* TRB, National Research Council, Washington, D.C., pp. 126-134, 2001.

Roberts, F.L., Khandal, P.S., Brown, E.R., Lee, D-Y, Kennedy, T.W., "Hot Mix Asphalt Material, Mixture Design and Construction", NAPA Research and Education Foundation, Second Edition, 1996.

Strategic Highway Research Program, SHRP-A-404, "Fatigue Response of Asphalt-Aggregate Mixes", National Research Council, Washington DC, 1994.

Tseng, K-H, Lytton, R. L., "Fatigue Damage Properties of Asphaltic Concrete Pavements", *Transportation Research Record 1286,* National Research Council, Washington, D.C., 1990.

Van Dijk, W., Visser, W., "The Energy Approach to Fatigue for Pavement Design", *Journal of the Association of Asphalt Paving Technologists, Vol. 46,* pp. 1-40, 1977.

Zaitsev, J.W. "Fatigue Response of Asphalt-Aggregate", Report SHRP-A-404, National Research Council, 1994.

APPENDIX A

Characteristics of the HMA Beam Samples

Table A1 Mix A

Sample	Molded	WT air	WT SSD	Gmm	Gmb	AV %	Height (mm)					Width (mm)				
							A	B	C	D	E	A	B	C	D	E
111	6/4/2002	2957.2	2963.8	2.445	2.279	6.8	51	50	50	50	50	62	62	62	62	62
116	6/4/2002	2884.7	2890.3	2.445	2.302	5.8	51	50	50	50	49	60	60	60	60	60
117	6/4/2002	3017.8	3024.5	2.445	2.295	6.1	50	49	50	50	50	63	63	62	62	62
118	6/6/2002	3026.5	3034.1	2.445	2.295	7.0	50	51	51	51	51	63	63	62	62	62
119	6/6/2002	2895.4	2904.3	2.445	2.288	7.3	51	51	51	51	51	58	59	58	58	59
113	6/6/2002	2950.1	2960.5	2.445	2.272	7.1	52	52	52	52	52	64	63	62	62	62
19	7/25/2002	2981.5	2960.5	2.445	2.283	6.6	51	51	51	51	51	62	62	62	62	62
20	7/25/2002	3019.8	3028.6	2.445	2.285	6.5	52	52	52	52	52	60	60	60	60	60
21	7/25/2002	2998.5	3008.9	2.445	2.268	7.2	52	52	52	52	52	62	62	62	62	62
22	7/25/2002	2996.2	3004.4	2.445	2.295	6.1	51	51	51	51	51	62	62	62	62	62
23	7/25/2002	3002.1	3011.0	2.445	2.275	7.0	52	51	50	50	50	65	65	65	65	65
24	7/25/2002	2946.4	2955.1	2.445	2.281	6.7	50	50	50	50	50	64	64	64	64	64
25	7/25/2002	2942.6	2953.3	2.445	2.265	7.4	50	50	50	50	50	64	64	64	64	64
26	7/25/2002	3172.9	3184.5	2.445	2.281	6.7	50	50	50	50	50	68	68	68	68	68
27	7/29/2002	2886.3	2894.7	2.445	2.274	7.0	50	50	50	50	50	62	62	62	62	62
28	7/29/2002	2999.3	3008.0	2.445	2.277	6.9	52	52	52	52	52	62	62	62	62	62
29	7/29/2002	2986.6	2996.9	2.445	2.277	6.9	52	52	52	52	52	62	62	62	62	62
30	7/29/2002	2936.2	2946.9	2.445	2.269	7.2	53	53	53	53	53	60	60	60	60	60
31	7/29/2002	3078.2	3089.4	2.445	2.266	7.3	53	53	53	53	53	63	63	63	63	63
32	7/30/2002	3007.0	3015.0	2.445	2.268	7.2	50	50	50	50	50	62	62	62	62	62
33	7/30/2002	3015.1	3025.6	2.445	2.250	8.0	52	52	52	52	52	62	62	62	62	62
34	7/30/2002	3036.6	3044.6	2.445	2.276	6.9	52	52	52	52	52	65	65	65	65	65
35	7/30/2002	2976.3	2984.0	2.445	2.278	6.8	50	50	50	50	50	62	62	62	62	62
36	8/14/2002	3134.4	3147.2	2.445	2.264	7.4	52	52	52	52	52	64	64	64	64	64
37	8/14/2002	3120.6	3131.0	2.445	2.251	7.9	52	52	52	52	52	64	64	64	64	64
38	8/14/2002	3114.7	3124.1	2.445	2.274	7.0	52	52	52	52	52	65	65	65	65	65
39	8/14/2002	3191.3	3203.0	2.445	2.273	7.0	51	51	51	51	51	66	66	66	66	66
40	8/14/2002	3136.1	3145.4	2.445	2.276	6.9	51	51	51	51	51	64	64	64	64	64
41	8/14/2002	3122.6	3139.6	2.445	2.272	7.1	51	51	51	51	51	64	64	64	64	64
43	8/14/2002	3088.0	3099.1	2.445	2.269	7.2	52	52	52	52	52	63	63	63	63	63
44	8/14/2002	3115.5	3131.1	2.445	2.259	7.6	52	52	52	52	52	63	63	63	63	63
45	8/15/2002	3130.2	3139.9	2.445	2.276	6.9	51	51	51	51	51	64	64	64	64	64
46	8/27/2002	2987.0	2995.3	2.445	2.269	7.2	50	50	50	50	50	62	62	62	62	62
47	8/27/2002	2999.6	3004.7	2.445	2.290	6.3	50	50	50	50	50	62	62	62	62	62
48	8/27/2002	3020.7	3026.3	2.445	2.282	6.7	50	50	50	50	50	62	62	62	62	62
49	8/27/2002	3042.6	3050.4	2.445	2.280	6.7	50	50	50	50	50	62	62	62	62	62
50	8/27/2002	2969.2	2977.3	2.445	2.272	7.1	50	50	50	50	50	62	62	62	62	62
51	8/27/2002	2930.7	2940.4	2.445	2.274	7.0	50	50	50	50	50	61	61	61	61	61
52	9/4/2002	3059.2	3065.7	2.445	2.260	7.6	50	50	50	50	50	64	64	64	64	64
53	9/4/2002	2548.0	2554.7	2.445	2.276	6.9	51	51	51	51	51	53	53	53	53	53
54	9/4/2002	2977.3	2985.9	2.445	2.280	6.7	50	50	50	50	50	62	62	62	62	62
55	9/4/2002	3074.7	3088.2	2.445	2.269	7.2	50	50	50	50	50	65	65	65	65	65

Table A1 Mix A - continued

Sample	Molded	WT air	WT SSD	Gmm	Gmb	AV %	Height (mm)					Width (mm)				
							A	B	C	D	E	A	B	C	D	E
56	9/4/2002	3139.8	3149.9	2.445	2.273	7.0	51	52	52	52	52	65	65	65	66	66
57	9/5/2002	3168.2	3177.7	2.445	2.280	6.7	51	51	51	52	52	68	67	67	67	67
58	9/5/2002	3033.9	3038.2	2.445	2.285	6.5	51	51	52	52	52	65	65	65	64	64
59	9/5/2002	3008.7	3020.9	2.445	2.289	6.4	51	51	51	51	51	63	63	63	64	65
60	9/5/2002	3133.8	3142.7	2.445	2.274	7.0	51	51	52	52	52	68	66	65	65	64
61	9/16/2002	3095.6	3101.7	2.445	2.280	6.7	51	52	52	52	53	66	66	66	67	68
62	9/16/2002	3084.5	3097.8	2.445	2.251	7.9	51	52	52	52	53	66	66	66	67	67
63	9/16/2002	2910.0	2919.6	2.445	2.262	7.5	51	51	51	52	52	62	62	62	62	62
64	9/16/2002	3068.3	3076.9	2.445	2.274	7.0	51	51	51	51	51	67	67	66	66	65
65	9/16/2002	3025.4	3031.5	2.445	2.293	6.2	51	51	51	51	51	64	64	64	64	65
66	9/16/2002	3069.6	3078.3	2.445	2.269	7.2	52	52	52	52	52	65	66	66	66	67
67	9/17/2002	3143.0	3150.5	2.445	2.266	7.3	52	52	52	52	52	67	67	66	66	66
68	9/17/2002	2981.8	2990.9	2.445	2.254	7.8	52	52	52	52	53	65	64	64	64	63
70	9/17/2002	2982.7	2992.1	2.445	2.258	7.6	53	53	53	52	52	63	63	63	63	63
71	10/21/2002	2976.4	2987.0	2.445	2.242	8.3	52	52	52	52	52	63	63	63	63	63
72	10/21/2002	2926.7	2943.4	2.445	2.208	9.7	54	54	54	53	53	60	61	62	63	65
73	10/21/2002	2868.5	2882.6	2.445	2.226	9.0	53	53	53	53	53	61	61	61	60	60
74	10/21/2002	2572.2	2582.2	2.445	2.263	7.5	48	48	48	48	48	57	58	59	60	61
75	10/22/2002	2664.8	2674.9	2.445	2.269	7.2	46	46	47	47	47	60	61	62	63	64
76	10/22/2002	2601.6	2608.5	2.445	2.269	7.2	49	48	48	48	48	60	60	59	58	55
77	10/22/2002	2523.0	2532.4	2.445	2.287	6.4	46	45	45	45	45	55	59	60	60	61
78	10/22/2002	2718.1	2729.4	2.445	2.295	6.1	45	45	45	45	45	65	64	63	63	65
79	10/23/2002	2514.7	2519.3	2.445	2.303	5.8	45	45	45	45	45	59	58	58	59	62
80	10/23/2002	2980.7	2992.3	2.445	2.264	7.4	47	45	45	45	45	69	70	70	70	74
81	10/23/2002	2631.5	2638.1	2.445	2.286	6.5	47	45	45	45	47	63	62	62	62	62
82	10/23/2002	2709.0	2717.7	2.445	2.272	7.1	45	45	45	45	45	64	66	66	65	60

Table A2 Mix B

Sample	Molded	WT air	WT SSD	Gmm	Gmb	AV %	Height (mm)					Width (mm)				
							A	B	C	D	E	A	B	C	D	E
9	1/17/2003	2990.6	2996.3	2.407	2.264	6.0	53	53	53	53	53	64	64	65	65	65
10	1/17/2003	2829.7	2838.1	2.407	2.253	6.4	52	52	52	52	52	63	62	62	61	60
11	1/17/2003	2518.3	2524.8	2.407	2.245	6.7	52	52	52	52	52	65	65	65	65	65
12	1/17/2003	2938.7	2945.4	2.407	2.264	6.1	53	53	53	53	53	64	64	63	62	62
13	1/17/2003	3017.5	3024.9	2.407	2.239	7.0	54	54	54	54	54	65	65	65	65	65
14	1/17/2003	2931.7	2939.5	2.407	2.225	7.7	53	53	53	53	53	63	63	63	63	63
15	1/17/2003	2964.9	2975.2	2.407	2.263	8.5	53	53	53	53	53	65	65	65	65	65
16	1/17/2003	2994.8	3004.1	2.407	2.240	7.0	53	53	53	53	53	64	64	64	64	64
17	1/17/2003	3157.0	3162.9	2.407	2.282	5.2	53	53	53	53	53	66	66	66	66	66
18	1/17/2003	3052.8	3060.5	2.407	2.258	6.2	53	53	53	53	53	65	65	65	65	65
24	1/22/2003	2966.9	2977.2	2.407	2.267	5.8	53	53	53	53	53	63	63	63	63	63
25	1/22/2003	2997.9	3008.2	2.407	2.256	6.3	53	53	53	53	53	63	63	63	63	63
26	1/22/2003	3074.4	3083.2	2.407	2.257	6.2	53	53	53	53	53	66	66	66	66	66
27	1/22/2003	2959.0	29.68.2	2.407	2.247	6.7	53	53	53	53	53	64	64	64	64	64
28	1/22/2003	3057.6	3070.2	2.407	2.218	7.8	53	53	53	53	53	66	66	66	66	66
29	1/22/2003	3193.8	3202.0	2.407	2.278	5.3	54	54	54	54	54	65	65	65	65	65
30	1/22/2003	3143.1	3169.9	2.407	2.252	6.4	54	54	54	54	54	65	65	65	65	65
31	1/22/2003	3111.2	3124.5	2.407	2.260	6.1	54	54	54	54	54	65	65	65	65	65
32	1/22/2003	3142.4	3157.4	2.407	2.263	6.0	54	54	54	54	54	65	65	65	65	65
33	1/24/2003	3138.1	3145.8	2.407	2.260	6.1	52	52	52	52	52	67	67	67	67	67
34	1/24/2003	3072.2	3077.9	2.407	2.272	5.6	53	53	53	53	53	65	65	65	65	65
35	1/24/2003	2984.4	2988.7	2.407	2.266	5.9	53	53	53	53	53	63	63	63	63	63
36	1/24/2003	3082.9	3090.0	2.407	2.243	6.8	53	53	53	53	53	66	66	66	66	66
37	1/24/2003	3109.5	3116.1	2.407	2.256	6.3	52	52	52	52	52	66	66	66	66	66
38	1/24/2003	3045.0	3050.2	2.407	2.267	5.8	52	52	52	52	52	64	64	64	64	64
39	1/24/2003	3008.6	3014.2	2.407	2.276	5.4	52	52	52	52	52	64	64	64	64	64
40	1/24/2003	2988.8	2997.2	2.407	2.251	6.5	53	53	53	53	53	64	64	64	64	64
41	1/24/2003	3090.0	3097.1	2.407	2.275	5.5	53	53	53	53	53	65	65	65	65	65
42	1/24/2003	3138.6	3144.6	2.407	2.278	5.4	53	53	53	53	53	66	66	66	66	66
43	1/24/2003	3152.1	3158.2	2.407	2.272	5.6	53	53	53	53	53	66	66	66	66	66
44	1/24/2003	2988.3	2996.0	2.407	2.250	6.5	53	53	53	53	53	63	63	63	63	63
45	1/24/2003	3104.3	3114.5	2.407	2.252	6.4	53	53	53	53	53	67	67	67	67	67
46	1/24/2003	2896.3	2902.6	2.407	2.259	6.1	53	53	53	53	53	62	62	62	62	62
47	1/24/2003	2855.7	2861.0	2.407	2.262	6.0	53	53	53	53	53	61	61	61	61	61
48	1/24/2003	2992.9	3000.8	2.407	2.238	7.0	53	53	53	53	53	65	65	65	65	65
49	1/29/2003	3130.7	3139.4	2.407	2.238	7.0	52	52	52	52	52	67	67	67	67	67
51	1/29/2003	3064.8	3072.3	2.407	2.257	6.2	53	53	53	53	53	64	64	64	64	64
52	1/29/2003	3151.7	3161.5	2.407	2.250	6.5	52	52	52	52	52	66	66	66	66	66
54	1/29/2003	3095.7	3101.4	2.407	2.257	6.2	53	53	53	53	53	65	65	65	65	65
55	1/29/2003	3075.6	3080.5	2.407	2.273	5.6	53	53	53	53	53	64	64	64	64	64
56	1/29/2003	3132.0	3138.0	2.407	2.268	5.8	53	53	53	53	53	65	65	65	65	65
57	2/20/2003	3196.2	3206.9	2.407	2.244	6.8	53	53	53	53	53	69	69	69	69	69

Table A2 Mix B – continued

Sample	Molded	WT air	WT SSD	Gmm	Gmb	AV %	Height (mm)					Width (mm)				
							A	B	C	D	E	A	B	C	D	E
59	2/20/2003	2832.8	2847.0	2.407	2.198	8.7	52	52	52	52	52	62	62	62	62	62
60	2/20/2003	3232.5	3239.2	2.407	2.245	6.7	53	53	53	53	53	69	69	69	69	69
61	2/20/2003	2999.3	3006.0	2.407	2.236	7.1	53	53	53	53	53	65	65	65	65	65
62	2/20/2003	3023.3	3033.4	2.407	2.259	6.1	53	53	53	53	53	66	66	66	66	66
75	2/212003	2957.8	2966.9	2.407	2.255	6.3	51	51	51	51	51	64	64	64	64	64
76	2/212003	3231.5	3237.0	2.407	2.313	3.9	52	52	52	52	52	66	66	66	66	66
77	2/212003	3053.0	3058.6	2.407	2.276	5.4	52	52	52	52	52	65	65	65	65	65
81	3/10/2003	2849.1	2874.2	2.407	2.181	9.4	53	53	53	53	53	63	63	63	63	63
82	3/10/2003	2992.5	3005.4	2.407	2.217	7.9	53	53	53	53	53	64	64	64	64	64
83	3/10/2003	2990.6	3001.0	2.407	2.233	7.2	53	53	53	53	53	63	63	63	63	63
84	3/10/2003	2828.2	2939.7	2.407	2.225	7.6	53	53	53	53	53	60	60	60	60	60
85	3/10/2003	3028.9	3049.1	2.407	2.214	8.0	53	53	53	53	53	65	65	65	65	65
86	3/10/2003	3258.1	3267.5	2.407	2.254	6.4	53	53	53	53	53	68	68	68	68	68
87	3/10/2003	3009.5	3016.6	2.407	2.254	6.4	53	53	53	53	53	63	63	63	63	63
88	3/10/2003	3103.2	3118.0	2.407	2.227	7.5	53	53	53	53	53	66	66	66	66	66
89	3/10/2003	3106.2	3120.1	2.407	2.224	7.6	53	53	53	53	53	66	66	66	66	66
90	3/10/2003	9098.6	3107.4	2.407	2.245	6.7	53	53	53	53	53	65	65	65	65	65
92	3/10/2003	2965.2	2983.0	2.407	2.213	8.1	52	52	52	52	52	64	64	64	64	64
93	3/10/2003	3204.2	3214.0	2.407	2.247	6.6	53	53	53	53	53	68	68	68	68	68
94	3/10/2003	2935.2	2941.5	2.407	2.248	6.6	53	53	53	53	53	62	62	62	62	62
95	3/10/2003	3009.3	3016.4	2.407	2.247	6.6	53	53	53	53	53	65	65	65	65	65
96	3/10/2003	3005.3	3015.5	2.407	2.215	8.0	53	53	53	53	53	65	65	65	65	65

Table A3 Mix C

Sample	Molded	WT air	WT SSD	Gmm	Gmb	AV %	Height (mm)					Width (mm)				
							A	B	C	D	E	A	B	C	D	E
1	6/4/2003	3147.9	3154.4	2.414	2.291	5.1	51	50	50	50	50	62	62	62	62	62
3	6/4/2003	3169.9	3013.3	2.414	2.297	4.9	53	53	53	53	53	66	66	66	66	66
4	6/4/2003	3006.4	3162.1	2.414	2.281	5.5	52	52	52	52	52	63	63	63	63	63
5	6/4/2003	3152.4	3160.2	2.414	2.268	6.1	53	53	53	53	53	66	66	66	66	66
6	6/4/2003	3154.3	3062.4	2.414	2.298	4.8	53	53	53	53	53	64	64	64	64	64
7	6/4/2003	3056.6	3102.5	2.414	2.287	5.3	53	53	53	53	53	65	65	65	65	65
9	6/4/2003	3090.7	2931.5	2.414	2.267	6.1	53	53	53	53	53	65	65	65	65	65
10	6/4/2003	2924.7	2931.1	2.414	2.284	5.4	53	53	53	53	53	60	60	60	60	60
11	6/4/2003	3202.0	3209.3	2.414	2.283	5.4	53	53	53	53	53	67	67	67	67	67
12	6/4/2003	2983.6	2993.7	2.414	2.272	5.9	53	53	53	53	53	63	63	63	63	63
13	6/4/2003	3128.3	3135.7	2.414	2.271	5.9	53	53	53	53	53	67	67	67	67	67
14	6/4/2003	3120.9	3127.0	2.414	2.305	4.5	53	53	53	53	53	65	65	65	65	65
15	6/4/2003	3121.6	3127.7	2.414	2.294	5.0	53	53	53	53	53	66	66	66	66	66
16	6/4/2003	2867.4	2879.5	2.414	2.270	6.0	53	53	53	53	53	62	62	62	62	62
19	6/4/2003	3202.7	3210.0	2.414	2.272	5.9	53	53	53	53	53	67	67	67	67	67
20	6/4/2003	2940.5	2950.0	2.414	2.278	5.6	53	53	53	53	53	61	61	61	61	61
21	6/4/2003	3037.6	3049.4	2.414	2.251	6.7	53	53	53	53	53	64	64	64	64	64
22	6/4/2003	3134.9	3142.8	2.414	2.287	5.2	54	54	54	54	54	63	63	64	65	65
23	6/4/2003	3092.2	3098.3	2.414	2.283	5.4	54	54	54	54	54	65	65	65	65	65
24	6/4/2003	2900.2	2913.1	2.414	2.249	6.8	53	53	53	53	53	62	62	62	62	62
25	6/4/2003	3065.1	3070.8	2.414	2.290	5.2	53	53	53	53	53	63	63	63	63	63
26	6/4/2003	3146.9	3151.5	2.414	2.307	4.4	55	55	55	55	55	65	65	65	65	65
27	6/4/2003	3149.0	3155.1	2.414	2.297	4.8	53	53	53	53	53	65	65	65	65	65
28	6/4/2003	3089.4	3100.2	2.414	2.255	6.6	53	53	53	53	53	65	65	65	65	65
29	6/4/2003	2945.3	2953.1	2.414	2.268	6.0	53	53	53	53	53	63	63	63	63	63
30	6/4/2003	3126.4	3132.4	2.414	2.287	5.3	53	53	53	53	53	65	65	65	65	65
31	6/4/2003	3088.7	3094.4	2.414	2.290	5.1	53	53	53	53	53	65	65	65	65	65
32	6/4/2003	3045.6	3053.0	2.414	2.266	6.1	52	52	52	52	52	65	65	65	65	65
33	6/4/2003	2955.9	2962.5	2.414	2.284	5.4	53	53	53	53	53	62	62	62	62	62
34	6/4/2003	3073.8	3079.2	2.414	2.308	4.4	53	53	53	53	53	64	64	64	64	64
35	6/4/2003	2992.3	2996.7	2.414	2.301	4.7	53	53	53	53	53	62	62	62	62	62
36	6/4/2003	3058.1	3065.9	2.414	2.271	5.9	53	53	53	53	53	64	64	64	64	64
37	6/4/2003	3109.3	3121.0	2.414	2.260	6.4	53	53	53	53	53	65	65	65	65	65
38	6/4/2003	3170.3	3177.8	2.414	2.266	6.1	53	53	53	53	53	66	66	66	66	66
39	6/4/2003	3120.7	3128.2	2.414	2.267	6.1	53	53	53	53	53	64	64	64	64	64
40	6/4/2003	2905.5	2914.7	2.414	2.245	7.0	53	53	53	53	53	62	62	62	62	62
41	6/4/2003	3054.0	3062.7	2.414	2.266	6.1	54	54	54	54	54	64	64	64	64	64
42	6/4/2003	3183.8	3190.3	2.414	2.293	5.0	54	54	54	54	54	66	66	66	66	66
43	6/4/2003	3159.3	3167.5	2.414	2.290	5.1	54	54	54	54	54	65	65	65	65	65
44	6/4/2003	3015.9	3026.9	2.414	2.232	7.6	53	53	53	53	53	64	64	64	64	64
45	6/4/2003	2988.7	3002.6	2.414	2.224	7.9	53	53	53	53	53	64	64	64	64	64
46	6/4/2003	3129.7	3135.4	2.414	2.264	6.2	53	53	53	53	53	66	66	66	66	66

Table A3 Mix C - continued

Sample	Molded	WT air	WT SSD	Gmm	Gmb	AV %	Height (mm)					Width (mm)				
							A	B	C	D	E	A	B	C	D	E
50	6/4/2003	3070.1	3079.2	2.414	2.253	6.7	53	53	53	53	53	64	64	64	64	64
51	6/4/2003	3038.3	3046.5	2.414	2.251	6.7	53	53	53	53	53	64	64	64	64	64
52	6/4/2003	2923.1	2936.0	2.414	2.223	7.9	53	53	53	53	53	64	64	64	64	64

APPENDIX B

Summary of Fatigue Test Results

Table B1 Summary of Number of Cycles to Failure, Mix A - Uncorrected Stiffness

Temp (^{0}C)	Strain (microstrain)	Sample	AV %	Sini	Sfin	b_0	$b_1 * 1000$	R^2	N_f
4	125	113	8.3	10,514	5,257	10,606	-1.307	0.92	4,091,394
		71	8.3	10,153	5,077	11,666	-0.418	0.70	15,746,282
		78	6.1	7,866	3,933	7,985	-0.131	0.50	31,003,136
		79	5.8	12,916	6,458	14,197	-0.342	0.52	22,629,279
	250	72	9.7	9,679	4,839	9,175	-6.275	0.97	690,897
		73	9.0	10,431	5,215	9,484	-4.984	0.93	856,391
		76	7.2	10,639	5,319	11,109	-2.589	0.16	2,235,798
		77	6.4	12,194	6,097	11,229	-2.413	0.92	2,126,817
	375	116	5.8	11,078	5,539	10,468	-53.588	0.42	91,978
		74	7.5	10,820	5,410	9,595	-72.859	0.99	57,434
		75	7.2	10,530	5,265	8,163	-28.509	0.97	101,644
		80	7.4	12,177	6,088	10,483	-68.982	0.99	63,710
	500	111	6.8	8,834	4,417	7,522	-36.324	0.99	85,477
		117	6.1	10,867	5,433	9,470	-202.121	0.59	19,970
		118	7.0	9,886	4,943	9,386	-389.258	0.99	11,415
		119	7.3	10,587	5,293	9,626	-278.439	1.00	15,559
10	125	27	7.0	10,425	5,212	10,018	-0.584	0.66	8,230,155
		45	6.9	10,910	5,455	10,179	-0.258	0.65	18,324,552
		46	7.2	8,780	4,390	9,147	-0.574	0.77	8,294,908
		47	6.3	10,961	5,480	10,581	-0.467	0.54	10,914,917
	250	26	6.7	9,062	4,531	7,672	-1.055	0.96	2,978,133
		43	7.2	9,573	4,787	8,180	-1.096	0.96	3,095,123
		44	7.6	9,697	4,848	8,537	-4.374	0.97	843,168
		48	6.7	11,047	5,524	8,820	-1.022	0.93	3,225,877
	375	24	6.7	8,829	4,414	6,465	-6.690	0.98	306,499
		25	7.4	10,354	5,177	7,223	-17.792	0.89	114,993
		28	6.9	9,262	4,631	7,335	-26.717	0.99	101,201
		32	7.2	8,723	4,362	7,508	-26.948	0.96	116,742
	500	23	7.0	8,325	4,163	7,315	-70.194	1.00	44,905
		29	6.9	9,248	4,624	8,224	-73.167	0.99	49,204
		30	7.2	8,460	4,230	6,742	-113.740	0.99	22,083
		31	7.3	7,892	3,946	5,912	-52.035	0.96	37,780

Table B1 - continued

Temp (^{0}C)	Strain (microstrain)	Sample	AV %	Uncorrected Stiffness (MPa)					
				Sini	Sfin	b_0	$b_1 * 1000$	R^2	N_f
20	125	22	6.1	7,070	3,535	6,577	-1.249	0.79	2,436,025
		41	7.1	7,163	3,582	6,633	-2.369	0.83	1,287,998
		50	7.1	8,103	4,051	7,167	-1.053	0.34	2,957,291
		82	7.1	5,212	2,606	4,804	-0.216	0.37	10,189,251
	250	20	6.5	5,147	2,574	4,219	-0.669	0.91	2,460,754
		40	6.9	5,534	2,767	5,043	-2.822	0.64	806,348
		49	6.7	5,289	2,645	4,733	-1.421	0.93	1,469,716
		39	7.0	5,392	2,696	4,342	-0.666	0.87	2,469,898
	375	21	7.2	4,504	2,252	3,717	-2.559	0.94	572,478
		37	7.9	4,338	2,169	3,465	-2.120	0.91	611,324
		38	7.0	4,875	2,438	3,205	-3.339	0.93	229,977
		81	6.5	4,424	2,212	3,219	-0.712	0.93	1,413,938
	500	19	6.6	5,324	2,662	3,996	-26.670	0.95	50,004
		33	8.0	3,463	1,732	2,526	-4.468	0.94	177,897
		34	6.9	5,035	2,517	3,111	-4.863	0.76	122,106
		35	6.8	6,674	3,337	5,055	-41.277	0.96	41,628
30	125	64	7.0	3,518	1,759	2,565	-0.299	0.53	2,699,254
		65	6.2	3,390	1,695	3,151	-0.104	0.23	14,058,676
		66	7.2	3,743	1,871	3,083	-0.101	0.25	12,047,443
		67	7.3	3,157	1,578	2,381	-0.240	0.54	3,342,622
	250	59	6.4	4,566	2,283	3,365	-4.461	0.84	242,619
		60	7.0	3,749	1,874	2,580	-2.960	0.78	238,314
		61	6.7	1,701	850	1,462	-0.792	0.88	772,255
		70	7.6	3,495	1,747	2,727	-0.647	0.80	1,515,842
	375	55	7.2	2,507	1,253	1,731	-0.478	0.59	997,936
		56	7.0	2,824	1,412	1,872	-1.220	0.79	376,757
		57	6.7	1,726	863	1,362	-0.907	0.87	550,050
		58	6.5	2,797	1,398	1,925	-2.667	0.93	197,277
	500	51	7.0	2,200	1,100	1,470	-1.510	0.69	245,228
		52	7.6	2,199	1,099	1,468	-2.927	0.93	126,117
		53	6.9	2,074	1,037	1,318	-0.934	0.73	300,714
		54	7.2	2,330	1,165	1,618	-3.364	0.98	134,788

Table B2 Summary of Number of Cycles to Failure, Mix A - Temperature Corrected Stiffness

Temp (^{0}C)	Strain (microstrain)	Sample	AV %	Temperature Corrected Stiffness (MPa)					
				Sini	Sfin	b_0	$b_1 * 1000$	R^2	N_f
4	125	113	8.3	11,167	5,583	10,843	-1.130	0.92	4,654,410
		71	8.3	10,677	5,339	11,352	-0.424	0.76	14,191,910
		78	6.1	7,744	3,872	8,034	-0.148	0.57	28,098,740
		79	5.8	13,360	6,680	14,272	-0.341	0.59	22,289,642
	250	72	9.7	9,438	4,719	8,894	-6.498	0.97	642,561
		73	9.0	10,847	5,423	9,476	-6.675	0.96	607,129
		76	7.2	11,604	5,802	11,450	-6.857	0.70	823,624
		77	6.4	12,490	6,245	11,070	-2.430	0.92	1,985,918
	375	116	5.8	11,392	5,696	10,719	-61.864	0.50	81,195
		74	7.5	11,064	5,532	9,828	-78.001	0.99	55,080
		75	7.2	10,980	5,490	8,604	-31.051	0.98	100,294
		80	7.4	12,476	6,238	10,762	-72.623	0.99	62,295
	500	111	6.8	9,274	4,637	7,912	-46.422	0.99	70,561
		117	6.1	10,990	5,495	9,578	-210.494	0.60	19,396
		118	7.0	11,296	5,648	10,774	-418.297	0.99	12,255
		119	7.3	11,577	5,789	10,684	-301.535	1.00	16,236
10	125	27	7.0	9,797	4,898	9,739	-0.456	0.78	10,617,833
		45	6.9	11,143	5,572	10,592	-0.285	0.58	17,611,689
		46	7.2	9,186	4,593	9,391	-0.659	0.78	7,277,840
		47	6.3	10,987	5,494	10,620	-0.334	0.59	15,368,420
	250	26	6.7	10,137	5,069	7,671	-1.343	0.96	1,937,552
		43	7.2	10,388	5,194	8,072	-1.344	0.98	2,141,900
		44	7.6	10,528	5,264	8,823	-4.925	0.98	722,667
		48	6.7	11,002	5,501	8,914	-0.906	0.96	3,768,604
	375	24	6.7	9,974	4,987	6,959	-4.972	0.97	396,666
		25	7.4	10,794	5,397	7,176	-18.329	0.89	97,080
		28	6.9	9,609	4,805	7,757	-32.967	0.99	89,551
		32	7.2	9,083	4,542	8,021	-36.038	0.98	96,545
	500	23	7.0	8,252	4,126	7,171	-69.440	1.00	43,852
		29	6.9	8,201	4,101	7,203	-61.993	0.99	50,040
		30	7.2	8,315	4,157	6,691	-113.367	1.00	22,347
		31	7.3	8,609	4,305	6,596	-55.919	0.96	40,979

Table B2 Summary of Number of Cycles to Failure for Temperature Corrected Stiffness for Mix A - continued

Temp (^{0}C)	Strain (microstrain)	Sample	AV %	Temperature Corrected Stiffness (MPa)					
				Sini	Sfin	b_0	$b_1 * 1000$	R^2	N_f
20	125	22	6.1	6,670	3,335	6,088	-0.332	0.42	8,286,897
		41	7.1	7,095	3,547	6,453	-2.683	0.82	1,082,647
		50	7.1	7,758	3,879	6,893	-0.940	0.34	3,208,223
		82	7.1	5,293	2,646	4,813	-0.169	0.45	12,837,241
	250	20	6.5	5,523	2,761	4,296	-0.645	0.92	2,380,640
		40	6.9	5,445	2,722	4,785	-2.997	0.65	688,214
		49	6.7	5,338	2,669	4,722	-0.743	0.85	2,762,175
		39	7.0	5,703	2,851	4,360	-0.641	0.88	2,352,435
	375	21	7.2	4,968	2,484	3,966	-3.442	0.89	430,420
		37	7.9	4,617	2,309	3,624	-2.979	0.87	441,673
		38	7.0	5,134	2,567	3,461	-5.581	0.92	160,115
		81	6.5	5,181	2,590	3,453	-0.753	0.87	1,146,761
	500	19	6.6	5,436	2,718	3,891	-23.452	0.92	50,007
		33	8.0	3,254	1,627	2,329	-2.666	0.87	263,483
		34	6.9	5,735	2,867	3,806	-12.574	0.96	74,688
		35	6.8	5,646	2,823	4,095	-28.087	0.95	45,293
30	125	64	7.0	3,434	1,717	2,555	-0.203	0.64	4,133,675
		65	6.2	3,413	1,707	3,144	-0.106	0.40	13,614,791
		66	7.2	3,538	1,769	2,952	-0.098	0.47	12,010,778
		67	7.3	2,965	1,483	2,190	-0.184	0.76	3,842,851
	250	59	6.4	4,398	2,199	3,128	-3.569	0.80	260,238
		60	7.0	3,627	1,813	2,381	-2.231	0.72	254,494
		61	6.7	1,495	747	1,246	-0.811	0.86	614,674
		70	7.6	3,310	1,655	2,265	-0.567	0.82	1,076,216
	375	55	7.2	2,725	1,363	1,861	-1.307	0.76	381,482
		56	7.0	2,876	1,438	1,872	-1.721	0.82	252,150
		57	6.7	1,684	842	1,302	-0.957	0.84	481,101
		58	6.5	2,632	1,316	1,746	-1.656	0.80	259,910
	500	51	7.0	2,152	1,076	1,412	-1.543	0.70	217,973
		52	7.6	2,086	1,043	1,359	-2.654	0.89	118,880
		53	6.9	2,046	1,023	1,365	-0.932	0.82	366,554
		54	7.2	2,364	1,182	1,637	-2.684	0.95	169,605

Table B3 Summary of Number of Cycles to Failure, Mix B - Uncorrected Stiffness

Temp (^{0}C)	Strain (microstrain)	Sample	AV %	Uncorrected Stiffness (MPa)					
				Sini	Sfin	b_0	$b_1 * 1000$	R^2	N_f
4	125	51	6.2	9,504.17	4,752.08	10,071	-0.496	0.89	10,730,476
		60	6.7	9,359.84	4,679.92	10,927	-0.891	0.87	7,010,746
		61	7.1	9,441.61	4,720.80	10,221	-0.130	0.16	42,463,041
		62	6.1	9,474.06	4,737.03	11,147	-0.440	0.46	14,583,788
	250	33	6.1	9,936.66	4,968.33	9,004	-2.677	0.96	1,507,535
		47	6.0	8,173.87	4,086.94	8,724	-6.721	0.97	689,936
		57	6.8	9,890.49	4,945.25	9,175	-4.655	0.98	908,576
		59	8.7	8,301.27	4,150.64	7,663	-2.355	0.97	1,491,426
	375	46	6.1	9,268.50	4,634.25	7,993	-24.315	0.98	138,144
		83	7.2	9,056.32	4,528.16	8,931	-68.669	0.97	64,121
		84	7.6	9,601.73	4,800.86	8,625	-65.053	0.99	58,789
		86	6.4	9,352.44	4,676.22	8,483	-23.454	0.97	162,292
	500	44	6.5	9,918.61	4,959.30	8,036	-92.066	0.98	33,421
		45	6.4	10,470.53	5,235.27	8,182	-117.892	0.97	24,993
		85	8.0	9,676.97	4,838.48	7,315	-74.691	0.98	33,158
		92	8.1	9,470.99	4,735.50	8,547	-165.932	0.99	22,972
10	125	11	6.7	9,111.61	4,555.81	8,851	-0.647	0.90	6,637,255
		12	6.1	9,104.15	4,552.07	8,940	-0.257	0.46	17,057,682
		14	7.7	8,965.12	4,482.56	9,017	-0.806	0.86	5,624,300
		17	5.2	11,373.15	5,686.58	9,740	-0.502	0.65	8,077,353
	250	29	5.3	8,962.53	4,481.26	7,360	-2.019	0.93	1,425,982
		30	6.4	6,321.40	3,160.70	5,366	-0.987	0.95	2,234,673
		31	6.1	7,115.51	3,557.76	5,690	-1.043	0.94	2,044,923
		32	6.0	6,243.97	3,121.98	4,564	-1.299	0.91	1,110,389
	375	81	9.4	5,410.40	2,705.20	4,412	-7.214	0.98	236,618
		82	7.9	6,826.80	3,413.40	5,825	-14.877	0.98	162,083
		95	6.6	7,546.65	3,773.33	6,849	-21.447	0.98	143,405
		96	8.0	6,936.39	3,468.20	6,021	-21.768	0.98	117,285
	500	87	6.4	8,353.93	4,176.96	6,492	-63.732	0.97	36,326
		88	7.5	6,887.74	3,443.87	5,591	-68.892	0.99	31,162
		89	7.6	7,007.73	3,503.87	5,732	-62.718	0.97	35,531
		90	6.7	6,214.35	3,107.17	5,019	-37.202	0.96	51,379

,

Temp (^{0}C)	Strain (microstrain)	Sample	AV %	Uncorrected Stiffness (MPa)					
				Sini	Sfin	b_0	$b_1 * 1000$	R^2	N_f
20	125	34	5.6	3,196.38	1,598.19	3,016	-0.205	0.66	6,918,111
		35	5.9	4,317.53	2,158.77	3,480	-0.334	0.81	3,959,373
		36	6.8	3,848.68	1,924.34	3,485	-0.297	0.85	5,246,822
		37	6.3	3,806.14	1,903.07	3,611	-0.340	0.78	5,016,012
	250	39	5.4	3,662.65	1,831.33	3,051	-0.736	0.89	1,657,987
		40	6.5	3,766.02	1,883.01	2,798	-2.174	0.82	420,697
		41	5.5	4,199.22	2,099.61	3,318	-3.932	0.69	309,847
		48	7.0	2,976.27	1,488.13	3,057	-0.913	0.94	1,718,670
	375	38	5.8	3,580.26	1,790.13	2,930	-5.776	0.96	197,322
		54	6.2	3,710.19	1,855.09	2,893	-3.378	0.94	307,413
		55	5.6	3,429.33	1,714.66	2,648	-3.669	0.94	254,306
		56	5.8	3,118.48	1,559.24	2,512	-3.247	0.91	293,336
	500	42	5.4	3,553.10	1,776.55	2,877	-21.041	0.95	52,293
		43	5.6	3,674.52	1,837.26	2,975	-32.134	0.97	35,407
		93	6.6	3,435.85	1,717.93	2,904	-20.639	0.95	57,473
		94	6.6	3,630.73	1,815.36	2,831	-25.847	0.95	39,288
30	125	10	6.4	2,566.61	1,283.31	2,006	-2.910	0.88	248,539
		75	6.3	2,296.92	1,148.46	2,109	-1.141	0.64	841,814
		76	3.9	3,124.57	1,562.28	2,871	-0.392	0.56	3,337,204
		77	5.4	2,602.97	1,301.48	2,324	-1.714	0.79	596,658
	250	15	8.5	1,904.30	952.15	1,397	-2.024	0.85	220,033
		24	5.8	1,912.08	956.04	1,516	-2.709	0.89	206,535
		25	6.3	1,954.97	977.49	1,419	-1.267	0.88	348,727
		26	6.2	1,819.78	909.89	1,264	-1.427	0.72	248,052
	375	9	6.0	1,929.75	964.87	1,539	-11.995	0.94	47,833
		13	7.0	1,765.64	882.82	1,454	-10.643	0.91	53,691
		16	6.2	1,405.58	702.79	1,122	-1.424	0.95	294,340
		27	6.7	1,922.42	961.21	1,561	-12.864	0.96	46,650
	500	18	6.2	1,416.94	708.47	1,182	-12.363	0.79	38,284
		28	7.8	1,420.36	710.18	1,131	-9.965	0.97	42,267
		49	7.0	1,341.22	670.61	1,075	-6.994	0.95	57,829
		52	6.5	1,015.50	507.75	794	-2.272	0.97	126,020

Table B4 Summary of Number of Cycles to Failure, Mix B - Temperature Corrected Stiffness

Temp (^{0}C)	Strain (microstrain)	Sample	AV %	Temperature Corrected Stiffness (MPa)					
				Sini	Sfin	b_0	$b_1 * 1000$	R^2	N_f
4	125	51	6.2	10,162.30	5,081.2	10,170	-0.449	0.82	11,325,902
		60	6.7	10,118.29	5,059.1	11,487	-0.529	0.71	12,157,376
		61	7.1	9,770.47	4,885.2	9,997	-0.303	0.53	16,847,955
		62	6.1	10,207.22	5,103.6	11,108	-0.368	0.55	16,322,560
	250	33	6.1	10,147.75	5,073.9	8,429	-2.747	0.94	1,221,361
		47	6.0	8,911.30	4,455.7	8,607	-6.853	0.98	605,760
		57	6.8	10,185.46	5,092.7	9,096	-4.633	0.97	864,053
		59	8.7	8,869.83	4,434.9	7,299	-2.315	0.89	1,237,357
	375	46	6.1	9,204.25	4,602.1	7,874	-24.933	0.97	131,233
		83	7.2	8,411.08	4,205.5	8,249	-61.857	0.97	65,366
		84	7.6	9,267.50	4,633.7	8,321	-68.276	0.99	54,000
		86	6.4	9,696.57	4,848.3	8,588	-27.085	0.97	138,061
	500	44	6.5	10,027.61	5,013.8	8,067	-97.264	0.98	31,392
		45	6.4	10,590.36	5,295.2	8,293	-122.374	0.98	24,497
		85	8.0	9,453.75	4,726.9	7,023	-75.208	0.98	30,527
		92	8.1	9,382.93	4,691.5	8,365	-164.503	0.99	22,330
10	125	11	6.7	8,742.86	4,371.4	8,421	-0.492	0.85	8,237,066
		12	6.1	9,361.22	4,680.6	8,676	-0.242	0.65	16,534,290
		14	7.7	9,250.15	4,625.1	8,563	-0.618	0.91	6,376,474
		17	5.2	11,350.02	5,675.0	10,134	-0.742	0.84	6,010,326
	250	29	5.3	8,788.47	4,394.2	6,878	-2.084	0.93	1,192,004
		30	6.4	6,233.16	3,116.6	4,540	-0.846	0.97	1,682,494
		31	6.1	7,313.57	3,656.8	5,955	-1.041	0.95	2,207,519
		32	6.0	6,576.41	3,288.2	4,548	-1.236	0.87	1,019,397
	375	81	9.4	5,605.37	2,802.7	4,309	-7.086	0.96	212,560
		82	7.9	6,733.06	3,366.5	5,650	-15.211	0.98	150,102
		95	6.6	7,854.82	3,927.4	6,920	-25.123	0.99	119,134
		96	8.0	7,028.07	3,514.0	6,101	-21.973	0.98	117,718
	500	87	6.4	8,344.97	4,172.5	6,541	-65.634	0.97	36,088
		88	7.5	7,115.38	3,557.7	5,779	-60.153	0.99	36,934
		89	7.6	6,911.34	3,455.7	5,629	-59.823	0.97	36,324
		90	6.7	6,121.03	3,060.5	4,938	-37.122	0.96	50,576

Table B4 - continued

Temp (^{0}C)	Strain (microstrain)	Sample	AV %	Temperature Corrected Stiffness (MPa)					
				Sini	Sfin	b_0	$b_1 * 1000$	R^2	N_f
20	125	34	5.6	3,243.62	1,621.8	3,074	-0.130	0.75	11,130,141
		35	5.9	4,391.85	2,195.9	3,681	-0.235	0.88	6,308,757
		36	6.8	3,691.41	1,845.7	3,378	-0.268	0.88	5,724,338
		37	6.3	3,726.76	1,863.4	3,733	-0.349	0.91	5,352,335
	250	39	5.4	3,572.60	1,786.3	2,935	-0.707	0.93	1,625,837
		40	6.5	3,747.67	1,873.8	2,731	-1.618	0.68	529,399
		41	5.5	4,304.53	2,152.3	3,366	-4.598	0.74	263,921
		48	7.0	3,094.10	1,547.0	2,797	-0.668	0.88	1,871,224
	375	38	5.8	3,565.50	1,782.8	2,920	-5.643	0.96	201,560
		54	6.2	3,596.09	1,798.0	2,813	-2.941	0.95	345,175
		55	5.6	3,346.66	1,673.3	2,603	-3.077	0.96	302,023
		56	5.8	3,249.87	1,624.9	2,570	-2.762	0.94	342,293
	500	42	5.4	3,621.01	1,810.5	2,827	-24.090	0.95	42,203
		43	5.6	3,488.56	1,744.3	2,688	-25.960	0.96	36,367
		93	6.6	3,333.65	1,666.8	2,595	-21.325	0.90	43,535
		94	6.6	3,690.27	1,845.1	2,812	-17.671	0.92	54,712
30	125	10	6.4	2,454.89	1,227.4	1,856	-1.907	0.74	329,464
		75	6.3	2,261.57	1,130.8	2,076	-1.080	0.62	875,342
		76	3.9	3,167.43	1,583.7	2,916	-0.469	0.62	2,840,996
		77	5.4	2,575.98	1,288.0	2,331	-0.554	0.53	1,882,117
	250	15	8.5	1,688.06	844.03	1,119	-1.014	0.64	271,187
		24	5.8	1,707.72	853.86	1,327	-1.808	0.81	261,640
		25	6.3	1,874.66	937.33	1,222	-1.575	0.83	180,741
		26	6.2	1,690.44	845.22	1,124	-0.888	0.61	313,910
	375	9	6.0	1,955.32	977.66	1,543	-11.746	0.94	48,128
		13	7.0	1,731.61	865.8	1,385	-11.734	0.92	44,239
		16	6.2	1,241.27	620.63	916	-0.750	0.82	393,966
		27	6.7	1,788.50	894.25	1,406	-12.491	0.94	40,978
	500	18	6.2	1,449.37	724.69	1,209	-13.237	0.81	36,558
		28	7.8	1,291.05	645.52	977	-6.952	0.95	47,623
		49	7.0	1,415.80	707.9	1,127	-8.357	0.96	50,159
		52	6.5	1,100.36	550.18	884	-2.522	0.98	132,554

Table B5 Summary of Number of Cycles to Failure, Mix C - Uncorrected Stiffness

Temp (^{0}C)	Strain (microstrain)	Sample	AV %	Uncorrected Stiffness (MPa)					
				Sini	Sfin	b_0	$b_1 * 1000$	R^2	N_f
4	250	44	7.6	7,834.67	3,917.33	6,449	-0.658	0.82	3,844,490
		48	5.6	4,639.72	2,319.86	4,286	-0.117	0.74	16,810,785
		51	6.7	8,186.32	4,093.16	7,100	-0.579	0.82	5,193,251
		52	7.9	7,680.43	3,840.22	6,449	-0.353	0.93	7,394,860
	375	12	5.9	7,632.79	3,816.40	6,117	-1.237	0.94	1,859,197
		11	5.4	9,274.65	4,637.32	6,984	-5.320	0.96	441,045
		47	5.7	7,937.98	3,968.99	6,739	-4.823	0.96	574,447
		10	5.4	7,861.43	3,930.71	6,085	-1.603	0.96	1,344,035
	500	46	6.2	5,397.49	2,698.74	4,958	-33.382	0.98	67,677
		14	4.5	7,677.55	3,838.77	5,615	-6.149	0.97	288,853
		15	5.0	7,369.60	3,684.80	4,980	-5.610	0.97	230,858
		13	5.9	7,232.29	3,616.14	5,889	-11.941	1.00	190,329
	625	39	6.1	1,931.80	965.90	1,506	-4.293	0.97	125,882
		45	7.9	1,689.19	844.60	1,288	-4.360	0.93	101,635
		49	7.2	2,791.90	1,395.95	1,879	-2.315	0.94	208,601
		50	6.7	7,343.31	3,671.66	5,611	-46.059	0.98	42,106
20	500	40	7.0	1,372.37	686.19	1,166	-0.188	0.47	2,554,822
		41	6.1	1,694.52	847.26	1,193	-0.122	0.77	2,843,139
		42	5.0	2,333.76	1,166.88	1,533	-1.517	0.86	241,370
		43	5.1	2,102.08	1,051.04	1,237	-0.150	0.79	1,235,480
	625	30	5.3	1,654.05	827.02	1,101	-1.087	0.78	3,149,265
		31	5.1	1,606.25	803.12	1,131	-0.137	0.90	2,401,217
		37	6.4	1,459.78	729.89	960	-0.098	0.75	2,338,526
		38	6.1	1,467.54	733.77	953	-0.144	0.81	1,524,509
	750	33	5.4	1,879.39	939.70	1,188	-0.244	0.88	1,016,888
		34	4.4	1,982.39	991.20	1,240	-0.252	0.84	984,005
		35	4.7	2,010.72	1,005.36	1,380	-1.056	0.93	355,129
		36	5.9	1,561.75	780.87	1,148	-1.145	0.97	320,527
	875	27	4.8	1,586.47	793.23	1,076	-1.657	0.96	170,877
		28	6.6	1,092.13	546.06	789	-0.569	0.98	427,050
		29	6.0	1,419.22	709.61	890	-0.365	0.82	494,174
		32	6.1	1,495.89	747.95	954	-0.392	0.83	527,040

Temp	Strain	Sample	AV	Uncorrected Stiffness (MPa)					
(^{0}C)	(microstrain)		%	Sini	Sfin	b_0	b_1 * 1000	R^2	N_f
30	750	5	6.1	795.75	397.88	515	-0.091	0.83	1,283,099
		6	4.8	797.10	398.55	544	-0.056	0.79	2,578,516
		19	5.9	805.40	402.70	536	-0.056	0.81	2,366,131
		26	4.4	778.07	389.04	542	-0.056	0.85	2,732,944
	875	1	5.1	751.47	375.74	489	-0.042	0.82	2,667,966
		3	4.9	674.93	337.47	463	-0.043	0.82	2,919,938
		4	5.5	734.73	367.36	504	-0.057	0.89	2,391,010
		7	5.3	824.88	412.44	534	-0.103	0.89	1,179,052
	1000	16	6.0	563.01	281.50	345	-0.059	0.84	1,092,600
		21	6.7	502.15	251.07	364	-0.059	0.81	1,914,723
		22	5.2	800.41	400.21	483	-0.109	0.84	754,593
		23	5.4	711.10	355.55	458	-0.044	0.81	2,320,847
	1125	9	6.1	628.33	314.17	391	-0.126	0.95	610,329
		20	5.6	738.47	369.23	476	-0.427	0.88	248,908
		24	6.8	672.85	336.43	425	-0.142	0.93	620,897
		25	5.2	633.86	316.93	416	-0.109	0.91	906,656

Table B6 Summary of Number of Cycles to Failure, Mix C - Temperature Corrected Stiffness

Temp (^{0}C)	Strain (microstrain)	Sample	AV %	Temperature Corrected Stiffness (MPa)					
				Sini	Sfin	b_0	$b_1 * 1000$	R^2	N_f
4	250	44	7.6	7,853.28	3,926.6	6,484	-0.627	0.86	4,078,603
		48	5.6	4,725.13	2,362.6	4,295	-0.079	0.24	24,490,792
		51	6.7	8,761.51	4,380.8	7,107	-0.625	0.81	4,360,000
		52	7.9	7,771.28	3,885.6	6,393	-0.356	0.86	7,047,723
	375	12	5.9	7,684.01	3,842.0	5,717	-1.127	0.90	1,664,041
		11	5.4	9,042.98	4,521.5	7,009	-5.346	0.97	465,417
		47	5.7	8,302.00	4,151.0	6,845	-4.925	0.94	547,021
		10	5.4	8,116.90	4,058.5	6,102	-1.568	0.93	1,303,217
	500	46	6.2	5,510.42	2,755.2	5,045	-32.658	0.98	70,122
		14	4.5	7,972.45	3,986.2	5,722	-6.723	0.95	258,125
		15	5.0	7,703.84	3,851.9	4,628	-5.598	0.94	138,565
		13	5.9	7,434.77	3,717.4	5,472	-12.613	0.95	139,116
	625	39	6.1	1,959.75	979.88	1,524	-4.654	0.96	116,935
		45	7.9	1,759.75	879.87	1,355	-4.385	0.93	108,420
		49	7.2	2,799.96	1,400.0	1,832	-2.485	0.93	173,770
		50	6.7	7,728.93	3,864.5	5,946	-50.019	0.98	41,606
20	500	40	7.0	1,468.21	769.11	1,001	-0.124	0.32	2,158,772
		41	6.1	1,738.60	869.30	988	-0.068	0.28	1,730,317
		42	5.0	2,254.11	1,127.1	1,458	-0.810	0.70	409,151
		43	5.1	2,267.35	1,133.7	1,288	-0.145	0.64	1,063,251
	625	30	5.3	1,680.67	840.34	1,124	-0.097	0.79	2,935,977
		31	5.1	1,613.78	806.89	1,112	-0.132	0.89	2,306,225
		37	6.4	1,382.24	691.12	985	-0.113	0.76	2,601,255
		38	6.1	1,587.99	793.99	1,137	-0.199	0.78	1,725,218
	750	33	5.4	1,874.07	937.04	1,155	-0.213	0.87	943,631
		34	4.4	2,030.69	1,015.3	1,299	-0.326	0.95	869,545
		35	4.7	2,100.41	1,050.2	1,390	-0.769	0.66	442,364
		36	5.9	1,613.48	806.74	1,108	-0.995	0.92	303,132
	875	27	4.8	1,593.37	796.68	1,075	-1.661	0.96	167,757
		28	6.6	1,040.18	520.09	729	-0.582	0.97	358,258
		29	6.0	1,396.02	698.01	850	-0.353	0.77	430,084
		32	6.1	1,529.35	764.68	975	-0.398	0.86	528,275

Table B6 - continued

Temp (^{0}C)	Strain (microstrain)	Sample	AV %	Temperature Corrected Stiffness (MPa)					
				Sini	Sfin	b_0	$b_1 * 1000$	R^2	N_f
30	750	5	6.1	754.22	377.11	481	-0.061	0.67	1,708,703
		6	4.8	765.92	382.96	550	-0.066	0.82	2,508,549
		19	5.9	780.37	390.19	515	-0.048	0.76	2,577,497
		26	4.4	776.11	388.05	542	-0.044	0.77	3,547,810
	875	1	5.1	742.99	371.49	474	-0.039	0.67	2,634,202
		3	4.9	665.09	332.54	455	-0.037	0.75	3,340,890
		4	5.5	738.95	369.48	504	-0.042	0.69	3,236,043
		7	5.3	840.01	340.00	542	-0.103	0.82	1,178,308
	1000	16	6.0	566.40	283.20	362	-0.052	0.81	1,513,988
		21	6.7	563.45	281.72	407	-0.082	0.84	1,528,215
		22	5.2	830.38	415.19	511	-0.099	0.82	964,465
		23	5.4	704.75	352.37	446	-0.042	0.72	2,248,515
	1125	9	6.1	624.83	312.42	386	-0.075	0.74	982,182
		20	5.6	704.19	352.09	446	-0.375	0.85	249,820
		24	6.8	643.23	321.62	420	-0.095	0.92	1,040,490
		25	5.2	604.58	302.29	390	-0.064	0.72	1,373,204

Table B7 Summary of Number of Cycles to Failure, Mix D - Uncorrected Stiffness

Temp (^{0}C)	Strain (microstrain)	Sample	AV %	Uncorrected Stiffness (MPa)					
				Sini	Sfin	b_0	$b_1 * 1000$	R^2	N_f
4	125	413		11,395	5,697	10,963	-0.250	0.50	21,060,315
		42		10,418	5,209	10,948	-0.540	0.81	10,635,859
		48		11,290	5,645	10,692	-0.157	0.46	32,087,269
		49		10,680	5,340	10,179	-0.103	0.16	47,093,465
	250	426		9,760	4,880	9,071	-1.790	0.96	2,342,100
		430		11,824	5,912	9,155	-1.140	0.97	2,845,751
		439		11,881	5,940	8,740	-1.206	0.97	2,321,108
		448		9,783	4,892	8,094	-1.132	0.99	2,828,543
	375	412		10,832	5,416	8,165	-2.695	0.04	1,019,857
		429		12,384	6,192	10,847	-39.901	0.96	116,658
		431		10,103	5,051	8,728	-28.529	1.00	128,867
		432		10,370	5,185	9,469	-41.147	0.98	104,114
	500	410		10,699	5,349	10,962	-598.718	0.93	9,375
		44		9,961	4,980	7,959	-104.688	0.99	28,457
		45		10,510	5,255	8,585	-67.740	1.00	49,159
		47		11,123	5,562	9,879	-215.479	0.98	20,036
20	125	434		1,838	919	1,508	-0.076	0.66	7,741,386
		435		4,914	2,457	4,053	-0.050	0.10	32,168,981
		465		4,483	2,241	4,863	-0.187	0.51	14,000,317
		467		3,554	1,777	3,092	-0.068	0.36	19,449,526
	250	438		5,113	2,556	3,694	-0.404	0.78	2,818,036
		440		4,186	2,093	3,218	-0.284	0.91	3,968,284
		456		3,959	1,979	2,853	-0.286	0.83	3,052,363
		451		2,982	1,491	2,257	-0.505	0.90	1,517,955
	375	436		3,181	1,590	2,396	-7.750	0.94	103,929
		437		4,097	2,049	2,846	-4.853	0.98	164,344
		443		3,488	1,744	2,481	-2.579	0.96	285,578
		452		1,491	745	1,203	-0.933	0.73	490,697
	500	444		2,490	1,245	2,272	-43.017	0.02	23,876
		447		3,372	1,686	2,274	-7.911	0.98	74,254
		449		2,701	1,350	1,774	-3.613	0.97	117,120
		450		2,480	1,240	1,698	-4.986	0.98	91,855

Table B7 - continued

Temp (^{0}C)	Strain (microstrain)	Sample	AV %	Uncorrected Stiffness (MPa)					
				Sini	Sfin	b_0	$b_1 * 1000$	R^2	N_f
30	125	457		2,305	1,152	1,674	-0.023	0.05	22,719,494
		468		2,824	1,412	2,453	-0.086	0.38	12,161,701
		473		3,420	1,710	2,739	-0.159	0.77	6,459,335
		474		3,530	1,765	2,648	-0.075	0.31	11,708,908
	250	459		2,161	1,081	1,445	-0.065	0.10	5,620,689
		460		2,798	1,399	1,772	-0.094	0.78	3,959,191
		466		1,529	765	1,132	-0.150	0.70	2,440,882
		475		2,030	1,015	1,436	-0.165	0.74	2,548,283
	375	461		2,467	1,233	1,459	-0.294	0.53	769,767
		463		2,022	1,011	1,320	-1.342	0.89	229,853
		464		1,801	901	1,226	-0.255	0.90	1,274,945
		477		2,004	1,002	1,272	-0.821	0.85	329,534
	500	469		2,160	1,080	1,317	-1.203	0.92	197,172
		470		1,972	986	1,339	-3.399	0.95	103,772
		476		2,056	1,028	1,326	-2.521	0.90	118,308
		567		1,193	597	800	-1.438	0.93	141,155

Table B8 Summary of Number of Cycles to Failure, Mix D - Temperature Corrected Stiffness

Temp (^{0}C)	Strain (microstrain)	Sample	AV %	Temperature Corrected Stiffness (MPa)					
				Sini	Sfin	b_0	$b_1 * 1000$	R^2	N_f
4	125	413		11,416	5,708	11,049	-0.370	0.40	14,443,006
		42		10,634	5,317	11,060	-0.387	0.84	14,820,904
		48		11,143	5,572	10,583	-0.041	0.10	122,251,683
		49		10,942	5,471	10,131	-0.139	0.30	33,537,712
	250	426		9,823	4,911	9,094	-1.752	0.95	2,386,818
		430		11,804	5,902	9,194	-1.159	0.98	2,840,947
		439		12,166	6,083	8,764	-1.145	0.97	2,341,403
		448		9,880	4,940	8,203	-1.065	0.99	3,064,742
	375	412		10,747	5,374	8,060	-2.425	0.03	1,107,977
		429		12,447	6,223	11,048	-40.586	0.96	118,866
		431		10,027	5,014	8,639	-27.580	1.00	131,429
		432		10,446	5,223	9,437	-44.613	0.98	94,449
	500	410		10,807	5,404	11,073	-603.509	0.93	9,394
		44		9,738	4,869	7,752	-103.081	0.99	27,971
		45		10,300	5,150	8,319	-69.416	1.00	45,655
		47		11,104	5,552	9,853	-216.353	0.98	19,881
20	125	434		1,821	911	1,683	-0.072	0.46	10,664,770
		435		5,020	2,510	4,261	-0.104	0.53	16,822,496
		465		4,621	2,310	4,281	-0.167	0.57	11,815,680
		467		3,708	1,854	3,085	-0.089	0.44	13,906,724
	250	438		5,229	2,615	3,651	-0.455	0.84	2,279,073
		440		4,298	2,149	3,227	-0.307	0.80	3,511,588
		456		3,972	1,986	2,798	-0.326	0.89	2,491,914
		451		2,929	1,464	2,179	-0.499	0.94	1,432,645
	375	436		3,137	1,569	2,342	-6.918	0.92	111,829
		437		4,071	2,035	2,747	-4.724	0.97	150,592
		443		3,554	1,777	2,542	-2.621	0.97	291,634
		452		1,551	775	1,242	-0.962	0.76	484,710
	500	444		2,600	1,300	2,321	-55.644	0.03	18,353
		447		3,428	1,714	2,327	-8.122	0.98	75,457
		449		2,799	1,399	1,878	-3.355	0.97	142,729
		450		2,510	1,255	1,672	-5.399	0.97	77,210

Table B8 - continued

Temp (^{0}C)	Strain (microstrain)	Sample	AV %	Temperature Corrected Stiffness (MPa)					
				Sini	Sfin	b_0	$b_1 * 1000$	R^2	N_f
30	125	457		2,356	1,178	1,785	-0.070	0.51	8,686,167
		468		2,765	1,383	2,451	-0.089	0.46	12,072,023
		473		3,401	1,700	2,730	-0.142	0.77	7,230,640
		474		3,493	1,746	2,741	-0.138	0.68	7,223,624
	250	459		2,178	1,089	1,645	-0.178	0.89	3,131,634
		460		2,754	1,377	1,780	-0.115	0.77	3,497,127
		466		1,579	789	1,120	-0.127	0.71	2,613,403
		475		2,017	1,009	1,431	-0.133	0.75	3,177,658
	375	461		2,511	1,256	1,550	-0.343	0.81	858,796
		463		1,953	976	1,347	-0.405	0.81	914,579
		464		1,871	935	1,159	-0.119	0.65	1,874,678
		477		2,013	1,007	1,293	-0.513	0.69	558,310
	500	469		2,187	1,094	1,334	-1.112	0.91	216,109
		470		1,936	968	1,310	-3.056	0.95	112,046
		476		2,011	1,005	1,301	-1.857	0.88	159,180
		567		1,231	616	816	-0.719	0.79	279,206

APPENDIX C

Dynamic Resilient Modulus Test Results

Table C1 Dynamic Resilient Modulus Mix A

Temp. (°C)	Sample No.	Air Voids (%)	Average Dynamic Modulus (MPa)				
			10 Hz	5 Hz	1 Hz	0.5 Hz	0.1 Hz
4	14	7.2	32,352	29,899	26,551	26,086	22,875
	15	7.2	17,168	16,832	15,016	14,199	11,558
	23	7.1	34,671	36,544	32,694	31,129	37,341
	26	6.7	27,450	26,073	23,489	22,079	19,832
	29	7.2	31,420	29,921	26,874	25,495	22,477
	Average		**28,612**	**27,854**	**24,925**	**23,797**	**22,816**
10	10	7.2	20,731	19,355	17,013	15,839	12,613
	12	7.0	19,508	19,575	16,463	15,262	11,701
	24	7.0	18,426	17,603	15,458	14,649	11,656
	28	7.2	25,364	25,526	21,825	21,073	16,962
	30	7.0	24,897	23,552	21,353	19,647	16,002
	Average		**21,785**	**21,122**	**18,423**	**17,294**	**13,787**
20	8	7.3	12,805	11,150	8,284	7,575	5,101
	11	7.1	14,046	12,804	9,817	9,016	6,301
	17	7.3	16,130	14,797	10,732	9,755	6,795
	18	6.7	16,027	14,806	11,886	10,980	8,183
	25	7.1	13,571	12,401	10,114	9,381	6,878
	Average		**14,516**	**13,192**	**10,167**	**9,341**	**6,651**
30	20	7.0	6,484	5,205	3,027	2,464	1,380
	31	7.1	7,591	6,027	3,721	3,091	1,872
	33	7.3	6,510	5,127	3,087	2,498	1,469
	34	7.1	6,150	5,287	3,627	3,062	1,827
	35	6.7	7,663	6,512	4,310	3,648	2,307
	Average		**6,880**	**5,631**	**3,554**	**2,952**	**1,771**
35	21	6.6	5,437	4,241	2,355	1,780	1,060
	22	6.8	4,900	3,559	1,886	1,439	832
	27	7.2	4,224	2,845	1,420	1,130	699
	42	6.5	6,058	4,699	2,859	2,272	1,442
	48	6.7	4,722	3,821	1,776	1,321	933
	Average		**5,068**	**3,833**	**2,059**	**1,588**	**993**

Table C2 Dynamic Resilient Modulus Mix B

Temp. (°C)	Sample No.	Air Voids (%)	Average Dynamic Modulus (MPa)				
			10 Hz	5 Hz	1 Hz	0.5 Hz	0.1 Hz
4	11	7.1	28,038	26,949	23,407	23,225	18,392
	17	7.1	19,750	18,394	15,760	15,306	12,461
	22	7.4	30,332	29,290	27,324	25,367	22,075
	2	7.2	18,635	17,430	14,957	14,299	11,676
	9	7.3	11,978	11,230	9,859	9,300	7,525
	Average		**21,747**	**20,658**	**18,261**	**17,499**	**14,426**
10	16	7.0	13,548	12,858	10,577	10,130	7,886
	18	6.6	19,814	18,609	15,851	15,012	12,155
	23	7.1	16,617	15,245	12,542	11,256	8,330
	6	7.5	16,466	15,406	12,707	11,896	9,304
	7	7.0	13,126	12,291	10,119	9,170	6,978
	Average		**15,914**	**14,882**	**12,359**	**11,493**	**8,931**
20	12	7.5	15,707	13,760	9,443	8,264	4,716
	13	7.4	9,706	8,883	6,344	5,472	3,664
	15	7.3	9,903	8,423	5,712	4,993	3,169
	21	6.9	10,560	9,299	6,994	6,204	4,288
	25	7.3	11,169	10,154	7,694	6,804	4,789
	Average		**11,409**	**10,104**	**7,237**	**6,347**	**4,125**
30	10	6.7	3,457	2,701	1,642	1,341	878
	14	7.4	6,063	5,065	3,136	2,442	1,481
	19	7.4	5,752	4,083	2,242	1,769	1,074
	3	7.0	6,718	5,522	3,559	2,985	1,970
	8	6.7	5,223	3,997	2,316	1,849	1,151
	Average		**5,443**	**4,274**	**2,579**	**2,077**	**1,311**
35	1	7.1	3,690	3,050	1,977	1,614	1,009
	20	6.9	3,558	2,775	1,618	1,324	923
	24	7.1	3,621	2,862	1,665	1,364	918
	4	7.4	6,762	5,343	2,966	2,349	1,452
	5	7.0	7,243	6,057	3,891	2,865	2,008
	Average		**4,975**	**4,017**	**2,423**	**1,903**	**1,262**

Table C3 Dynamic Resilient Modulus Mix C

Temp. (°C)	Sample No.	Air Voids (%)	Average Dynamic Modulus (MPa)				
			10 Hz	5 Hz	1 Hz	0.5 Hz	0.1 Hz
4	10	6.6	32,683	31,769	28,833	27,092	21,975
	13	6.9	16,518	14,686	12,304	11,181	9,053
	14	6.8	26,924	25,519	20,891	19,650	14,094
	13a	6.9	17,828	16,178	13,238	12,032	9,740
	14a	6.8	25,954	24,062	20,521	19,477	13,913
	Average		**23,981**	**22,442**	**19,157**	**17,886**	**13,755**
10	11	7.1	10,248	8,864	6,397	5,649	3,875
	12	7.3	18,545	16,215	11,763	10,906	7,002
	15	6.7	21,543	19,660	15,489	14,416	10,141
	11a	7.1	10,750	9,235	6,895	5,983	4,140
	12a	7.3	18,583	16,018	12,312	11,143	7,533
	Average		**15,934**	**13,998**	**10,571**	**9,619**	**6,538**
20	7	6.8	13,528	11,251	7,838	6,943	4,471
	8	6.9	11,336	9,513	6,786	5,792	4,232
	9	6.7	18,586	15,297	10,459	9,057	6,161
	8a	6.9	11,089	9,467	6,945	5,621	3,996
	9a	6.7	16,015	13,513	9,219	8,090	5,416
	Average		**14,111**	**11,808**	**8,249**	**7,101**	**4,855**
30	1	7	5,252	4,426	3,137	2,688	2,032
	2	7.3	5,744	4,809	3,281	2,623	1,810
	3	7.2	5,240	3,492	2,050	1,679	1,152
	2a	7.3	5,933	4,938	3,428	2,768	1,977
	3a	7.2	3,911	3,038	1,986	1,618	1,168
	Average		**5,216**	**4,141**	**2,777**	**2,275**	**1,628**
35	4	6.9	3,034	2,457	1,702	1,420	1,066
	5	7.6	2,673	2,208	1,465	1,219	906
	6	6.8	2,708	1,985	1,262	999	759
	5a	7.6	2,699	2,216	1,490	1,233	921
	6a	6.8	2,501	1,969	1,246	998	775
	Average		**2,723**	**2,167**	**1,433**	**1,174**	**886**

Table C4 Dynamic Resilient Modulus Mix D

Temp. (°C)	Sample No.	Air Voids (%)	Average Dynamic Modulus (MPa)				
			10 Hz	5 Hz	1 Hz	0.5 Hz	0.1 Hz
4	15	5.3	34,935	35,756	33,352	32,587	28,603
	18	6.8	21,004	20,392	17,531	16,750	13,841
	19	6.6	23,083	22,650	20,066	19,560	16,599
	21*	7.1	6,908	6,280	5,288	4,536	4,342
	Average		**26,340**	**26,266**	**23,650**	**22,965**	**19,681**
10	2	6.6	27,452	25,000	22,524	21,853	18,146
	8	4.9	25,225	23,685	21,569	20,072	17,176
	17	7.3	24,411	22,417	18,354	17,064	12,853
	20	6.7	18,330	16,900	14,690	14,905	12,781
	Average		**23,854**	**22,000**	**19,284**	**18,473**	**15,239**
20	1	6	6.9	17,594	15,758	12,491	11,737
	3	6.8	7.1	13,752	12,009	9,470	8,594
	4	6.9	7.3	14,095	10,260	7,690	6,807
	11	7.1	6.8	15,517	14,000	11,501	10,673
	12	7.3	6	19,638	17,475	14,024	13,036
	Average		**16,119**	**13,900**	**11,035**	**10,170**	**7,505**
30	9	5.4	5.4	14,855	13,163	9,575	8,146
	10	5.7	6.2	9,803	8,302	5,775	4,914
	13	5.8	6.8	8,710	7,426	5,357	4,674
	14	6.2	5.7	14,246	12,464	9,171	8,009
	16	6.8	5.8	12,477	10,878	7,830	6,773
	Average		**12,018**	**10,447**	**7,542**	**6,503**	**4,575**
35	5	5.3	6.9	4,948	4,129	2,900	2,484
	6	6.7	7.1	7,495	6,198	4,344	3,721
	7	6.9	5.3	6,358	5,205	3,582	3,001
	20	7.1	6.7	6,685	5,635	3,972	3,422
	Average		**6,372**	**5,292**	**3,700**	**3,157**	**2,330**

Outlier – this sample was not considered in the calculation of average dynamic modulus

K - TRAN

KANSAS TRANSPORTATION RESEARCH
AND
NEW - DEVELOPMENTS PROGRAM

A COOPERATIVE TRANSPORTATION RESEARCH PROGRAM BETWEEN:

KANSAS DEPARTMENT OF TRANSPORTATION

THE UNIVERSITY OF KANSAS

KANSAS STATE UNIVERSITY